Improving The Fire Resistance Rating of Concrete Masonry Walls Through the Use of Insulations

An Experimental and Numerical Study

by

Oprite Bobmanuel

A thesis submitted to the Faculty of Graduate and Postdoctoral Affairs in partial fulfillment of the requirements for the degree of

Master of Applied Science

In

Civil Engineering

Department of Civil and Environmental Engineering
Carleton University
Ottawa, Ontario
September 2021

Abstract

For non-loadbearing applications, the 15 cm blocks are usually used. They are lightweight, easy to install, and are cost effective. The fire resistance rating of the 15 cm block is about 1 h, while that of a 20 cm block is about 2 h. This reduced fire resistance rating is due to smaller cells which leads to more convective and radiative heat transfer inside of the block cells, as well as the reduced face cells that cause the blocks to heat up quicker. With the use of lightweight insulation materials as cell fillers, an improvement in the fire resistance rating was achieved for the 15 cm block. These materials were able to reduce the convective and radiative heat transfer in the cells. For the experimental and numerical analysis carried out, vermiculite, and gypsum were able to improve the fire ratings by at least 1h.

Acknowledgement

My appreciation goes to God, my parent, siblings and friends for their encouragement and support all through my studies

I would like to thank my esteemed supervisor Professor Ehab Zalok for his invaluable supervision, support, and tutelage during the course of my master's program. My gratitude extends to the Department of Civil and Environmental Engineering, Carleton University, for the knowledge instilled upon me. Additionally, I would like to express gratitude to Professor Heng Khoo for his guidance with the finite element modelling and analysis software, ABAQUS.

My profound gratitude goes to the Canadian Masonry Design Centre (CMDC) and Canadian Concrete Masonry Producers Association (CCMPA) for their financial and in-kind support. I would like to specially extend my gratitude to Dr. Bennett Banting (CMDC) for his personal involvement in various ways during the entire research. Also, grateful to the National Science and Engineering Research of Canada (NSERC) for the funding support, and to Peter McBride and Sean Tracey (Ottawa Fire Services) for their support to the fire laboratory.

I would like to thank my research team, past and present – Hamish Pope and Hannah Keelson for their treasured support which was really influential in shaping my research and critiquing my results.

Table of contents

List of tables

List of figures

List of abbreviations

ACI	American concrete institute
ASTM	American Society for Testing and Materials
BEM	Boundary element method
BS	British standards
BSI	British standards institution
CAD	Computer-aided design
CAE	Complete Abaqus environment
CCMPA	Canadian concrete masonry producers' association
CFD	Computational Fluid Dynamics
CPU	Computation time
DFLUX	Distributed flux
DOF	Degrees of freedom
EN	Eurocode
EPS	Expanded polystyrene
FDM	Finite difference method
FEA	Finite element ANALYSIS
FEM	Finite element method
FORTRAN	Formula translation
IS	Indian standard
ISO	International Organization for Standardization
LWAC	Lightweight aggregate concrete
LWC	Lightweight concrete
MK	Metakaolin
NWC	Normal weight concrete
OPC	Ordinary Portland cement
PCM	Phase change material
PET	Polyethylene terephthalate
PP	Polystyrene particles
SF	Silica fume
SFPE	Society of Fire Protection Engineers
ULC	Underwriters Laboratories of Canada
XPS	Extruded polystyrene

Chapter 1: Introduction

Masonry construction is one of the oldest and most common building techniques in the history of mankind, besides wood construction. The issue of burning/charring of timber due to a fire, fungi attacks, or insect attacks on timber resulted in the initial practice of roofing permanent structures in masonry. The evidence of masonry's durability, acoustic insulation, cost-effectiveness, versatility, non-combustibility, strength, weather change resistance and availability can be observed in the world's most significant ancient/historical structures like the Egyptian pyramids, the Great Wall of China and the Coliseum in Rome [1]. The architectural and structural properties of masonry both distinguish it from other building materials in its application. Natural stones were the first type of masonry used, and over time, sun-dried clay bricks, sand-lime bricks, and concrete block units with varying shapes and sizes have been manufactured. The type of masonry to be used in any construction depends on the load-bearing capacity of the wall.

Over the years, critical events like the collapse of the World Trade Center towers within 1 hour and 42 minutes on September 11th in Manhattan, causing over billions of dollars in infrastructure and property damage [2], 2996 deaths and over 6000 injured have led to the

increasing interest in the behavior of building materials in a fire [3]. The mechanical and thermal properties of masonry constituents largely influence the behavior of masonry walls in fire. Concrete is able to remain in place during a fire, with the cooler inner section performing its load bearing function. The performance of masonry walls at elevated temperatures is deemed excellent due to the exceptional thermal properties of its components. Under elevated temperature, the cement paste in concrete undergoes an endothermic reaction [4]. This phase assists in limiting the temperature rise in the fire-exposed concrete. A few researchers have reported a loss of strength, reduced moisture content, thermal expansion, thermal bowing, cracking, spalling, cosmetic blemishes, etc., in masonry units at elevated temperatures.

1.1. Basis of research

In the present-day building industry, normal weight concrete (NWC) hollow blocks with vertically oriented cells are normally used in the construction of masonry walls because they are lightweight, cost-effective, and easy to handle compared with solid or semi-solid blocks. However, the fire resistance rating of hollow blocks is comparatively lower than solid or semi-solid blocks and so researchers have been looking for ways to further improve the fire resistance these hollow blocks so that their fire ratings would be as good or even better than solid blocks, semi-solid blocks, or lightweight concrete blocks (LWC).

Hollow blocks generally have a ratio of less than 0.75 between the net cross-sectional area and the total cross-sectional area. The smaller this ratio, the lower the rate of heat transfer through the masonry block, in ambient conditions. Air filling up the cells of hollow blocks have a lower thermal conductivity than concrete, and so in actual sense, the thermal performance of hollow blocks should be better than solid blocks, but that is not the case. This is due to the effect of radiation and convection that are the predominant modes of heat transfer in concrete masonry blocks. When hollow blocks are heated, the hot gases in the cells travel upward and increase the heat flow of the blocks. This heat transfer phenomena gives rise to the need to further improve the fire resistance of hollow blocks by using lightweight insulating materials in the cells to obstruct heat flow.

1.2. Objectives of research

This is research is part of a much larger research at Carleton university that aims at improving the fire resistance of a nonloadbearing masonry wall by minimizing the heat flow through the wall. The first part of this research involves a full-scale fire resistance test carried out at the research facility at Barnsdale, Ottawa. The tests were carried out on walls of different types of different block geometries. The second part of the research involved a numerical analysis of the tested control wall, and the use of different lightweight insulating

materials with known thermal properties from existing literature in the cells with the objectives:

- Improve the fire resistance rating of a 15 cm wall beyond 1 h, through experimental work and numerical analysis, using lightweight insulation materials as cell fillers.
- To develop a reliable finite element model for simulating the thermal behaviour of normal weight concrete (NWC) masonry walls.
- To verify the numerical model using the experimental test results of a 20 cm NWC control wall.
- To validate the model using the experimental test results of the 15 cm NWC wall with insulation in the cells

1.3. Layout of the thesis

This thesis will contain five (5) chapters, which are detailed as follows:

- Chapter one is based on the introduction of the research, basis of the research, objectives of the research, and the research's general outline.
- Chapter two presents a literature review of past research relevant to this thesis. This section covers the effects of elevated temperatures on concrete masonry units. It discusses the thermal and mechanical properties of masonry constituents, the rate

of heat flow through walls, problems associated with concrete masonry exposed to elevated temperatures, and various methods to improve the fire resistance of wall assemblies through the use of insulation materials as fillers, mix designs, or cell configurations.

- Chapter three focuses on the general description of the work. The experimental work done on the first part of the research program is reviewed in this chapter, following the finite element model to simulate masonry walls thermal behavior when subjected to a fire.
- Chapter four focuses on the validation and verification of the developed finite element model. The choice of meshing technique, interaction module, and emissivity are discussed in this chapter along with the results from both the experimental and numerical analysis.
- Chapter five focuses on the conclusion, limitations of the study, and recommendations for future study.

Chapter 2: Literature review of masonry in fire

Masonry units can be made with various materials: stone, glass, shale, (calcium silicate) sand-lime, clay, and concrete, with concrete or clay bricks or blocks being the most commonly available masonry materials [5]. Masonry blocks or bricks vary in size.

Regardless of its good sound properties, low cost, and good thermal properties, unfired clay bricks are susceptible to water damage. A small amount of lime can help stabilize clay bricks, resulting in an improved building material [6]. Notwithstanding, there are durability problems that exist with the use of lime alone for the stabilization process [7]. Fired clay bricks also begin to exhibit serious durability problems when exposed to the humidity of the environment. The absorbed moisture causes complex chemical reactions within the clay, leading to an irreversible moisture expansion within the clay [5]. Unlike clay brick, concrete masonry blocks are a more recent development that started being used as a building material in the mid-19th century. They also have good thermal and sound insulating properties but are prone to irregular shaped whitish deposits (efflorescence) on their surfaces that are generally not expansive. These deposits are formed when salts migrate from the interior to the exterior surfaces of the masonry blocks. However, they do not affect the integrity of the masonry concrete blocks [9].

2.1. Types of masonry concrete blocks

Based on their net cross-sectional area, concrete blocks can be classified as solid, cellular, or hollow shaped blocks [8], as illustrated in Figure 2-1 below. Solid blocks are dense aggregate blocks with properties that make them ideal for load-bearing applications [9]. These blocks contain no formed cells. Cellular blocks are lightweight aggregate blocks with a lower strength than solid blocks, but with better insulating properties. This improved insulating property is as a result of the 30% recycled raw materials and air entrained during the mix. Cellular blocks can be used for both interior and exterior applications and fillings. These blocks contain formed cells that do not fully penetrate the block. Hollow blocks have the least densities and are better suited for partitioning [9]. They contain a void area greater than 25% of the gross area is more frequently used because of the ease of handling, ease of reinforcing, reduced weight, and overall economy [5]. These blocks contain formed cells that fully penetrate the block.

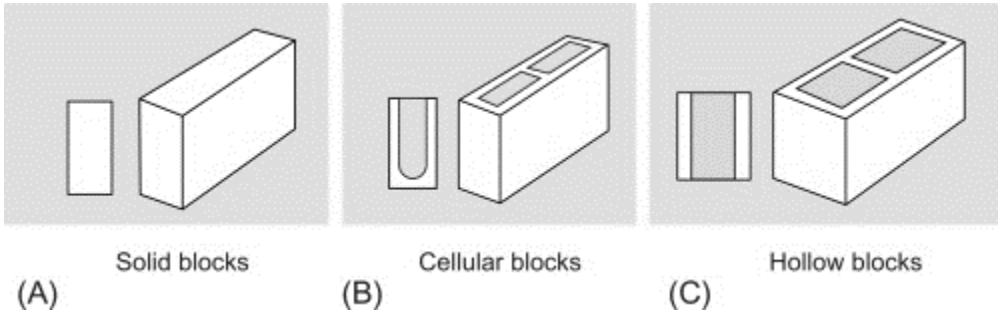

Figure 2-1 Types of blocks [10]

Masonry block unit divisions into dense or lightweight blocks are merely based on their densities [8]. Normal weight concrete has densities ranging from 2200 - 2300 kg/m^3 and compressive strengths ranging from 20 – 50 MPa [10]. Lightweight concretes are produced with lightweight aggregates. They can be further classified based on their use. Low-density LWC used for insulating purposes have compressive strengths ranging from 0.69 - 6.89 MPa. Moderate density LWC used as 'fill' concrete has compressive strengths ranging from 6.89 - 17.24 MPa, while high-density LWC for structural purposes has compressive strengths over 17.24 MPa [11], with densities ranging from 1400 – 1900 kg/m^3 [10].

2.1.1. **Masonry walls**

Masonry construction makes use of masonry units, mortar, grout, and reinforcements. The knowledge of the interaction of these materials in masonry assemblages and the factors affecting the physical, mechanical, or thermal properties of the composite is needed to understand the fundamental behavior of masonry. Concrete masonry blocks are manufactured from Portland cement, aggregate, and water. They can be used in the construction of loadbearing walls and non-loadbearing walls. A load-bearing wall is a type of construction where every wall element works together to carry the building load to the foundation and then transfer that weight to the soil. They are mainly used to construct

smaller residential buildings. Non-loadbearing walls, on the other hand, are not part of the structural frame system. They are mostly interior walls used as partitioning for high structures as they increase lateral stiffness. Both types of constructions involve the placement of a masonry unit as a layer, one at a time. The units are held together employing mortar, which imparts strength and stability to the whole unit.

2.2. Fire resistance

The fire-resistance rating is the time in minutes or hours that an element or assembly can resist fire or elevated temperatures. This concept applies to the elements of a structure and not the materials that make up the elements.

2.2.1. Assessment of fire resistance

In assessing fire resistance, three different approaches can be used: the full-scale fire test, prescriptive method, or performance-based method. The prescriptive method is based on generic codes. They are the cheapest to implement and are rigid compared to the performance-based method that allows for engineering thinking with its flexibility. The latter is based on engineering calculations. A full-scale fire resistance test, although expensive and time consuming, is the most common method of assessing fire resistance. However, as permitted by [12], calculations can now be substituted with full-scale tests to assess fire resistance.

2.2.2. **Fire standards**

Standards used for assessing fire resistance tests vary upon location, with their different requirements [4]. A few of them include ISO 834, CAN/ULC-S101, ASTM E119, BS 476 Parts 20-23. In Canada the CAN/ULC-S101 test, the standard methods of fire endurance tests of building construction and materials, is used. This test follows the standard time-temperature fire curve as shown in Figure 2-2. Although the standard fire curve does not directly depict a real fire, it can be used to test for the fire resistance of structural elements and create their standards for determining failure time or modes.

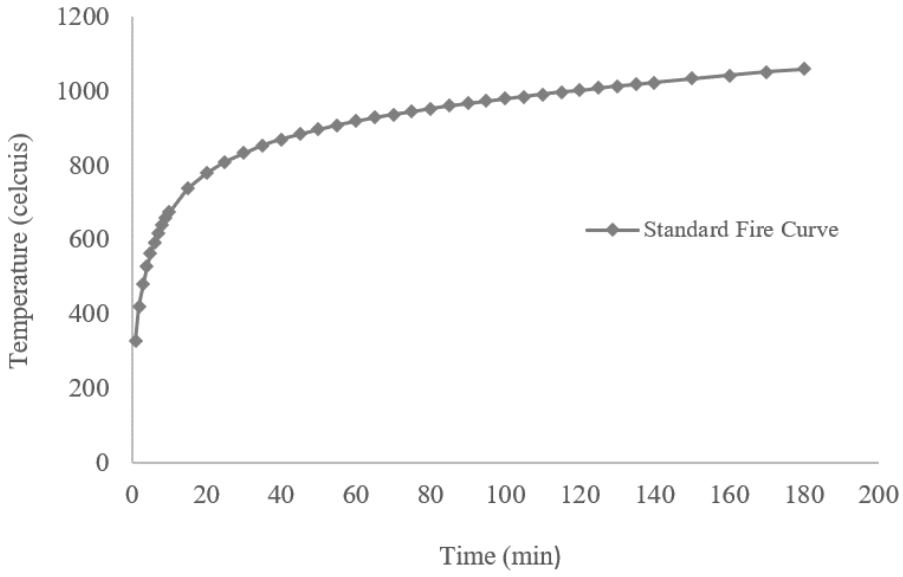

Figure 2-2 Time-temperature curve

2.2.3. **Failure criteria**

There are three (3) failure criteria for any fire resistance testing: insulation, stability, and integrity [4]. For a fire's duration, a structural element meets the stability criterion if it can perform its load-bearing functions without collapsing. It meets the integrity criterion if cracks allowing the passage of smoke or hot gases through the wall are not developed. Lastly, it meets the insulation criterion if the temperature on the unexposed face of the wall does not exceed an average temperature increase of 140°C or a maximum temperature increase of 180°C at a single thermocouple point. The failure criteria that govern is based on the structural element Table 2-1. Columns or beams are load-bearing structural elements and so they must meet the stability criterion to avoid a collapse of the entire structure when exposed to fire. On the other hand, load-bearing walls must be able to meet all three (3) criteria. The walls should be able to support the loads during a fire, remain uncracked and stay well below the insulation limits on the unexposed face of the wall.

Table 2-1 Failure criteria for structural elements (Modified from [4])

Building element	Stability	Integrity	Insulation
Partition		✓	✓
Load-bearing wall	✓	✓	✓
Floor/ceiling	✓	✓	✓
Beam	✓		
Columns	✓		

A few factors primarily control the fire resistance of a concrete masonry wall. They include cement type, aggregate type, thermal capacity, and thermal conductivity of the concrete [13]. These factors determine the extent of heat transfer through the concrete masonry, from the exposed face of the wall to the unexposed face.

2.3. Properties of masonry

The mechanical and thermal properties of masonry blocks or mortar largely influence the behavior of masonry walls in fire. It is important to study how these properties vary over a range of elevated temperatures, so as to determine appropriate changes that can be made in other to improve the fire resistance ratings of masonry.

2.3.1. Mechanical properties of concrete masonry at elevated temperatures

Although concrete has good fire resistance, its mechanical properties (density, compressive strength, and elasticity modulus) gradually decrease over time in a fire. This decrease in the mechanical properties is mainly due to the pore-structure coarsening of hardened cement paste (hcp) [14], crack formation, heating rate, maximum temperature, duration of the fire, the load applied during heating, water-cement ratio, aggregate type, etc. [13] [15].

2.3.1.1. Density of concrete masonry

Density values, regardless of the concrete type, vary according to the material's porosity, so that an increase in the porosity significantly reduces the density of the concrete. The density of concrete subjected to elevated temperatures reduces by 100 kg/m^3, after the evaporation of the free moisture in the concrete occurs [4]. However, this density reduction has an insignificant effect on the thermal behaviour of the masonry wall [4]. An experiment conducted on modified lightweight concrete, produced with different variations of glass and metakaolin revealed that as the temperature increased, there was a gradual decrease in the density from about 20 ºC. This behavior was tied to the pore water evaporation [16]. The aggregate type is another factor that affects the density at an elevated temperature. Depending on the type and temperature, aggregates degrade and begin to melt off.

Research conducted by Schnider [17] revealed that limestone, quartzite, and basalt concrete showed similar decreasing density trends in a fire until 800 ºC. At 800 ºC, there was a sudden drop in the density of limestone concrete. This phenomenon was linked to the decomposition of calcareous aggregates at 800 ºC [17].

2.3.1.2. Compressive strength of concrete masonry

The capacity of a structure to withstand its design loads without a reduction in its geometry is termed the compressive strength of that structure. The compressive strength of concrete masonry largely depends on the aggregate type. With their varying chemical compositions,

aggregates undergo degradation in a fire as the crack length and width increase, causing a reduction in the compressive strength of concrete. As illustrated in Figure 2-3, normal weight concrete begins to lose its strength at about 400 ºC, while lightweight concrete begins to lose theirs at 500 ºC. This gradual strength reduction continues till about 900 ºC for NWC and 1000 ºC for LWC, beyond which they both would have lost all of their strengths [4]. The density of LWC is generally much lower than that of NWC and has a much lower strength than the former at ambient temperature. However, at elevated temperatures, the LWC loss in compressive strength is much slower than NWC [4]. Researchers attributed the decrease in compressive strength of NWC to be as a result of the loss of water on the surface of concrete and the capillary water between 100 ºC and 300 ºC [15] [18], formation of hardened cement paste (hcp) below 600 ºC [14], further resulting in crack development and ruptures.

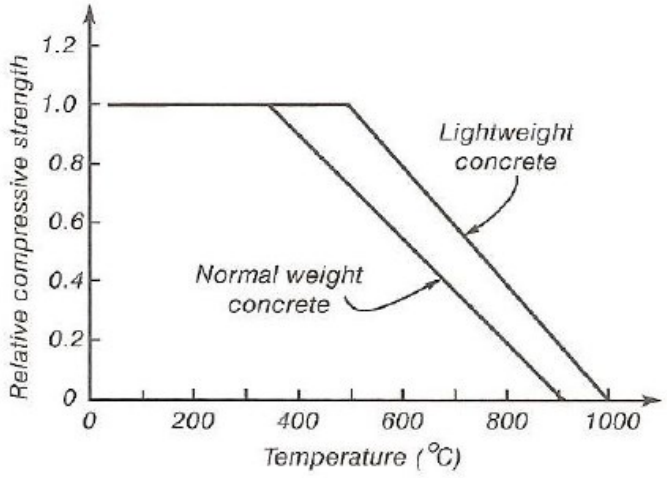

Figure 2-3 Compressive strength comparison of NWC and LWC [4]

Jonaitis et al. [19] investigated the effects of elevated temperatures and long-term loading on the compressive strength of normal-weight concrete. Some of the NWC specimens were tested at 72 days, and others at 400 days. The results indicated that the age of concrete had negligible effects on the compressive strength of concrete at elevated temperatures. Specimens that were preloaded before heating decreased faster in their compressive strength than those loaded after heating. This behavior could be associated with the compressive effect of the load on the structure, and crack formed at elevated temperatures [20]. Concrete experiences a significant loss of strength after exposure to temperatures between 250 - 300 ^{o}C. Its strength reduces rapidly between 300 ^{o}C - 500 ^{o}C, and in excess of 600 ^{o}C, it loses its structural capacity [21].

2.3.1.3. Modulus of elasticity of concrete masonry

Modulus of elasticity measures the resistance of an object to being deformed elastically when stress is applied to it; thus, a stiffer material will have a higher elastic modulus. Similar to the concretes compressive strength trend in a fire, the modulus of elasticity also decreases as the temperature increase. This is due to the aggregate degradation; thus, making concrete masonry more brittle. Conclusions can then be made that the aggregate type is also a significant factor to be considered. Granite which has a high bond strength with cement has a much slower rate of reduction of modulus of elasticity at elevated

temperatures [23]. The experimental investigation carried out by Jonaitis et al. [19], revealed that like the compressive strength of concrete, the elasticity modulus of concrete does not depend on exposure to elevated temperatures alone but also on the long-term loading. Schnider [17] stated that the cement type is not a significant factor that could affect the modulus of concrete elasticity. A list of factors and how they affect the modulus of elasticity of concrete in elevated temperatures are summarized in Table 2-2 [17].

Lightweight concrete was found to have a stiffness 20 – 30 % less than normal-weight concrete [17] [24]. Research carried out on lightweight concrete showed that there was a drastic reduction in the concretes stiffness between 0 – 200 ºC and a moderate reduction between 400 ºC and 600 ºC [8], Figure 2-4.

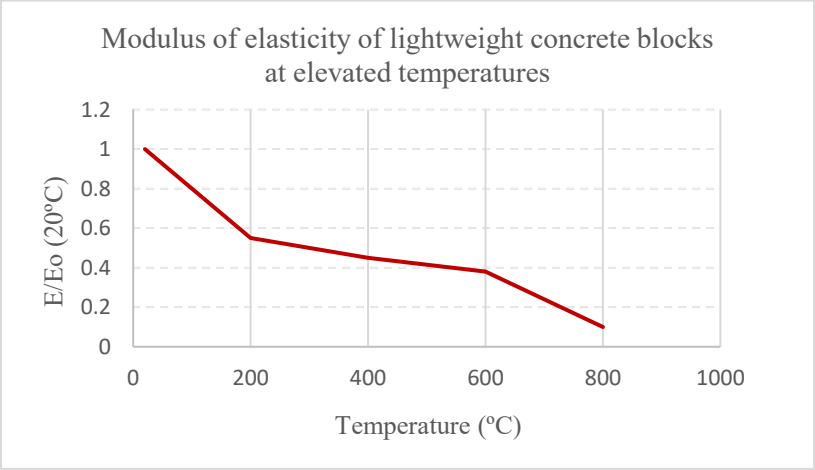

Figure 2-4 Reduced moduli of elasticity of LW concrete blocks at thermal conditions [8].

Table 2-2 Factors affecting the modulus of elasticity [17]

Type	Effect		
	Strong	Medium	Weak
Class of strength	-	-	*
w/c ratio	-	-	*
Aggregate	***	-	-
Type of cement	-	**	-
Agg. /cement ratio	-	**	-
Max. Agg.	-	-	*
Load level	***	-	-
Heating rate	-	-	*
Evaporation rate	***	-	-
Age of concrete	-	-	*
Type of curing	-	**	-
Sealing	***	-	-

2.3.2. **Thermal properties of concrete masonry at elevated temperatures**

The thermal properties of concrete masonry are the thermal conductivity, and specific heat. These time dependant properties of concrete largely depend on the moisture content and the entrapped air in the concrete. Hence, these properties are highly influenced by the heat transfer and moisture processes as they change the temperature and water distributions within the concrete mass with time.

2.3.2.1. Thermal conductivity of concrete masonry

Thermal conductivity is a measure of a material's capacity to conduct heat. This property is associated with the internal structure of the material, most influencing the temperature gradient of the concrete in a fire. The thermal conductivity of concrete can be kept low by

entrainment of air in the concrete or the use of lightweight aggregates in the mix. Hence, lightweight concrete is expected to have lower thermal conductivity values than normal-weight concrete [18]. An increase in the porosity of concretes structure due to the losses in pore water or dehydration of the cement paste leads to a decrease in the thermal conductivity of concrete. The pores produced on the concretes surface act as an insulating layer, reducing the rate of heat transfer through the concrete [13]. The variation of thermal conductivity for normal weight and lightweight concrete is illustrated in Figure 2-5 [25]. EN 1994-1-2 specified lower and upper limit conductivity values for NWC. The thermal conductivity of normal weight concrete at the upper limit is 2 W/m.K at ambient temperature and decreases gradually as the temperature increases until about 1000ºC, after which there is insignificant change in the property. Lightweight concrete, on the other hand, has a value of 1 W/m.K at ambient temperature. It has a similar decreasing trend like NWC until about 800 ºC, where it reaches a plateau, and there is no further change with temperature increase. Once evaporation occurs, the conductivity values drop and continue to decrease as temperature increases. This trend is also similar to the specific heat behaviors [16].

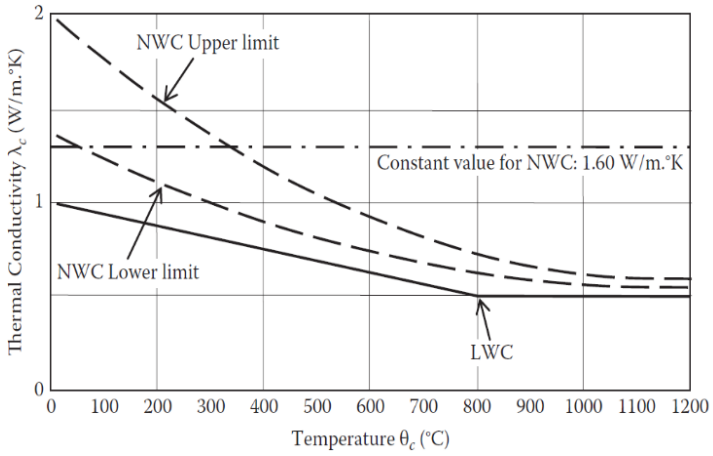

Figure 2-5 Thermal conductivity of normal weight concrete (NWC) and lightweight concrete (LWC) as a function of the temperature according to EN 1994-1-2 [25].

2.3.2.2. Specific heat capacity of concrete masonry

Gani [13] established that the heat capacity of concrete is mainly controlled by the heat capacity of the materials used in the manufacture of the concrete. The variation of the specific heat with temperature is illustrated below in Figure 2-6. Normal weight concrete made with normal-weight aggregates (siliceous and calcareous) increase in specific heat as the temperature increases whereas, lightweight concrete made from lightweight aggregates remains constant even with an increase in temperature. At 100 ºC, there is a spike in the specific heat value. This spike occurs because more energy is needed for evaporation of the pore water to occur. The intensity of the spike largely depends on the amount of moisture content in the concrete. Around 100 - 200 ºC, the specific heat of concrete with 0 % moisture content is around 950 J/Kg.K – 1050 J/Kg.K, and the specific heat of water is

4,185.5 J/Kg.K. To adequately take the effect of the spike in specific heat into consideration, the specific heat of water would need to be distributed between a range of temperatures to increase the energy needed for evaporation to occur [4].

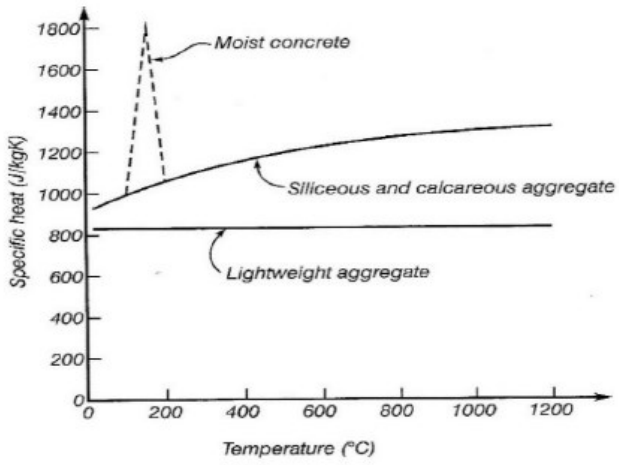

Figure 2-6 Specific heat of normal weight concrete (NWC) and lightweight concrete (LWC) as a function of the temperature [4].

Experimental research carried out on the comparison between modified lightweight concrete, and lightweight concrete reveal that modified lightweight concrete exhibit a much greater increase in specific heat at about 100 °C because they contain more evaporable moisture than lightweight concrete and hence require more time and energy to dry out Figure 2-7 [16]. The trend of modified lightweight concrete after all of the evaporable water has dried out shows better thermal properties than conventional lightweight.

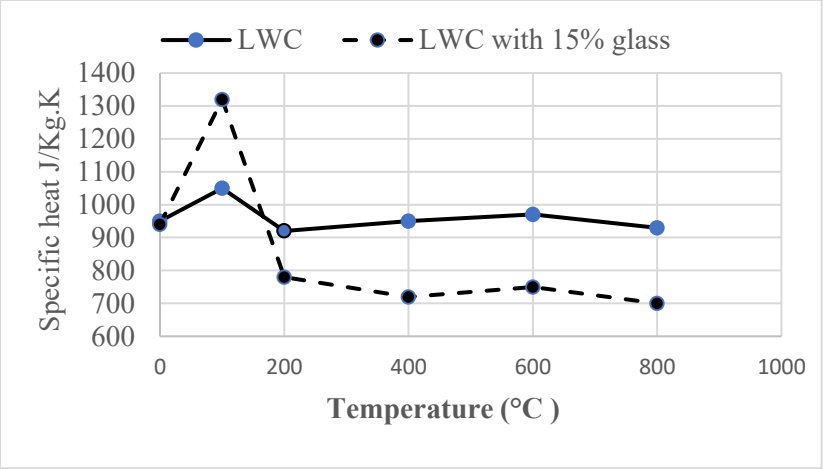

Figure 2-7 Specific heat values of LWC and modified LWC [16].

2.3.2.3. Thermal expansion of concrete masonry

Expansion occurs in materials exposed to high temperatures. The expansion coefficient is associated with the water in the material [18]. It is not very important to consider this property in fire designs; however, when the concrete masonry is restrained, then it should be considered [4]. This is because compressive stresses arise if the frames are ridged enough. At 575 ºC, siliceous aggregates undergo a quartz phase change resulting in its thermal expansion in concrete [26]. An experimental investigation carried out on concrete by Schneider [17] indicates that between 600 – 800 ºC, there is little or no thermal expansion in concrete, but rather, shrinkage occurring due to the chemical and physical reactions in the aggregates.

2.3.2.4. Emissivity of concrete masonry

The emissivity of the surface of a material is its effectiveness in emitting energy relative to a black body whose emissivity is 1. A material's ability to emit energy is directly dependent on the temperature of the material. As emissivity increases, the temperature of the material also increases [27]. The emissivity value of concrete is a parameter not clearly defined; however, Mikron [28] suggested 0.94, and EN 1992-1-2 [29] considers 0.7, Qin et al. [30] suggest values between 0.9-0.94, and MPA [31] suggested 0.85 – 0.95.

2.3.2.5. Moisture content

The presence of moisture during heating has vast effects on the outcome of the test and so should be taken into consideration. The moisture contained in concrete masonry is free evaporable and chemically bound water. Moisture begins to evaporate between 20 – 100 ^{o}C, thereby causing internal vapor pressure build-up [13]. High porosity, however, increases the water retention capacity of a structure. An increase in the pores moisture increases the thermal conductivity of the concrete [17] [18]. With an increase in moisture content, there is an increase in the evaporable water [32]. Lightweight aggregates act like water reservoirs for the evaporable water, making lightweight aggregate concrete (LWAC) behave worse in a fire than normal-weight concrete; thus, resulting in cracks. Lightweight aggregate impregnation is therefore recommended [33]. This procedure from past research

has been confirmed to improve the water tightness, strength recovery, and sorption properties of the aggregates. The sodium silicate deposits reduce water retention by capillary suction [33]. Moisture content is a major factor that affects spalling in concrete [33]. Determining the actual moisture in concrete is difficult. Several authors have tried to recommend the maximum allowable moisture content in hardened concrete to avoid spalling. The Eurocode [34] recommended 4% of the concretes weight for NWC and 5% for LWC.

2.3.3. **Mortar**

Mortar is a mix of cement, fine aggregates, and water. It is used to provide a bond between individual masonry blocks. The assemblage is built to withstand the imposed conditions of loads and weather. Hardened mortar is intended to provide strength, durability, and weather-tightness. Concrete mortar, in conjunction with air cells, contributes to the general thermal resistance of masonry units at elevated temperatures [35]. However, mortars are the weakest link in any masonry assembly, particularly, the bed joints [36].

2.3.3.1. Types of mortar used in masonry wall construction

There are several types of mortars with their recommended usages [5]. They include:

a) Type S mortar – this is an all-purpose mortar. It can also be used particularly for structural applications like loadbearing walls.

b) Type M mortar – this is used when a high compressive strength is a priority.

c) Type N mortar – this is intended for non-loadbearing applications and is used when a moderate compressive strength is required.

d) Type O mortar – this is used when low compressive strength is required. It is not recommended for use in severe exposure conditions.

e) Type K mortar – this is used when low compressive strength is required in areas where the moisture content is low.

2.3.3.2. Types of mortar joints for masonry wall construction

Various types of mortar joints can be used on masonry, depending on the desired objectives. The use of a particular mortar joint will largely depend on its aesthetics or its water penetration disabilities. These mortar joints are illustrated in Figure 2-8 [37]. For high resistance to rainwater penetration, a concave mortar joint is recommended. With Vee mortar joints, there is no form of water penetration or accumulation due to their geometry. For masonry blocks that require final finishes like plastering, etc., the flush mortar joint is recommended. Raked mortar joints are usually not recommended for exterior walls because of their geometry, which can accumulate water. Joints formed by placing the mortar in excess in between the blocks/bricks are called extruded mortar joints. Degradation may occur in the joints with varying weather exposure. Beaded mortar joints

are also not recommended for external use because of their exposed ledges. Like the raked mortar joints, the struck mortar joints are not recommended for use on exterior walls as they could result in water seepage issues. Weathered mortar joints are horizontal joints that permit watershed.

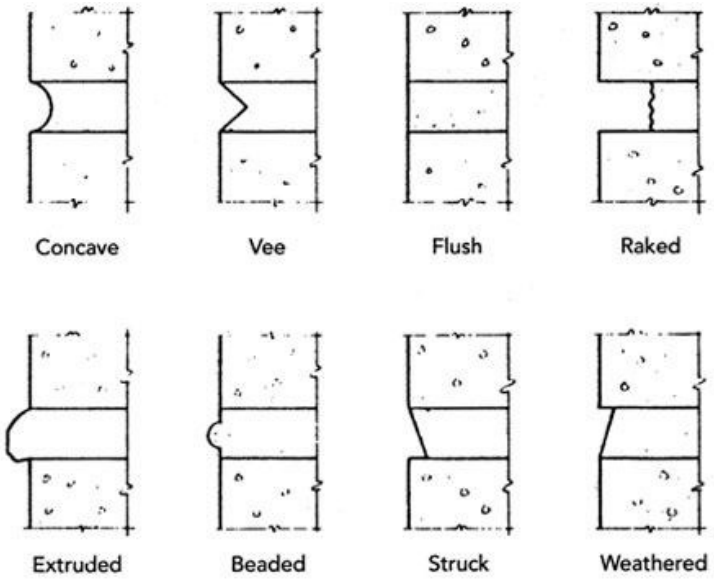

Figure 2-8 Types of mortar joints [5]

At elevated temperatures, mortar joints are the weaker link in any masonry assembly when moisture losses occur, and cracks form, particularly, bed joints [36]. The joints become a source of discontinuity in the insulation layer, thereby reducing the fire resistance of the wall and encouraging thermal bridging [38]. With thermal bridges, areas with the least thermal resistance for heat transfer is formed. However, from the research conducted by

Keelson et al. [39], the type of joint profile used in any concrete masonry construction has negligible effects on the fire-resisting property of the wall.

2.3.4. Mechanical & thermal properties of mortar at elevated temperatures

The following section discusses both the mechanical and thermal properties of mortar at elevated temperatures. It is important to see how these properties are affected at elevated temperatures.

2.3.4.1. Compressive strength of mortar

Like with cement, the compressive strength of mortar decreases when exposed to elevated temperatures. The compressive strength of two (2) specimens of cement mortar were investigated at room and elevated temperatures according to ASTM C39 [40]. Specimen G5 had the fine sand replaced by graphite powder, while specimen G0 had no graphite content. At an 8 °C/min heating rate and an exposure time of 1 h, specimen G0 had lost about 12% of its initial strength at 300 °C while specimen G5 retained all of its compressive strength. However, their compressive strength both dropped abruptly after 300 °C to about 50% of their initial compressive strengths Figure 2-10. Cülfik et al. [40] suggested that the decrease in strength of G0 may have been a result of calcium leaching or crack formations due to the differences in the thermal properties of the fine sand and cement. At 900 °C, G0 had completely disintegrated. In another experiment, the replacement of OPC (ordinary

Portland cement) with metakaolin (MK) and silica fume (SF) up to 20% in a mortar mix proved to perform better at elevated temperatures due to the pozzolanic activity resulting from their large surface areas [41]. The replacements act as void fillers in the hardened mortar, thereby increasing the mortar density and strength [42]. Across all samples presented in Figure 2-9, the initial increase in the strengths up to 200 °C is due to the hydration of the unhydrated particles, and the decrease after is as a result of the dehydration of the already hydrated particles.

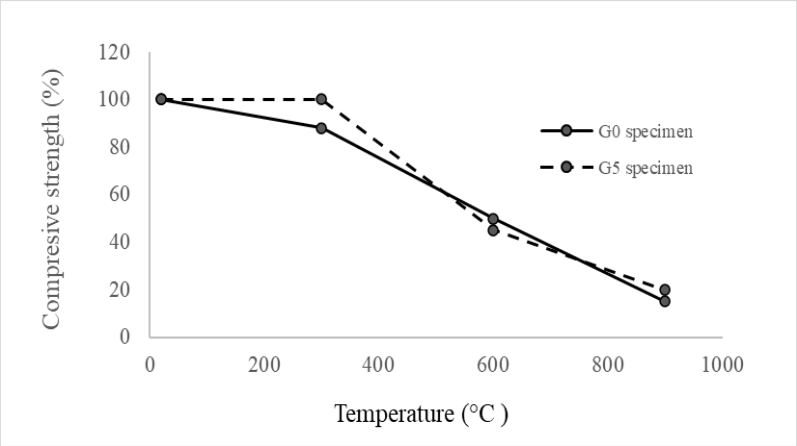

Figure 2-9 Compressive strengths of G0 and G5 mortar specimens at Tmax = 1 h and R = 2 C/min [40].

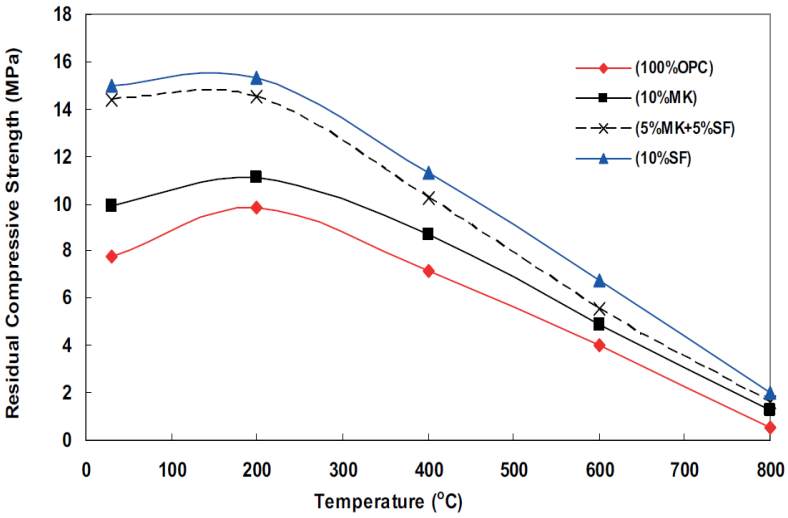

Figure 2-10 Compressive strength of mortar produced with replacements and OPC [41].

2.3.4.2. Modulus of elasticity

At elevated temperatures, the modulus of elasticity showed a considerable decrease. Tests conducted by Cülfik et al. [40] revealed that the trends were like those of the compressive strength for both G0 & G5 specimens, although more severe. The heating rate determined the level of strength losses in the mortar. Fast heated mortar showed better results than slow heater mortar. At 300 °C, the loss in the modulus of elasticity was over 44% of the initial value for both specimens. At 600 °C, the loss was over 20% of the initial value, and at 900 °C, it was impossible to measure their modulus of elasticity because both specimens had lost so much of their strength [40].

2.3.4.3. Thermal conductivity of mortar

According to an investigation carried out by a group of researchers [43], four (4) different cement mortar specimens (NL, TL, ML, MTL) were tested at different pre-treatment conditions. The NL specimen was unloaded and tested at the room temperature state. The TL specimen was also previously unloaded but was gradually exposed to an increasing temperature up to 800 °C for 2 h. ML specimen was preloaded with a design load of about 90% of its compressive strength. The MTL specimen combined both TL & ML, with further pre-treatment exposure to 800 °C for 2 h. The results from the high-temperature exposure tests indicate that TL samples achieved the highest conductivity values, followed by the MTL samples. NL & ML samples exhibited the lowest values, as illustrated in Figure 2-11 [43]. Thermal conductivity is affected by the hydration of cement. This endothermic factor can consume heat during a reaction, thereby decreasing the thermal conductivity values. The resulting pores formed also have the capacity to decrease thermal conductivity values. However, the pores formed may be accompanied by cracks, which could increase the radiative heat transfer and increase the thermal conductivity values. Černý et al. [43] stated that the effects of wide cracks due to thermal load were the leading cause of the high-temperature thermal conductivity values.

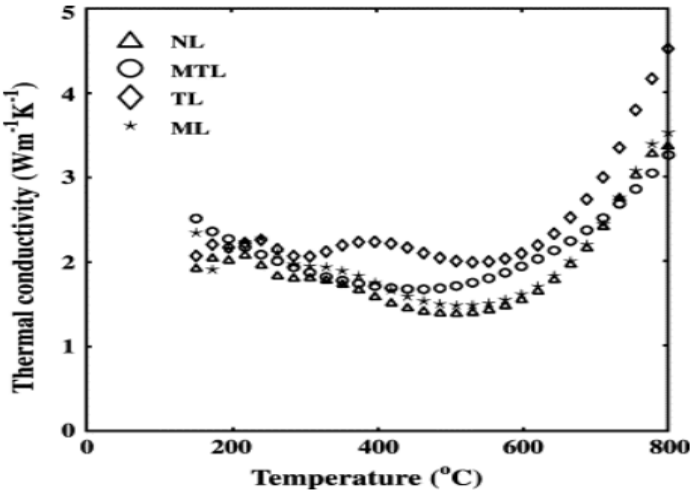

Figure 2-11 High-temperature values of the thermal conductivity of cement mortar for various types of previous loadings [43].

2.3.4.4. Specific heat capacity of mortar

Specific heat capacity tests carried out showed that there is a rapid increase in the property between 25 – 600 °C, and a decrease after [44] [45] Figure 2-12. The specific heat of mortar largely depends on the aggregate type. With a cement to sand ratio of 1:3, the increase in the specific heat capacity of mortar at elevated temperatures is attributed to the siliceous aggregates, which have a value of 730 J/Kg.K at 25 °C. On the other hand, the decrease of the specific heat capacity of mortar after 600 °C is attributed to the α → β transition of the siliceous aggregates at 573 °C, which has a specific heat capacity of 1125 J/Kg.K.

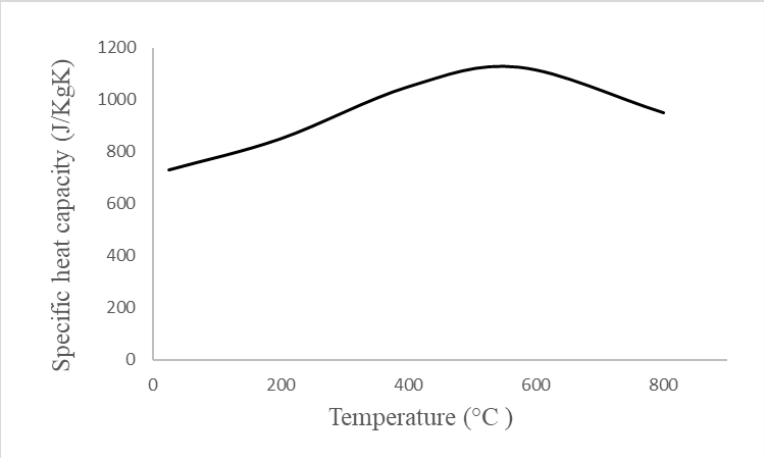

Figure 2-12 Specific heat capacity of studied cementitious composites [44].

2.3.4.5. Thermal expansion of mortar

Like concrete, the thermal expansion also occurs in the mortar at elevated temperatures. However, at a much lower rate. The shrinkage and moisture loss that occurs at elevated temperatures cause cracks to form. These cracks reduce the bond strength between the concrete masonry block and the mortar, making the mortar the weaker link [5].

2.4. Heat transfer in masonry walls

Heat is transferred in masonry blocks through conduction, convection, and radiation Figure 2-13. The hot gases from the flames are transmitted to the exposed side of the masonry block via convection and radiation, through the solid areas via conduction, through the cells via radiation, and further out to the environment via radiation and convection.

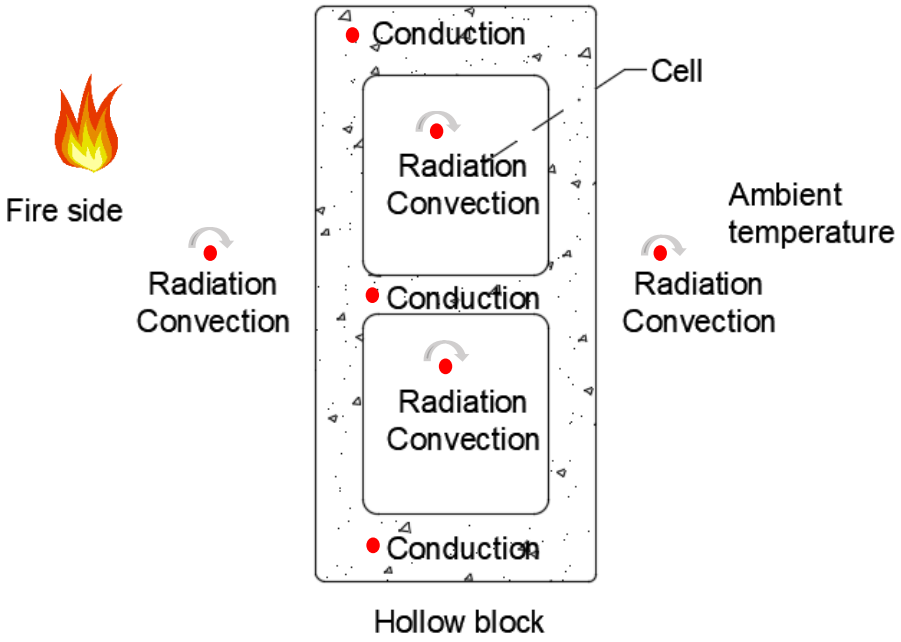

Figure 2-13 Heat transfer process through masonry block.

The equation that governs conduction is given as:

$$\frac{\partial}{\partial x}\left(k\frac{\partial T}{\partial x}\right)+\frac{\partial}{\partial y}\left(k\frac{\partial T}{\partial y}\right)+\frac{\partial}{\partial z}\left(k\frac{\partial T}{\partial z}\right)+q_v=\rho C_p\frac{\partial T}{\partial t} \qquad \text{Equation 2-1}$$

In Equation 2-1 [4], k = thermal conductivity [$W.m^{-1}.k^{-1}$], q_v = heat generation rate [$W.m^{-3}$], ρ = density [$kg.m^3$], C_p = specific heat capacity [$J.kg^{-1}.k^{-1}$], T = temperature [k], t is the time [h].

The equation that governs convection is given as:

$$Q = -hA\Delta T \qquad \text{Equation 2-2}$$

In Equation 2-2 [4], Q =heat transferred per unit time, h =convective heat coefficient [$W.m^{-2}k^{-1}$], ΔT is the temperature difference between the surface of the solid and the fluid [k], A is the area of the object [m^2].

The equation that governs radiation is given as:

$$Q = \int_A \sigma F_e F_a \{T_1^4 - T_2^4\}\, dA \qquad \text{Equation 2-3}$$

In Equation 2-3 [4], Q is the heat transferred from surface 1 to surface 2, σ is the Stefan-Boltzmann constant ($5.67 \times 10\text{-}8\ W/m^{-2}K^{-4}$), T is the temperature [K], F is the view factor.

The flow of hot gases through the blocks cells largely depends on the cell aspect ratio [46]. The-Duong et al. [47] in their research, concluded that convection and radiation are the main modes of heat transfer through a masonry wall because the horizontal partitions of the wall where conduction is the predominant mode of heat transfer had lesser temperature values than the vertical partitions as illustrated in Figure 2-14. The time required for heat transfer to occur through the wall depends on the geometry of the block, moisture content in the wall, and wall thickness.

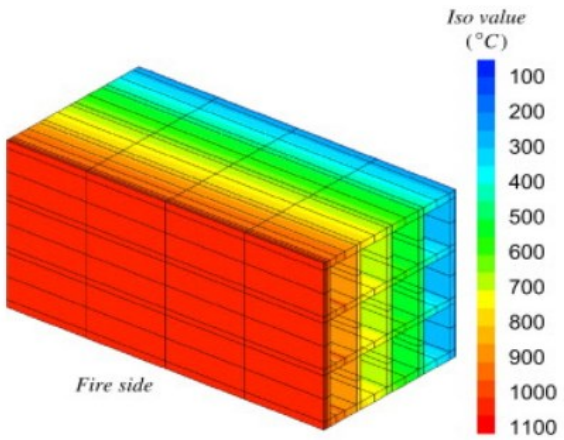

Figure 2-14 Heat movement through a concrete block [47].

As a result of the convective and radiative heat, the hollow cells heat up faster than the solid areas (webs) of the block or the mortar. Research conducted on the rate of heat transfer to the unexposed face of the wall showed that the temperature at the hollow cells, solid webs and mortar increased at similar rates at the start of the test. The mortar soon became the hottest section, after which it began to plateau for some time at 100 ºC Figure 2-15. While this plateau period occurred, the hollow cells and solid webs continued to heat up at a slightly higher rate. During the plateau period, evaporation of the free and chemically bound moisture occurred. This process caused the mortar to cool for some time while the other areas continued to heat up. It can then be concluded that the temperature profile of the unexposed side of the wall differs from point to point according to the amount of moisture contained in that region [48]. The amount of moisture determines the length of

the plateau. Conclusions can then be drawn that the mortar had the greatest amount of moisture, followed by the solid webs and then the hollow cells.

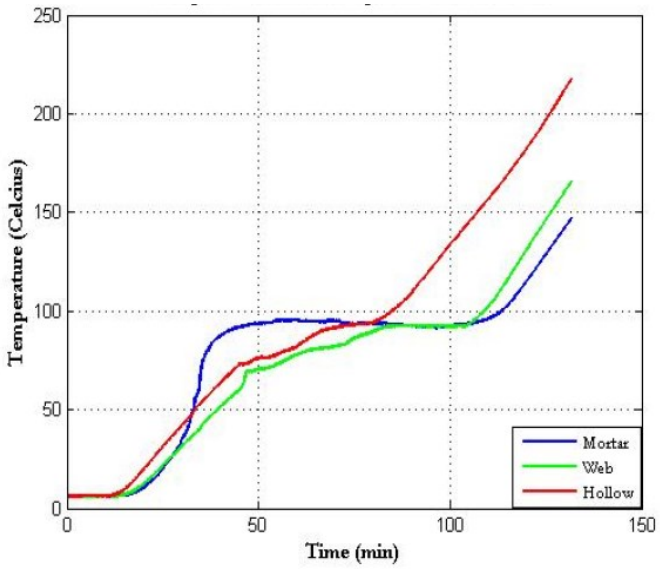

Figure 2-15 Temperature profile on the unexposed side of the wall [48].

In the case of a finite element analysis, researchers have tried to investigate the heat transfer through a masonry block using a one – dimensional model. Sala et al. [49] went on to conclude in their research that there are likely chances of attaining an error using a one-dimensional model. Most researchers have gone on to use two – dimensional and three – dimensional models that are more accurate in giving relatively close experimental results with little or no errors. Nagy [50] went on to conduct a comparison between a 1-D model and a 3-D model. The 1-D model showed a linear graph because it did not consider the varying geometry of a masonry block.

2.5. Problems associated with masonry walls exposed to elevated temperatures

Both the thermal and mechanical properties of concrete determine the influence of fire or elevated temperatures on concrete masonry. Concrete exposed to fire can experience damage like thermal bowing, spalling of various degrees, chemical transformations, or colour change.

2.5.1. Thermal bowing

When masonry wall is exposed to elevated temperatures, a temperature difference arises across the walls thickness. If unrestrained, expansion occurs on the exposed side of the wall, resulting in thermal bowing. The temperature distribution is curvilinear so that it is steeper on the exposed face of the wall as illustrated in Figure 2-16. With time, the bowed wall can recover because the unexposed side of the wall can heat up enough to close the temperature gap [47]. Further investigations conducted confirmed that a more severe heating rate affects the level or extent of deflection [51]. Thermal bowing can occur on loaded or unloaded walls. The tendency for a wall to collapse from thermal bowing is more severe in loaded walls than in unloaded walls. As the deflection towards the fire increases, the vertical loads shift from the center of the wall towards the fire, eventually aiding in the walls collapse [52].

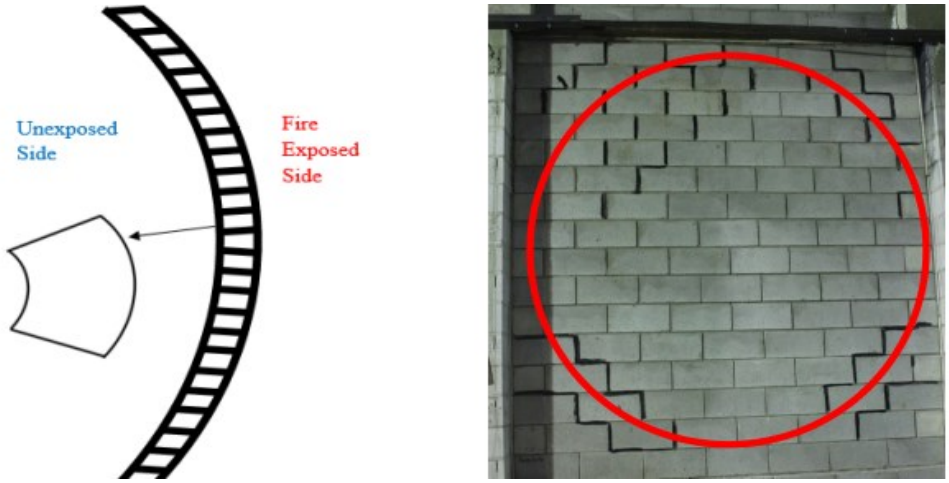

Figure 2-16 Thermal bowing of concrete masonry wall [48].

2.5.2. **Spalling**

The breakage of fragments of concrete, bricks, or blocks, when exposed to elevated temperatures or fire, is referred to as spalling [8]. There are different stages/types of spalling: aggregate spalling, corner spalling, and explosive spalling. Explosive spalling is the most extreme type of spalling that could affect the structure's stability. Several tests confirm that reduced moisture content reduces the chances of spalling occurring. According to [20] [53], spalling can occur due to high thermal stresses greater than the concretes tensile strength or due to high pore pressures in concrete caused by temperature difference within a block. When concrete is exposed to elevated temperatures, it expands. The heat penetrates deeper into the concrete, thereby heating the inner pores. The pressures in these pores increase even more due to the high saturation and temperature. With

continuous heating, moisture moves from the high-pressure areas to the low-pressure areas, Figure 2-17. Spalling occurs in the concrete when this moisture cannot be transported easily. The level of damage and spalling depends on the moisture content in the concrete, the porosity, the permeability, the stress conditions, the heating rate, aggregate type, the dimensions of the element, the rate of the temperature rise, and the strength of the concrete [20] [53] [54]. Lower heating rates have fewer effects on explosive spalling [55].

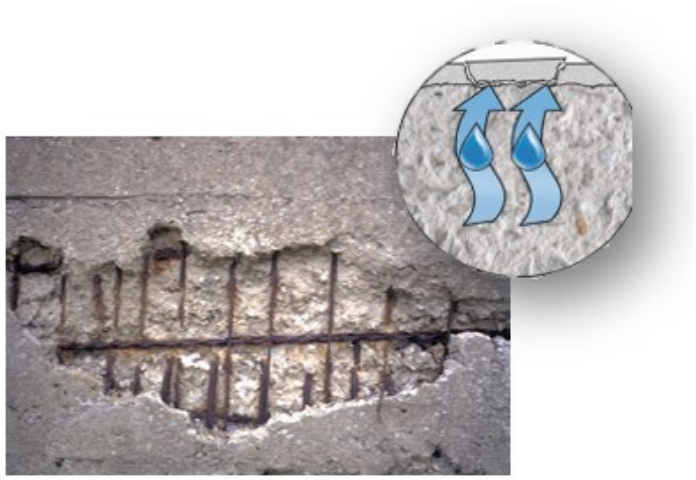

Figure 2-17 Mechanism of spalling due to moisture penetration [56]

Due to their high density and low permeability, NWC is more susceptible to explosive spalling than LWC. Often, the spalling resistance of LWC behaves worse than that of NWC in fire because of the ability of the lightweight aggregates to carry more evaporable water in their voids. Further experiments were conducted to compare the spalling results of NWC and modified lightweight concrete. The results indicated that spalling did not occur at

temperatures below 400ºC across all samples [57]. Spalling was less serious in the modified lightweight concrete because of reduced water retention and absorption capacity of the lightweight aggregates during heating. Another reason is because parts of the modified material melted below 400 ºC forming microcracks and connecting pores to provide a channel for the flowing water.

Sullivan et Zaman [54] experimented on NWC of different geometries (large and small), cured for different periods under varying heating rates. The experiment indicated that water loss from the concrete occurred at two points, 110 ºCand again at 180 ºC Figure 2-18. Only large specimens spalled, and they did so around the second moisture loss period, 180 ºC. Faris et al. [55] concluded that NWC spalls within the first 45miins of heating and that the design loads of up to 60% on the concrete have no significant effect on spalling at low or high heating rates. To reduce the effect of spalling, polypropylene fibers were added to the concrete mix. These fibers melted and relieved the pressure in the concrete by aiding the escape of the high vapor pressure. This reduced the degree of spalling from 22% to less than 1%.

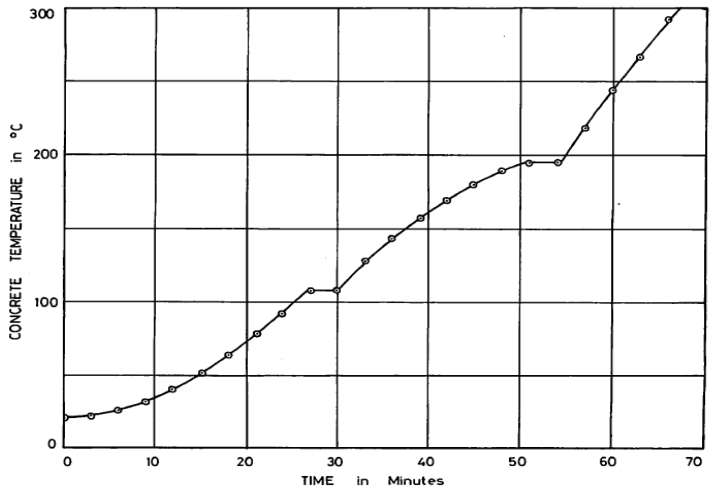

Figure 2-18 Time-temperature curve of specimens [54].

2.5.3. **Chemical transformation of cement stone and aggregates**

An overview of the chemical transformations of cement stone and aggregates at elevated temperature is summarized in Figure 2-19. At about 100 °C, evaporation of free water first takes place. At temperatures up to 300 °C, the aggregates expand while the cement paste contracts. This phenomenon results in cracks in concrete masonry due to the thermal property mismatch of both the cement paste and aggregates. At 400 °C, there is loss of water from the cement slurry resulting in the breakdown of $Ca(OH)_2$ into CaO and H_2O. At 575 °C, the siliceous aggregates undergo a quartz phase change resulting in its expansion. Above 700 °C, the limestone ($CaCO_3$) is broken down into CaO and CO_2. This chemical reaction is called “decarbonization”. Concrete left to cool down after being

exposed to temperatures over 700 °C form calcium hydroxide. At extremely high temperatures, say 1100 °C, the cement stones begin to melt off [26].

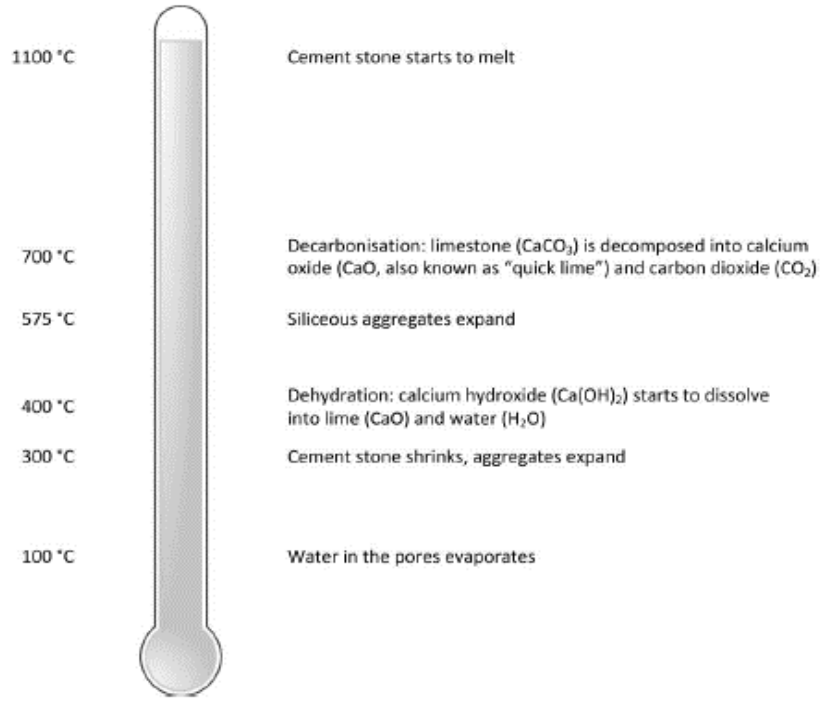

Figure 2-19 Overview of the chemical transformations of cement stone and aggregates [26].

2.5.4. **Colour change**

The color change in concrete is a result of exposure to high temperatures. This change largely depends on the aggregate type and is more pronounced in siliceous aggregates than in others. When siliceous aggregates begin to turn red at high temperatures, it indicates the temperature the concrete has reached. This color change usually occurs at 300 °C [21].

2.6. Insulation materials

The use of building insulation materials in construction has become increasingly popular over the years, in an attempt to improve the thermal behaviour of buildings. These insulating materials have a low thermal conductivity, poor conductors of heat, are lightweight and are able to form the thermal envelope of buildings. There are three (3) main sources of insulation materials: natural vegetation (cork, straw, wood, and cellulose fibre); renewable/petroleum materials (polystyrene); and natural minerals (perlite, vermiculite, aerated concrete) [58].

There are different factors that should be considered when deciding on the type or quantity of an insulation material to be used on a structure; thermal conductivity, sensitivity to moisture, durability, flammability, toxicity, impact on the environment, ease of installation, cost, etc. [59]. Insulation materials can be classified in many different ways, some of which are highlighted in the sections below.

2.6.1. Composition classification

Insulation materials can also be classified based on their compositions as organic, inorganic [60]. Organic insulation materials can be sourced from renewable/petroleum materials and natural vegetation. Examples of organic insulations are expanded polystyrene, extruded polystyrene, polyurethane, phenolic foam, polyisocyanurate foam, cellulose, wood fibre

board, flax wool, sheep wool, etc. while inorganic insulation materials can be sourced from non-renewable materials. Examples are mineral wool (glass wool and rock wool), cellular glass, ceramic fibres, aerogel, vacuum insulted panels, slag wool, stone wool, foamy glass, aerated concrete, perlite, vermiculite, gypsum, foamed concrete etc. [61]. Organic insulations have become attractive over the years because they are environmentally friendly, non-toxic, recyclable, renewable and a lesser amount of energy is required in their production. In producing organic insulation materials, temperatures below 200 °C are required, but in producing inorganic insulation materials, temperatures over 1000 °C is required [62]. Organic insulation materials also have better thermal insulating properties when compared with inorganic insulation materials. They also have a much lesser density compared to inorganic insulation materials. This may not always be desirable, but the thickness needs to be increased to match a certain level of thermal insulation.

Regardless of the advantages of organic insulation materials, they are highly flammable, and so for this reason they are not preferred in construction [62]. In regard to improving the energy efficiency of a building, organic insulation materials can be used but with regards to fire, organic insulation materials are not the best as they are not good flame retarders and generally would result in flame spread. There are also risks of emissions and diffusion of toxic gases during combustion. Very few research has taken into account the

fire hazards of organic insulation materials. Research done are always in relation to the energy efficiency. Inorganic insulation materials are able to resist moisture and fire better and so for this reason, they are preferred as a passive fire protection [61].

2.6.2. **Heat exchange classification**

Insulation materials can be categorized according to their heat exchange capacity as mass insulations or reflective insulations. Mass insulations are able to reduce the rate of heat transfer by conduction, especially in areas where heat transfer by convection or radiation does not occur. With their thermal mass, they are able to absorb heat and slow down the rate at which the retained heat is transferred to the cooler side. We can therefore conclude that the thickness of the mass insulation is of utmost importance as this determines its effectiveness in retarding the heat transfer. With an increase in thickness, the thermal performance of the mass insulation is improved and vice versa [61]. According to Victoria [63], the insulation capacity of mass insulations is as a result of the tiny pockets of trapped air contained in the material as shown in Figure 2-20a. As a result, when mass insulations are compressed, they lose their heat retarding property.

Reflective insulation has similar principles to mass insultations but in this case, they work to reduce the heat transfer by radiation to the cooler side by reflecting back a greater portion of heat while only radiating a small amount of heat as shown in Figure 2-20b. Emissivity is a major factor to be considered when dealing with radiation. This factor determines how much heat would be radiated. With a high emissivity, a high amount of heat would be radiated [61].

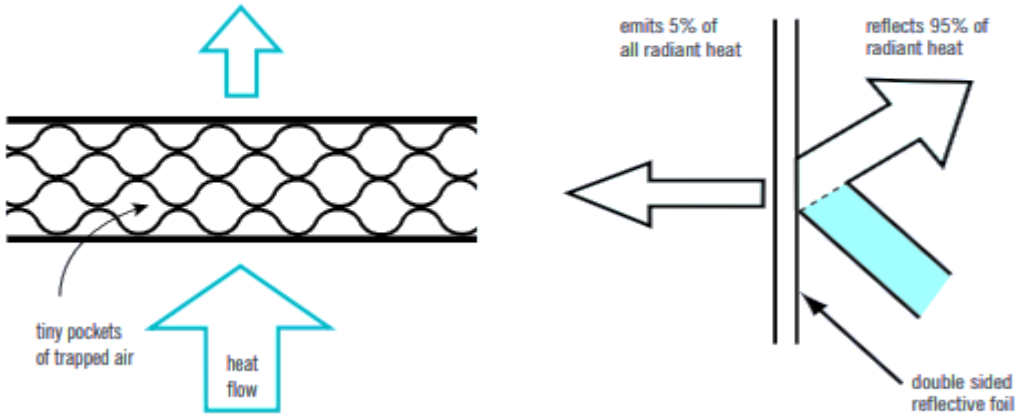

a. b.

Figure 2-20: Insulation classifications; a) Mass insulation, b) Reflective insulation [61].

2.7. Methods of Improving Fire Resistance

Past studies have shown that the convection currents in the cells of hollow concrete masonry blocks contribute significantly to the rate of heat transfer and thus, cannot be ignored. As a result, there is a need to further improve the thermal capacity of the block by any means possible. This can be achieved by increasing the number of cells in the direction perpendicular to the heat flow, using lightweight aggregates, modified lightweight

aggregates, or using insulating materials as inserts. They will be discussed further in this section.

2.7.1. **Insulation materials as filler - Introduction**

Nowadays, the convectional masonry wall requires additional thermal insulation to increase its thermal resistance. This can be added in the concrete block mix or as cell fillers in the concrete hollow blocks. Both methods have a significant positive effect on the thermal resistance of masonry blocks, however, the blocks filled in have a better thermal resistance than those block mixed [50] [64] [65]. This is due to the low water absorption of the blocks and the significant reduction in the thermal conductivity of the insulation filled blocks. Al-Hadhrami et al. [64] in their research concluded that for blocks filled with insulating materials, the type of insulation used is significant as the addition of perlite in the cells of a brick only showed a 10% improvement whereas, the addition of mineral wool in the same cells showed a 32% improvement in the thermal resistance.

Insulating materials like gypsum, polystyrene, mineral wool, perlite etc. have higher thermal conductivities than the buoyant air in the cells. In reality, this should counter the aim of trying to improve the thermal performance of an insulation filled block. When the block cells are filled with air, all the three modes of heat transfer (conduction, convection and radiation) are present. On the other hand, when the block cells are filled with insulating

materials, the effect of radiation and convection is reduced significantly [64]. These inserts in the cells reduce the volume for convective currents to circulate and this in turn can eliminate or suppress the cell convection to some degree [65]. Other experiments proved this assumption to be correct [64] [66] [67]. Pavlík et al. [66], in their experiment involving the use of expanded polystyrene as cell fillers showed a decrease in the effective thermal conductivity of the block as a result of a reduction in radiative heat transfer.

2.7.1.1. Gypsum

Amongst its many functions, gypsum and its products are lightweight materials that can be used for heat preservation and thermal insulation because of the moisture in the gypsum crystals [4]. It is highly porous and consists mainly of calcium sulfate and water [60]. Depending on the temperature, different types of gypsum binding materials can be produced [60] [68]. When subjected to heat above 90 ºC, gypsum undergoes a calcination process where 21% by weight chemically bound and free (absorbed) water is released into the pores. The pore pressure is increased, thereby transferring water vapor and air through the pores. The heat absorbed during the evaporation – dehydration process does not cause temperature increase [69]. This property of gypsum makes it of interest in fire protection, as it contributes to the fire resistance of gypsum. However, the fireproofing intensity of gypsum decreases when the moisture is stripped away [68].

The break down of the chemically bound water takes place in two stages [68]. As such, the specific heat of gypsum at elevated temperatures has two peak points. At temperatures between 90 ºC and 250 ºC during the first stage, the calcium sulphate dihydrate loses about 75% of its water, forming calcium sulphate hemihydrate $CaSO_4 \bullet \frac{1}{2} H_2O$ Equation 2-4, [68].

$$CaSO_4 \bullet 2H_2O + Q \leftrightarrow CaSO_4 \bullet \frac{1}{2} H_2O + \frac{3}{2} H_2O \uparrow \qquad \text{Equation 2-4}$$

With further heating, the second stage of the reaction occurs where the remaining 25% is lost. Calcium sulphate hemihydrate loses the remaining water to form calcium sulphate anhydrate $CaSO_4$ Equation 2-5, [68].

$$CaSO_4 \bullet \frac{1}{2} H_2O + Q \leftrightarrow CaSO_4 + \frac{1}{2} H_2O \uparrow \qquad \text{Equation 2-5}$$

Several research that has been conducted in the past all agree that the first peak point of moisture loss takes place at 100 ºC, but they all reported different temperatures for the second peak point. Sultan [70] conducted an experiment on type X gypsum boards at a heating rate of 2 ºC/min. The first recorded peak point was 18.0 kJ/kg°C at 100 ºCwhile the second recorded peak point was 3.07 kJ/kg.°C at 670 ºC. Harmathy [71] reported a first peak point of 7.32 kJ/kg°C at 100 ºC. However, his experiment only went as far as 650 ºC, and so did not reach a second peak point. Mehaffey et al. [72] in an experiment conducted

using a differential scanning calorimeter at scanning rates of 2 and 20 ºC min $^{-1}$ tested specimens conditioned at 40 ºCfor 24 hrs. They recorded a peak value of 30 kJ/kg.°C at 100 ºCfor the 2 ºCmin $^{-1}$ scanning rate and a peak value of 14 kJ/kg.°C at 140 ºCfor the 20 ºCC min $^{-1}$ scanning rate. The results of their experiment only went as far as 200 ºC, and so did not reach a second peak point.

Gypsum is fast condensing and hardening when mixed with water to form a slurry. The hardened product has a high porosity of over 50% that improves its thermal performance. The insulating material is then capable of slowing down the rate at which heat is transferred through walls and floors at elevated temperatures. Gypsum products are porous and hydroscopic, with poor water and frost resistance [68]. Heat transfer through gypsum occur via conduction, convection, and radiation. From the furnace to the exposed side of the gypsum, heat transfer occurs via convection and radiation, with radiation being the most predominant. Heat transfer through the solid gypsum occurs via conduction. However, convection and radiation are also modes of heat transfer through gypsum because of the porous nature of the material. Heat transfer from the unexposed side of the gypsum to the surrounding occurs via convection and radiation, with convection being the most predominant. At about 200 ºC, gypsum board begins to experience shrinkage [73]. This eventually leads to crack formation, but the cracks are usually not large enough to pose a

problem [69]. The cracks only widen after the test is terminated and gypsum plaster began to cool. Fire-rated gypsum, Type X and Type C, contain different amounts of glass fibre and vermiculite. These additives help improve the performance of gypsum at elevated temperatures by reducing the effect of shrinkage and cracks. Vermiculite is able to counterbalance the shrinkage by expanding when heated, while the glass fibre attempts to ensure that cracks do not occur [73].

Gypsum is usually found at the interior side of partition walls, usually as a cladding element, thereby guaranteeing the use of most of the thermal inertia [74]. The dehydration front of gypsum moves from the exposed side of the wall to the unexposed side, with a decreasing velocity due to the heat flux on the exposed side of the wall. This results in a smaller overall heat flux than the conductive heat flux, leading to a smaller temperature rise and longer temperature plateau [75].

2.7.1.2. Vermiculite

Vermiculite is a naturally occurring inorganic insulating material that has a low density, low thermal conductivity and a great fire resistance. It is made up of vermiculite, hydrobiotite and phlogopite, alongside aluminum and magnesium silicate as a result of factors like weathering, and movement of heated groundwater [76]

Like perlite, they are able to expand or exfoliate eight – twenty times their initial size, at temperatures above 1000 ^{o}C as a result of steam produced. When vermiculites cool off, they are able to retain their newly expanded form. They are also able to hold moisture within the voids of their particles after expansion [77]. Up to temperatures as high as 1100 ^{o}C, vermiculite does not lose its heat/fire resisting property [76]. It can be used as part of the block mix to replace cement, sand or just as a loose-fill materials.

2.7.1.3. Mineral Wool

Glass wool plus rock wool together is known as mineral wool. Mineral wool is a non-combustible fibrous lightweight insulating material formed from spun ceramic fibers. It is an environmentally friendly material with numerous tiny pores. It has an excellent fire resistance [68]. It has a low moisture content [82], and is hydrophobic in nature meaning that it does not mix freely with water. Researchers have attempted to block the routes for thermal current in masonry concrete blocks by wrapping the interior and exterior surface of an exterior wall with a high-performance heat insulating material. An experimental investigation carried out on mineral wool blankets revealed a noticeable improvement in the performance of the relined furnace [83]. Yang et al. [84], in their research, concluded that the use of mineral wool as an insulating material would only show significant improvements with heat preservations but little improvement on thermal insulation effects.

Pavlík et al. [67], in their research carried out an experiment on the use of air, hydrophobic mineral wool (repels water), hydrophilic mineral wool (has an affinity to water), polystyrene balls, and foam polyurethane as cell fillers. Their results showed that unlike the air-filled cell wall which had all the three modes of heat transfer present, the insulation filled walls had convection and radiation significantly reduced. Similar findings were also reported by Al-Hadhrami et al. [64]. The insulation filled walls all showed significant improvements in their thermal resistance, however, the two types of mineral wool (hydrophobic & hydrophilic) showed the greatest improvements than the others. The hydrophobic mineral wool had a 61% improvement in their resisting capacity, the hydrophilic mineral wool had a 67.7% improvement while polystyrene balls and foam polyurethane had a 50% and 53% improvement, respectively [67].

2.7.2. **Mix design**

Blocks can come in different mix designs to accommodate the use, required fore resistance, and water resistance. mix designs involves varying proportions of the water/content, aggregate size and type, and additives.

2.7.2.1. Use of lightweight aggregate

Concrete's behavior in fire depends on its constituents and mix proportions. The choice of the type of aggregate to be used in a mix is a crucial factor, as some aggregates break up at

relatively lower temperatures than others. Lightweight concrete or modified lightweight concrete performs better in fire or elevated temperatures because of their improved thermal properties and bonding capabilities than normal-weight concrete. The use of cost-effective recycled rubber aggregates made from used tires was reported to effectively reduce the heat transfer rate and increase the thermal resistance of concrete [85]. An experimental study conducted by Yesilata et al. [86] on rubberized concrete walls showed an improvement in the thermal properties of concrete as the percentage of the rubber aggregates increased from 0% to 10% and from 10% to 20% Figure 2-21. A greater improvement was observed with the 20% rubber aggregate sample. However, this improvement had an inverse effect on concretes compressive strength.

In another research conducted, polymeric waste materials like PET bottles and rubber were added to the concrete mix. This addition greatly improved the thermal insulation performance [87]. The degree of the improvement is, however, dependent on the amount and shape of the PET bottle and rubber tire. The square-shaped rubber showed a better performance than the strip or irregular shaped rubber or PET pieces [86] [87].

Al-Sibahy et al. [16] conducted research on the behavior of modified lightweight concrete made from metakaolin and recycled glass. At elevated temperature, the results showed that regardless of the percentage contents of both replacements, there was a general

improvement in the concretes thermal behavior. This can be attributed to their lower thermal conductivity values of both replacements compared to cement or natural sand.

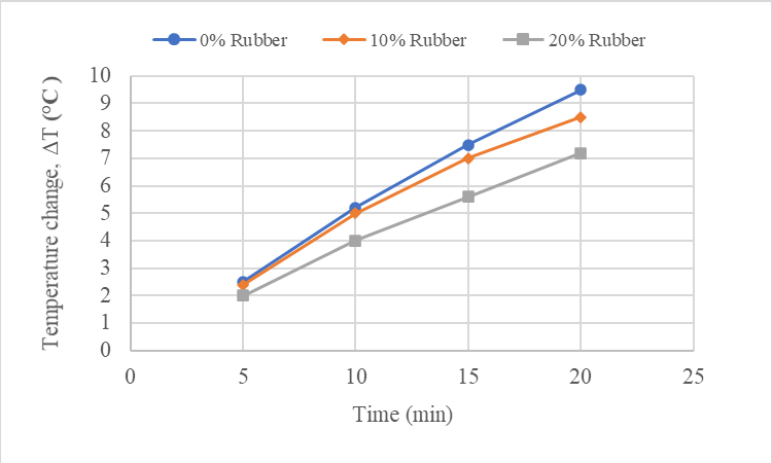

Figure 2-21 Heat transfer through concrete made with rubber aggregates [86].

2.7.2.2. Insulating mortar

Al-Hadhrami et al. [64] also highlighted another method of further improving the thermal resistance of a wall assembly through the use of insulating mortars. Using insulation materials as cell fillers alone is not adequate enough as the mortar joints also act as thermal bridges. This affects the overall thermal performance of the wall. Insulating mortars showed a 23–46% increase in the thermal resistance of walls when compared to conventional mortar [64]. This range of improvement was as a result of the differences in the insulation material used as the cell fillers. These insulating mortars consists of a

cementitious binder, water, and lightweight aggregate such as expanded perlite, polystyrene particles (PP), and vitrified microsphere [88].

The environmental problems associated with the use of ordinary Portland cement (OPC), led to the need for an alternative binder that emits a lesser amount of CO_2 and requires a lesser amount of energy [89]. This gave rise to the development of geopolymers. Geopolymers have better thermal resistance, greater compressive strength, and a quicker setting time than the convectional OPC. Duan et al. [90] in their research experimented on thermal insulating geopolymer composite made from polystyrene and metakaolin. They investigated the effects of an increase in the percentage of polystyrene particles from 25% to 100% on the mechanical and thermal properties of the composite.

Their result showed that as the polystyrene particle content increases in the composite, the compressive strength decreases [90]. This behaviour was attributed to the differences in the individual properties of the polystyrene particle and the geopolymer paste. This difference caused the formation of cracks in the composite and thus caused a reduction in strength with new additions of polystyrene particles. The thermal insulating geopolymer also had a considerably lower density and lower thermal conductivity due to the presence of the polystyrene particles [90]. Similar trends also occurred in research conducted with an increasing percentage of vitrified microsphere. The density, compressive strength and

thermal conductivity decreased as the vitrified microsphere content increased [88]. At elevated temperatures, the behaviour of the thermal insulating geopolymer with increasing PP content is shown in Figure 2-22. Between ambient temperatures and about 300 ºC, the geopolymer composite experiences an increase in the compressive strength. This increase is immediately followed by a steady and gradual decline in the strength values until 800 ºC. The moisture contained in the pores of the geopolymer composite was suggested as the reason behind its high thermal resisting performance [90].

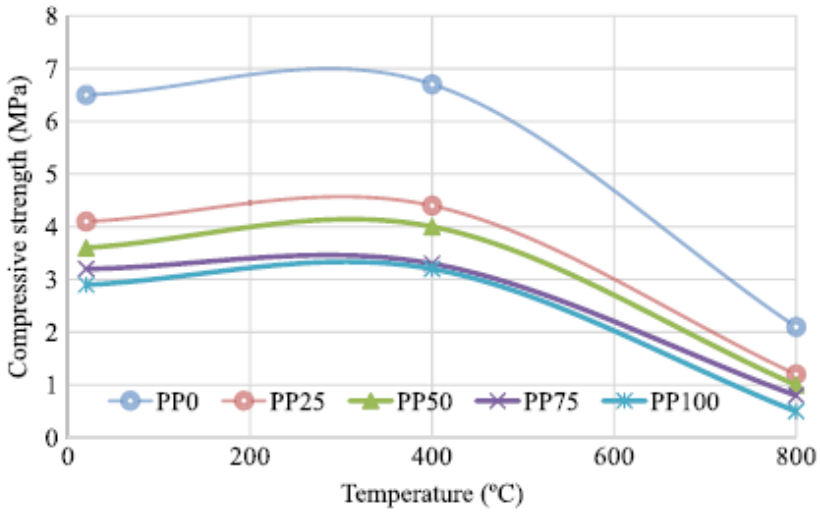

Figure 2-22: The compressive strength of geopolymer composites [90].

2.7.3. **Cell configuration**

In the present-day building industry, hollow lightweight blocks with vertically oriented cells are widely used to reduce heat transfer rates through masonry blocks [4]. Their

thermal resisting capacity can be further improved by cell shapes alterations [50], increasing the cell numbers [91], reducing the cell depths or altering the cell arrangements [67]. These methods shall be further discussed in detail in this section.

2.7.3.1. Cell shape

For manufacturability purposes, cell shapes are roughly rectangular. However, past research has shown that the shape of cells plays an important role in improving the thermal resistance of the block [50]. Nagy [50] conducted an experiment on hollow masonry blocks with four (4) different cell shapes, triangular shaped cells, small rectangular shaped cells, trapezoidal shaped cells and big rectangular shaped cells. The first three (3) shaped types were smaller in size. In the use of mineral wool, expanded perlite and polyurethane foam as cell fillers for these blocks, there was barely any significant change in the thermal conductivity for the smaller sized blocked shapes (triangular shaped cells, small rectangular shaped cells, trapezoidal shaped cells). However, there was a significant difference in the thermal conductivity for the blocks that had the big rectangular shaped cells. Their thermal conductivities were lowered significantly and were considered to have the most optimal cell shapes.

2.7.3.2. Cell number/cell arrangement and aspect ratio

The thermal performance of a concrete block can be improved by increasing the number of openings in the block. This can be achieved since the thermal conductivity of air is much less than that of concrete. Antar et al. [91] conducted research on the effect of increasing the number of cells on the thermal performance of hollow concrete blocks. For this research, the block width was kept constant, and a minimum requirement as specified by IS: 3952-1988 [92] was used as a guide in increasing the cells. The code [92] stated that for blocks to maintain their strengths the web thickness cannot be less than 8 mm and the shell thickness cannot be less than 11 mm. The result as shown in Figure 2-23 shows that the thermal resistance of the block increases with an increase in the number of cells. However, it was noticed that the increase from 4 to 5 cells only had a 3.18% increase in the thermal resistance while the increase from 5 to 6 cells only showed a 2.25% increase in the thermal resistance. It can therefore be concluded that the constant increase in the number of cells would always have a positive effect on the thermal resistance, until it gets to a point (5 cells) where a further increase in the number of cells would have an insignificant effect on the thermal resistance of a block [91].

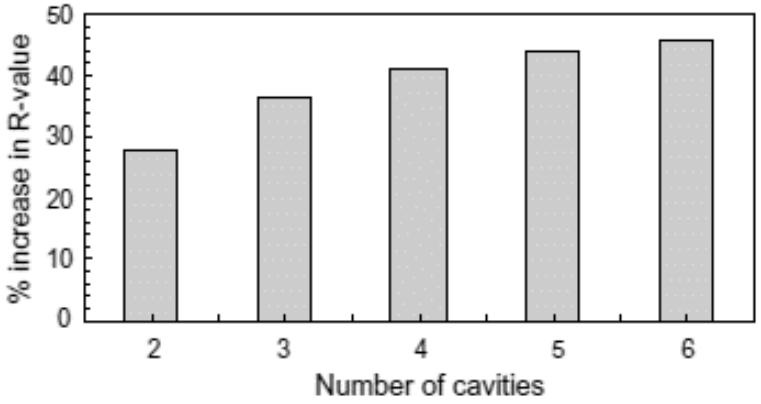

Figure 2-23: Percentage increase in the R-value with number of cells [91].

Li et al. [93] in their research went further to investigate the thermal performance of blocks with an increasing number of cells in both the widthwise direction and the lengthwise direction. Figure 2-24 shows the thermal conductivity values for the different configurations. Across all the widthwise hole configurations from 1-6, when the lengthwise hole increases from 1 to 2, there is a sharp decline in the thermal conductivity values. It further decreases when the number of holes increase from 2 to 4. The decrease in the conductivity values when the holes increase from 4 to 6 is almost insignificant. This result also correlated with the results from Antar et al. [91] experiment. As the lengthwise holes increase beyond 6, the thermal conductivioty values begin to rise gradually but only by a small percent. The L8W4 (length – 8 & width – 4) block sample was then concluded to be the most optimal configuration. The lengthwise cell arrangement had a greater effect on the thermal conductivity of the block than the widthwise arrangement.

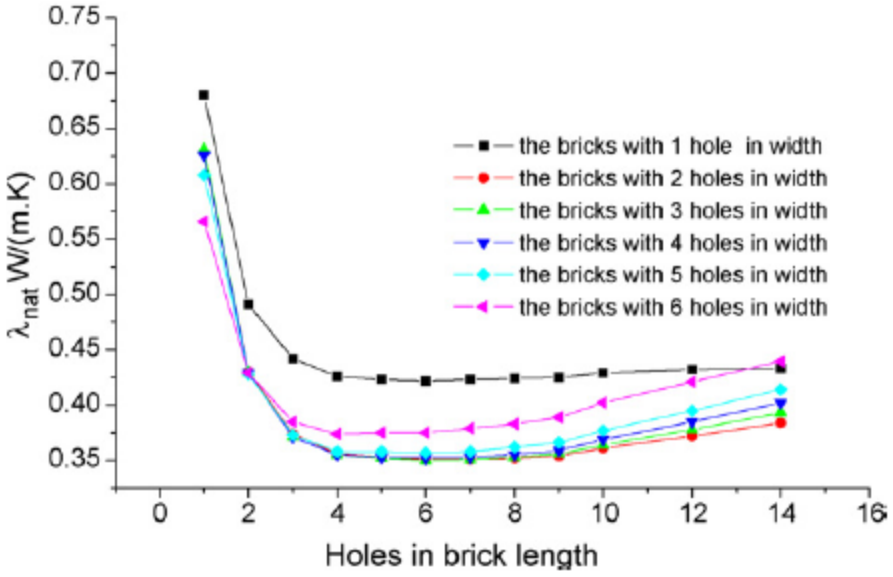

Figure 2-24: Thermal conductivity values of hollow block [93].

A cells aspect ratio can be increased by reducing the cell depths. Block cell depth reductions have similar effects as increasing the number of vertical cells [94]. This reduction in the cell depth reduces the vertical flow velocity and increases the thermal resistance of the block.

2.8. Numerical modeling of masonry walls in fire

The time consuming and expensive nature of the standard fire tests has resulted in the need to develop reliable numerical models to extrapolate test data and conduct extensive parametric studies on masonry wall behavior at elevated temperatures. Different numerical methods exist for the linear or non-linear behavior of masonry: finite element method (FEM), finite difference method (FDM), boundary element method (BEM), and many

others, but because the empirical calculations in the decay period are less accurate, finite element methods (FEM) calculations are recommended for thermal analysis of concrete structures exposed to real fire [4].

2.8.1. **Finite element method**

The finite element method is a numerical procedure widely used in any engineering analysis to solve complex mathematical problems. The step-by-step approach to solving any finite element problem is summarized in flowchart Figure 2-25. It involves the modeling of discretized bodies interconnected by nodes and boundary lines common to two or more elements or surfaces. Simultaneous equations are formulated for each discretized element and then combined to obtain the solution of the whole body. If the accuracy is not met, the model meshes are refined until a closer accuracy has been achieved. As illustrated in Figure 2-26, there are two (2) main modeling approaches in any FEM analysis: micro-model approach and macro-model approach. The choice of an approach depends on the level of simplicity and accuracy desired [95]. The micro-model approach involves the individual creation of individual parts, while the macro-model involves creating composites with no clear distinction between the units or mortar. This approach is adopted for complex structures and when the homogenous behavior of the structure is majorly of interest. Several commercial software packages like ABAQUS,

ANSYS, etc., can be used in the numerical evaluations of the linear and non-linear behavior of concrete and heat transfer modes.

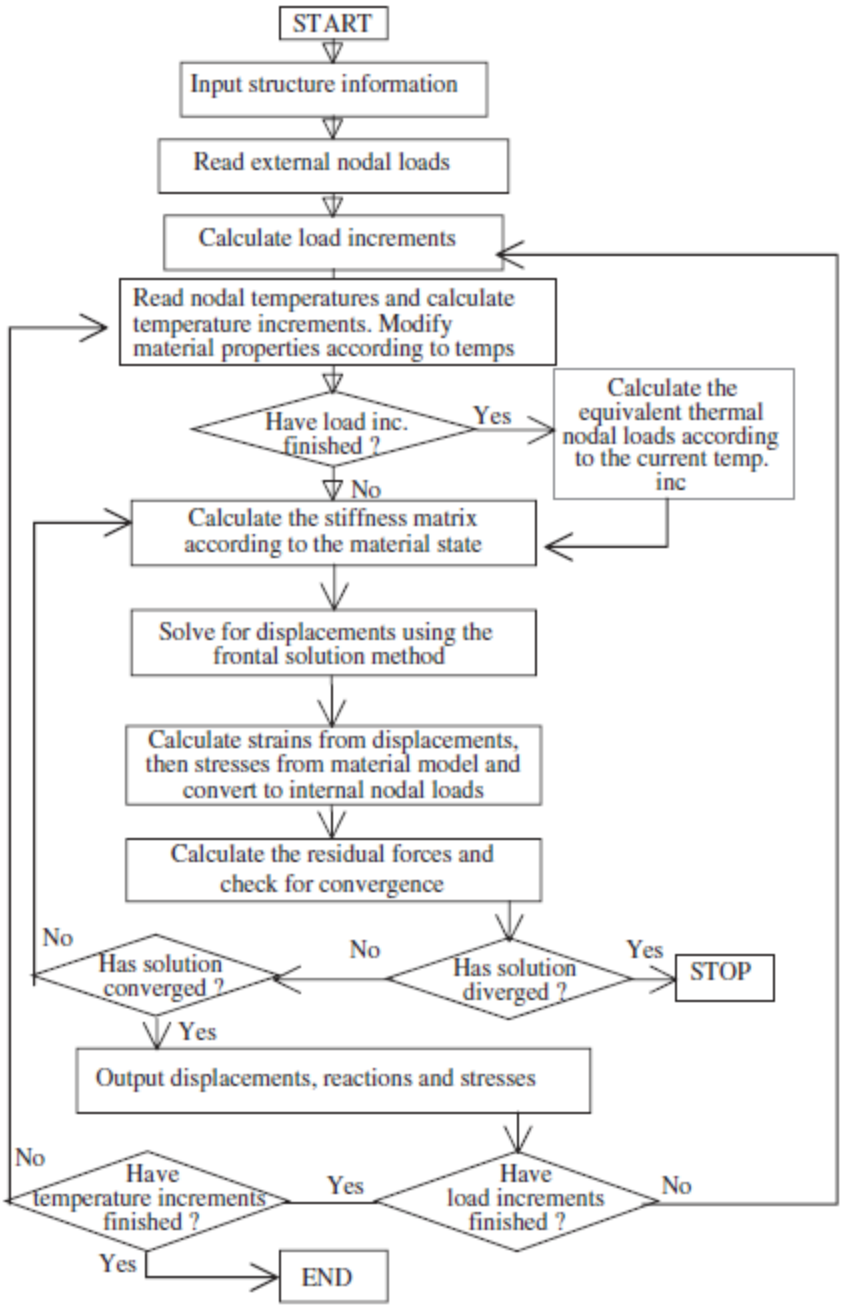

Figure 2-25 Flow chart showing solution procedure for an FEM analysis [96].

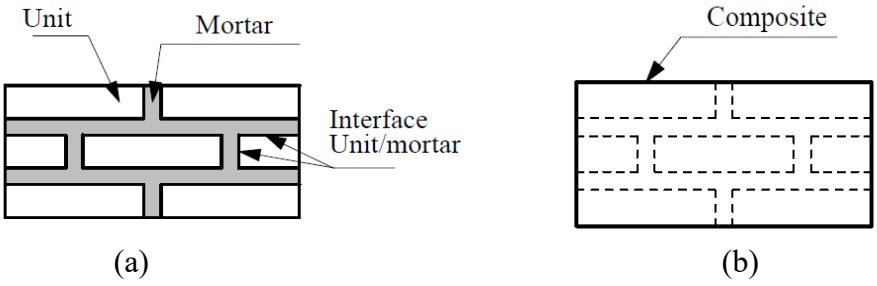

Figure 2-26 Micro-modelling (a), Macro-modelling (b) [95].

2.8.1.1. Abaqus FEA software package

Abaqus finite element analysis software was released in the early 1970s consisting of several core products for different engineering applications. Abaqus/CAE (Complete Abaqus Environment) is used for modeling, assembling, and visualizing FEA results. Abaqus/Standard is a versatile product that can solve linear and nonlinear thermal, static, or dynamic problems. Abaqus/Explicit is best suited for transient dynamic problems. Abaqus/CFD (computational Fluid Dynamics) is dedicated to the simulation of fluid dynamics and heat transfer and is good for thermal and fluid structural cases and Abaqus/Electromagnetic [97]. The Abaqus FEA package has better nonlinear capabilities that allow its users to fully customize inputs like user materials, user elements, user heat fluxes, etc. It can write a FORTRAN subroutine and have ABAQUS incorporate it into a run. Every finite element analysis involves three stages: Pre-processing/modeling stage,

the processing/finite element analysis stage, and the post-processing stage. The first stage involves a model created using a text editor or any compatible CAD software. The second stage can only be accomplished with the Abaqus/Standard, Explicit, or CFD cores, while the last stage is a visualization stage where the results from the analysis can be viewed, and reports can be generated, etc.

Chapter 3: Methodology

This chapter discusses the experimental tests carried out at the Barnsdale research facility in Ottawa, using the Canadian standard fire test. This research was conducted to study the thermal behavior of concrete masonry walls in fire when lightweight insulating materials and air are used as cell fillers. The walls were exposed to the CAN/ULC-S101 standard fire Equation 3-1, [98].

The CAN/ULC-S101 standard fire equation can be expressed as:

$$T_g = T_o + 750\,(1 - \exp(-0.49\sqrt{t})) + 22.0\sqrt{t} \qquad \text{Equation 3-1}$$

Where:

T_g = Furnace temperature, T_o = ambient temperature in degree Celsius, and t = time in minutes.

Further into the chapter, the processes taken to develop a reliable numerical finite element model that correctly depicts the behavior of masonry in fire are discussed. This numerical model is developed using a commercial finite element software, Abaqus/Standard 6.14.

The model will be verified using the results from a control wall (Test 1), with air as a cell filler. The emissivity, mesh sizing, film coefficient, and cell radiation will be used for calibrating the numerical model. The verified numerical model will then be validated using the results from another wall (Test 2), with a lightweight insulating material as a cell filler.

3.1. Experimental research description and procedure.

This section presents the experimental procedures carried out in the laboratory work. From the wall set-up to the thermocouple placements and then to the use of a thermal imaging camera.

3.1.1. Set-up

A full-scale fire resistance test was conducted on four walls that make up a room. One wall was the control wall and the other three walls had varying characteristics. Each test wall was 8 ft x 8 ft tall (6 blocks wide and 12 courses high) Figure 3-1. Detailed summary of the test walls are highlighted in Table 3-1.

These blocks were bonded together with a 10 mm Type S concave mortar joint and were built within steel frames. The NW 20 cm wall was left to cure for a month before testing while the NW 15 cm wall was left to cure for a week before testing. A propane burner was used to subject the walls to a standard fire as prescribed by the CAN/ULC S-101 [98].

Propane burners were built to produce up to a 7 MW fire which distributes the heat evenly between the test walls. The burner was manually controlled to ensure that the temperature recorded in the furnace at any given time matched the corresponding temperature of the standard fire curve.

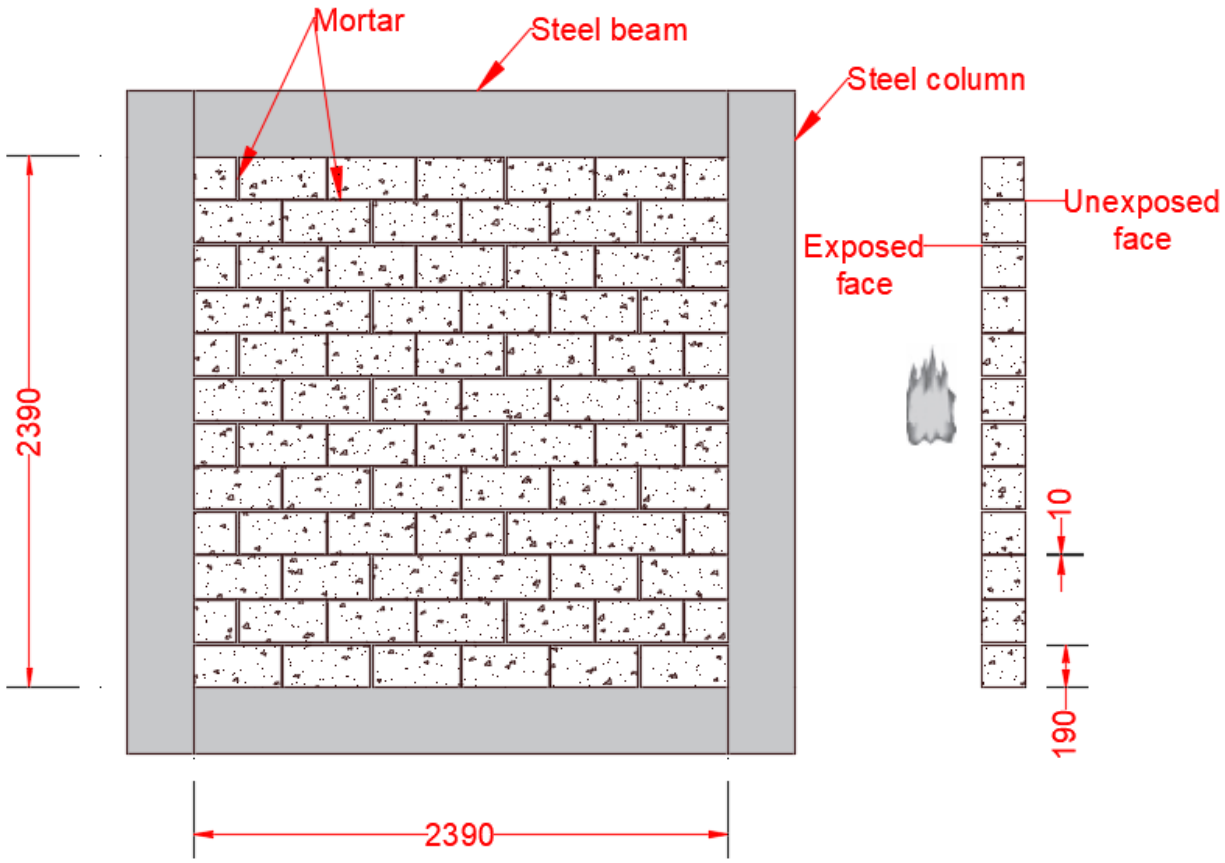

Figure 3-1 Wall geometry (units in mm).

Table 3-1 Test wall summary.

Test 1		20 cm Carbon cured block
Test 2		15 cm block with expanded vermiculite

3.1.2. **Thermocouple**

To monitor the heat transfer rate through the walls, Type K thermocouples were placed at unique locations on the exposed and unexposed face of the wall. Type K thermocouples are the most common thermocouples with a wide temperature range, −200 °C to +1350 °C [99]. As per the CAN/ULC S-101 [98], a minimum of 9 thermocouples are required to monitor the test walls. Five of the thermocouples are required to be placed in specific locations and the other four thermocouples can be placed at locations decided on by the testing authority. For the tests conducted, nine (9) thermocouples were placed on the

unexposed face of the wall Figure 3-2. As a result of the anisotropic nature of the blocks, the thermocouples were spread among the hollow sections, solid web and mortar joint.

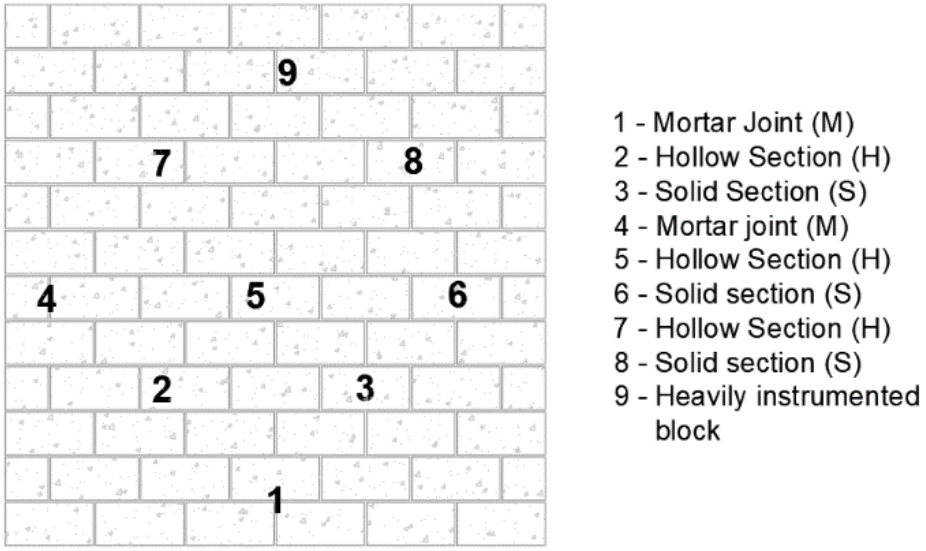

Figure 3-2 Thermocouple locations on wall.

One thermocouple was placed at the centre of the wall, four other thermocouples were placed at the mid point of each quarter. The last set of four thermocouples were placed to complete a diamond pattern as this gave the best coverage of the wall.

There was a need to further study the rate of heat transfer through a block. For this, three (3) distinct locations were also chosen to be studied: the hollow cell (H), solid web (S), and mortar joint (M). The block located at position #9 was heavily instrumented with thermocouples at these unique locations. This block was chosen because of its location

high up on the wall, as it is assumed that hot gases travel vertically upwards, leaving the top region of the wall hotter than the lower region. For the hollow cell, thermocouples were placed on the exposed face of the wall (H1), unexposed face of the wall (H5), on either sides of the interior cell (H2 and H4) and at the middle (H3). For the solid webs and mortar joint, the thermocouples were placed similarly. On both the exposed face (S1 and M1) and unexposed face (S3 and M3) of the wall, as well as the middle of the block/mortar (S2 and M2) Figure 3-3.

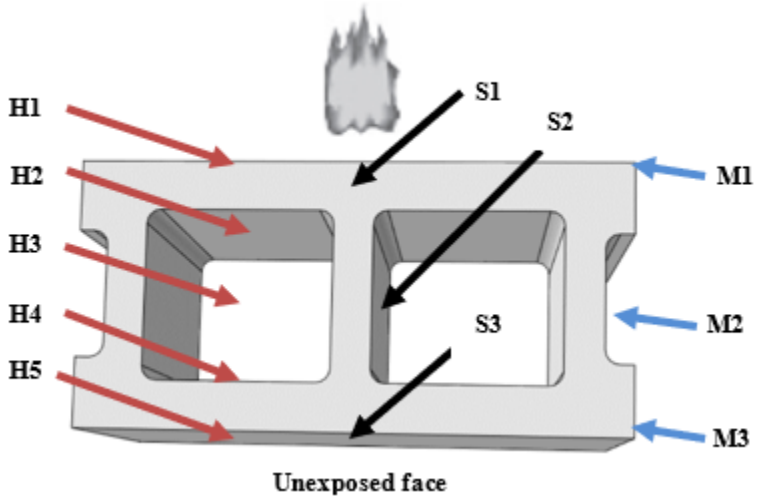

Figure 3-3 Thermocouple locations on heavily instrumented block.

Insulating pads were placed over the thermocouples on the unexposed face of the wall. The pads were made of fiberfrax and were roughly 150 mm in length and width, and 12.7 mm thick. The pads were securely placed to ensure that the thermocouples placed at specific points remain in place. The pads were also put in place to ensure that the temperature

readings recorded by the thermocouples are the actual temperature readings as a result of the furnace temperature and not the temperature readings after there must have been some exposure to the ambient conditions.

The thermocouple readings were recorded every five (5) seconds and so this was within the requirement of the CAN/ULC S-101 [98]. The measurements were taken with a National Instruments NI cDAQ-9188 data acquisition unit, and Labivew software was used to organize and export the data.

To take into account any deviation from the prescribed time temperature profile, a correction is provided by the CAN/ULC S-101 [98] for measuring the furnace temperature. The correct fire resistance period can be calculated using Equation 3-2, [98].

$$C = I + \frac{2I\,(A - A_s)}{3\,(A_s + L)} \qquad \text{Equation 3-2}$$

Where;

C = corrected fire endurance period (h), I = fire endurance period obtained before correction (h), A = area under the curve of indicated average furnace temperature, A_s = area under standard fire curve and L = lag correction.

3.1.3. **Thermal imaging**

As part of the testing, thermal imaging is used to monitor the test walls. The camera used was a high-resolution science grade LWIR CAMERAFLIR A655sc. Data from thermal imaging is used to draw contours of the non-uniform temperature profile on the unexposed surface of the walls, which allows for the determination of the critical points on the surface. Unlike thermocouples, thermal imaging allows for monitoring the whole wall surface, which is useful if the critical points happen to be somewhere where there are no thermocouples. Temperatures from the camera can be used to validate the thermocouple readings to ensure accuracy.

To calibrate the thermal imaging camera, an emissivity value of 0.94 is used, the relative humidity for each test day, the ambient temperature and the distance between the camera and the test walls are set. It was important to set these parameters in order to measure accurate temperature across the walls.

3.2. Finite element model

To further evaluate the behavior of masonry walls, a finite element model was developed using a commercial software package, ABAQUS. The finite element approach was adopted because of the complexities and difficulties in obtaining an analytical mathematical solution for the partial differential equations with numerous unknown variables at any point on the body. With the finite element method, getting an acceptable solution is possible. This approach involves the breaking down of the model into smaller discretized elements, all connected together by nodes, surfaces, or boundary lines. Simultaneous equations are then formulated for each discretized element and then amalgamated together to produce a single solution for the whole system [100]. ABAQUS is able to analyze the nonlinear behavior of the concrete masonry walls and the heat transfer modes accurately by adjusting the load increments and convergence tolerances during the analysis until an approximate solution is reached. The analysis was purely thermal with no interest in structural behavior. The standard fire curve, CAN/ULC S-101 [98], was inputted into the analysis for the fire model. For the temperature variations to be measured, the thermal properties of the concrete masonry must be specified [4]. The element type, interaction module, meshing, boundary conditions, and loadings are discussed further in this section.

3.2.1. **Element type**

The masonry units (full blocks, half block, head joint, and bed joint) were modeled as individual parts with their respective local coordinate systems Figure 3-4. They were coupled in the assembly module as independent instances of parts relative to each other in a global coordinate system**.** The mortar was modeled similar to those used in the experimental research, with a 10 mm depth. For simplicity, the concave joint was not incorporated. Rather, the joint was assumed to be rectangular on all sides.

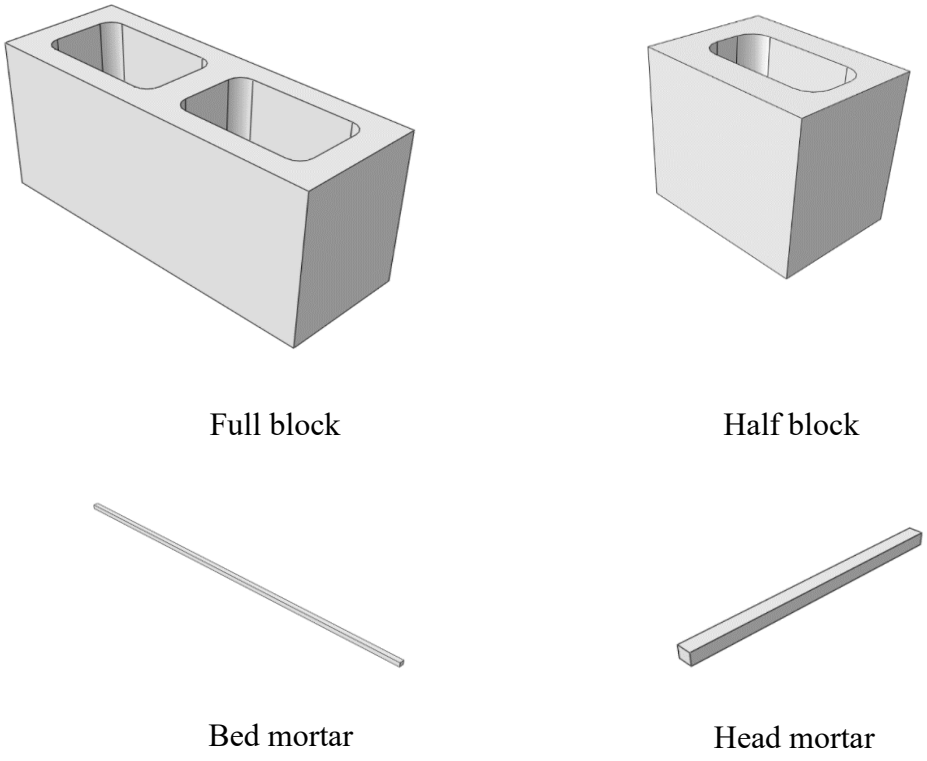

Figure 3-4 Masonry units.

3.2.2. **Material model**

For any heat transfer analysis, thermophysical properties have to be specified. These properties, density (ρ), specific heat capacity (Cp), and thermal conductivity (k), govern the thermal behavior of concrete masonry walls in fire or elevated temperatures. The properties were specified for both the concrete masonry blocks and mortar. These values were gotten from past literature [101] Appendix A1 and A2. However, using the stated thermal properties did not produce the expected results and so there was a need to tweak the thermal properties in such a way that an accurate model was achieved. For this analysis, the properties were temperature dependant properties that varied over a range of temperatures from 20 ºC and 800 ºC. This range was selected because beyond 800 ºC, aggregates like limestone would have completely disintegrated, forming cracks resulting in a drastic loss of strength and possibly collapse [17]. The issue with the model created using the earlier stated thermal properties is that the effect of the free moisture in the concrete was absent. As a result, there was no plateau phase resulting in the model being hotter than it should normally be. It is then important to incorporate this free water into the model.

When concrete is exposed to temperatures up to 100 ºC, the equivalent density of concrete is reduced by 100 kg/m^3. However, this density reduction has an insignificant effect on the

thermal behaviour of the masonry wall [4]. The presence of moisture during heating has vast effects on the outcome of the test and so should be taken into consideration. The heat transfer in the cells negatively impact the fire resistance of the masonry block, but the moisture plays a role in diminishing the heat transfer effects [102].

Energy is required for water to heat up and for vaporization to occur. Since this energy is directly related to the specific heat, the specific heat values around 100 ºC was increased to consider the effects of moisture. The amount of moisture content in concrete is a major factor in determining the amount of energy needed for evaporation of the pore water to occur. The higher the moisture content in the concrete, the greater the energy that is needed. In order to determine the total energy required for evaporation to occur, the specific heat of water, heat of vaporization of water, and the specific heat of concrete must be considered. This increase was done by calculating the free water content of the concrete (around 2.5%) and adding that percentage of water's specific heat value (4.2 kJ/kg.k) to the concrete. Since vaporising water takes more energy, the heat of vaporisation of water was found (2458.3 KJ/Kg), and that value was divided by the temperature range it would be spread over (20 K) in order to get a specific heat value (KJ/Kg.K). This value was also added to the specific heat at temperatures around 100 ºC.

$$Cp_{water} + \Delta Hvap_{water} + Cp_{concrete} = Cp_{total}$$

$$(0.025 \times 4.2) + [(0.025 \times (2458.3/20))] + 0.822 = 4.0 \text{ kJ/kg/k}$$

A much better result was achieved with this adjustment. However, the obvious horizontal plateau that occurs in a physical test did not occur in the model analysis. Rather, the model only showed a slower increase in temperature. During the physical test, the thermocouples read the temperature of the vaporized water which remains constant at 100 ºC until all the moisture has been evaporated. Since the model does not directly incorporate the water, and instead indirectly approximates the increase in specific heat due to the water, the graph at that point slightly diverges from the physical test data.

3.2.3. **Interaction module**

Interaction module is an important step-dependent module that must be assigned to selected regions in an assembly because Abaqus/CAE cannot recognize surfaces or edges as being in contact even in close proximity [103]. For surfaces or edges where the mode of heat transfer is via conduction, like the interaction between concrete blocks and mortar, a surface-to-surface contact was assigned to the initial step, as these are areas of discontinuities in the model. This can be done manually or automatically by using the 'contact pairs' feature. This interaction module involves grouping surfaces or edges in contact with the master or slave surfaces. The concrete masonry block surfaces were assigned master surfaces because they have larger surfaces, while the mortar joints were

assigned slave surfaces because they have smaller surfaces Figure 3-5. Abaqus requires that the slave surfaces are more finely meshed than the master surfaces [103]. A thermal conductance property of 0.80 W/m.K was specified for this interaction, as the results mimicked the experimental results better.

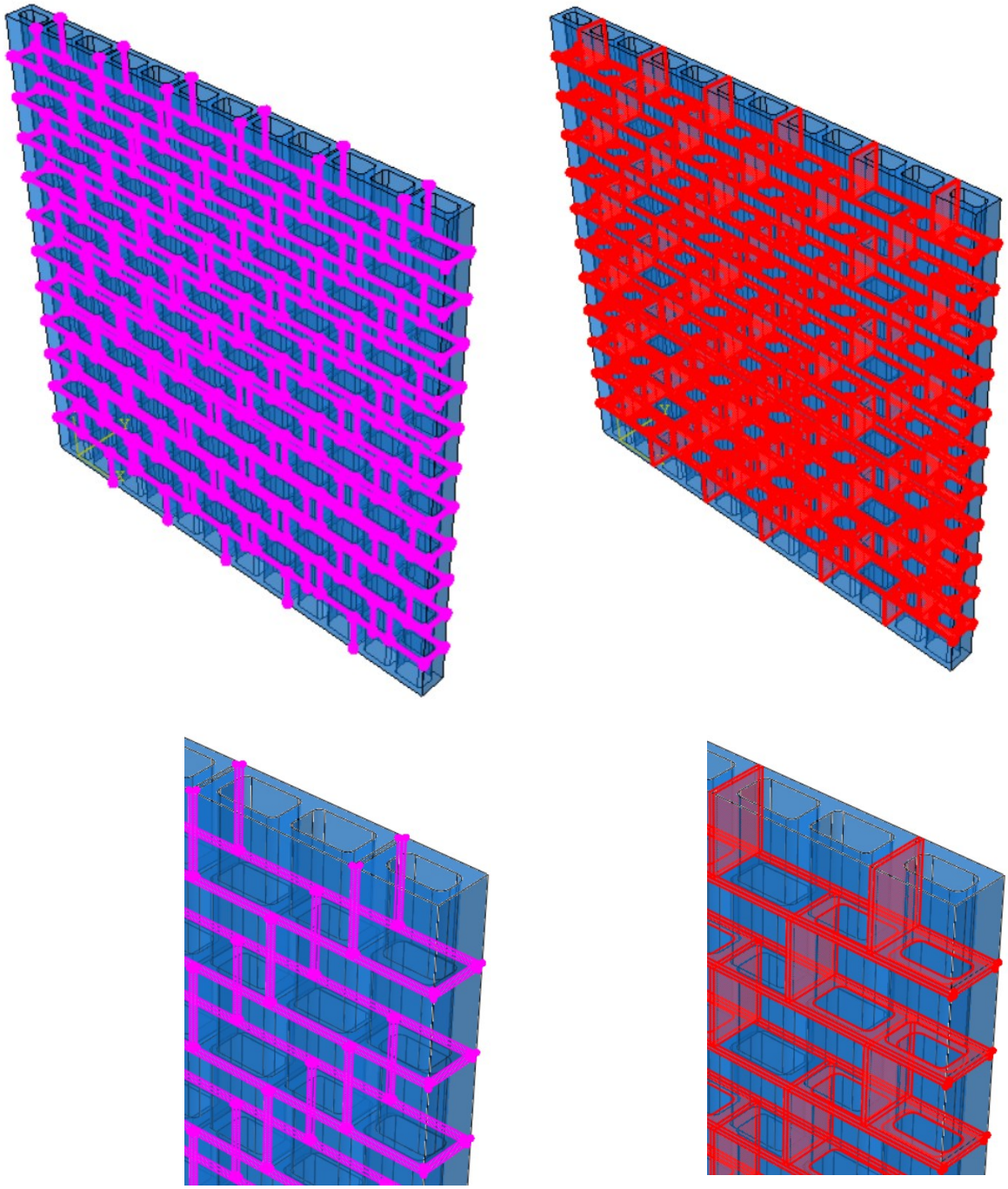

(a) (b)

Figure 3-5 Slave surface (a) and Master surface (b).

In the hollow cells and the frog cells formed when two blocks are married together, convection and radiation are the predominant heat transfer modes in these regions as a

result of the convective air moving freely in these cells. These interactions can only be applied in the heat transfer step [104]. They are applied to specific regions formed from manually selecting and creating surfaces or sets in the assembly module. For considering the effect of convection, temperature-dependent thermal film conditions were assigned to all of the hollow surfaces using the property reference definition. This property can define the heating due to the convective air from the hot gases. The film coefficient, h and sink temperature, θ were defined.

For accounting for radiation in enclosures, cell radiation interaction or cell radiation approximation in the surface radiation interaction can be used. Emissivity is defined in this interaction module. The choice of the radiation type to be used largely depends on the computation time and accuracy. However, by specifying the number of symmetries, the cell radiation interaction can reduce the overall computation time [103]. However, there are limitations to using this interaction module for cell radiation problems when nodes/degrees of freedom (DOF) are over 16,000 [103]. In that case, cell radiation approximation is adopted.

The selections for the hollow surfaces in which radiation was applied differed from that of the convection interaction. The radiative view factor was assumed to be a one-directional heat transfer simulation; even though, in reality, radiative heat transfer also occurred on the

adjacent cell faces. This simplification was made because it simulated the heat transfer through the concrete block better than when applied in both directions Figure 3-6. In the latter approach, the solid webs heated up faster than the hollow regions, which was typically not the case during the experimental research.

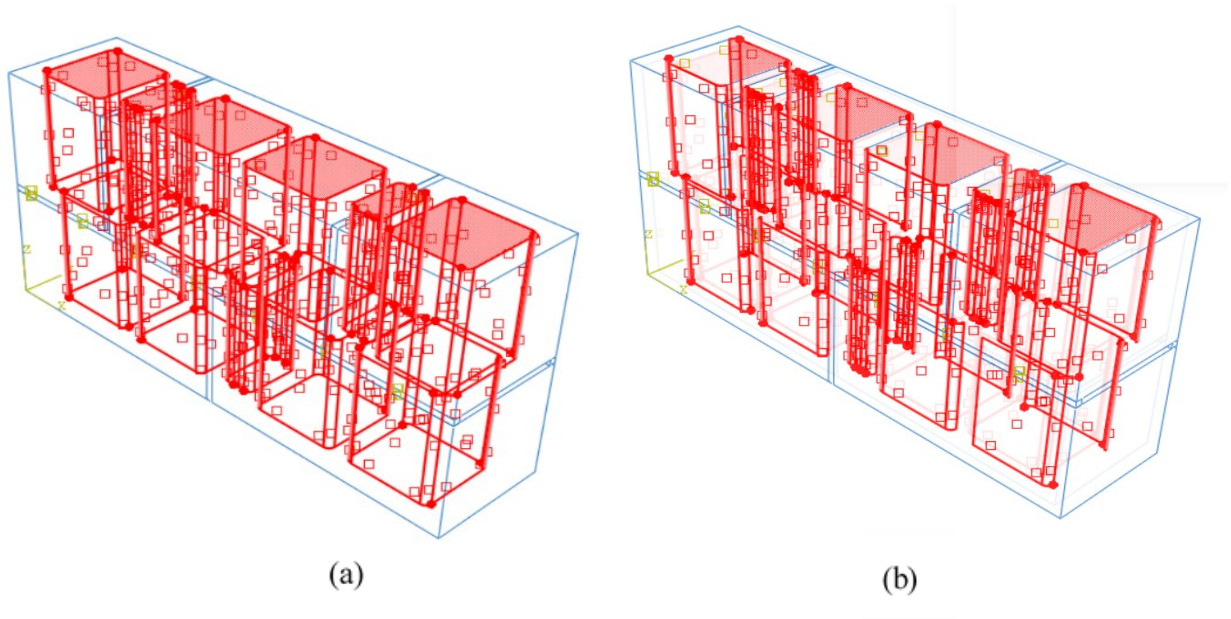

Figure 3-6 Selected convection surface (a) and Selected radiation surface (b).

3.2.4. **Boundary conditions and thermal loading**

During the experimental test, a propane burner was used as the heat source. The air in the furnace heated up, and the heat gradually transferred to the exposed face of the concrete masonry wall via convection and radiation. The uniform heat flux, q'' (W/m^3), subjected to the exposed surface of the wall as shown in Figure 3-7 was modeled using Equation 3-3.

$$q''=h_c\,(T_f-T_s) + \emptyset\varepsilon ff\sigma(T_f{}^4-T_s{}^4) \qquad \text{Equation 3-3}$$

Where;

h_c = coefficient of convection, T_f = furnace temperature (K), T_s = surface temperature of assembly (K), $\emptyset$ = configuration factor, ε_{ff} = surface emissivity, σ = Stefan-Boltzmann constant, (5.67 x 10^8 W/m^{2}K^4).

In the finite element model analysis, this heat flux was applied as a user-defined subroutine, DFLUX (Distributed Flux), written in Fortran (See Appendix B). The DFLUX file can define nonuniformly distributed heat flux over the selected surfaces of a wall as a function of time, temperature, etc. The surface heat flux is a step-dependant parameter. This parameter was applied in the heat transfer step to selected surfaces created under the assembly module. The governing equation for the 3-dimensional thermal analysis is as shown in Equation 3-4 [97]

$$\frac{\partial}{\partial \mathrm{x}}\left(\mathrm{k}\frac{\partial \mathrm{T}}{\partial \mathrm{x}}\right) + \frac{\partial}{\partial \mathrm{y}}\left(\mathrm{k}\frac{\partial \mathrm{T}}{\partial \mathrm{y}}\right) + \frac{\partial}{\partial \mathrm{Z}}\left(\mathrm{k}\frac{\partial \mathrm{T}}{\partial \mathrm{z}}\right) + \mathrm{qv} = \rho \mathrm{Cp}\frac{\partial \mathrm{T}}{\partial \mathrm{t}} \qquad \text{Equation 3-4}$$

Where;

k = the thermal conductivity (W/mk), ρ = density (kg/m3) and Cp = specific heat capacity (J/kg.K), t is the time (s), x,y,z are the distances from the heat source.

In the model attributes, two (2) properties must be inputted for any heat transfer analysis where radiation or emissivity will be considered. The absolute zero temperature (–273.15 ^{o}C) and the Stefan–Boltzmann constant (5.669 x 10^{-11} W.m^{-2}K^{-4}). Since Abaqus has no inbuilt unit system, care should be taken to ensure unit consistency in the model so that no errors or inconsistent results would be gotten.

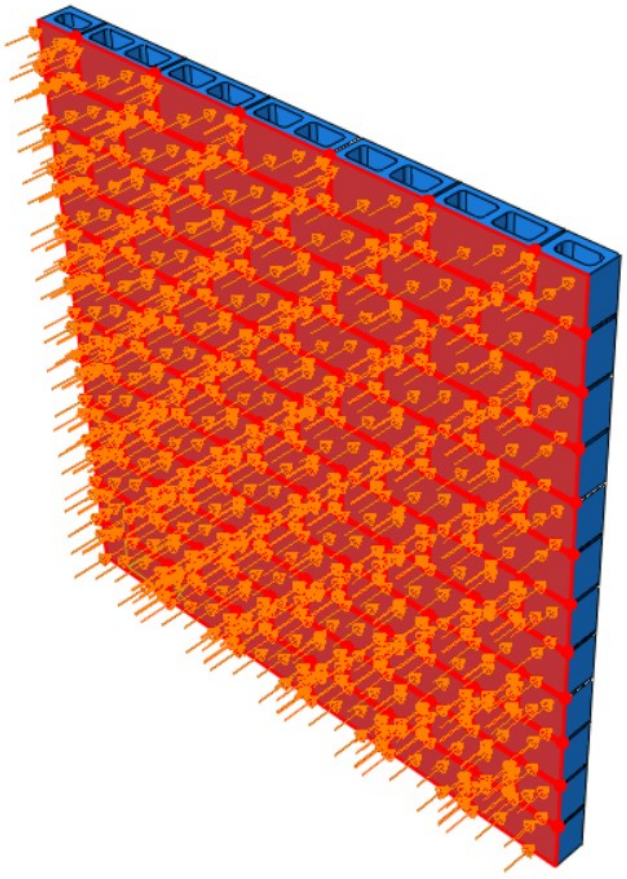

Figure 3-7 Heat flux applied to the exposed face of the wall.

3.2.5. **Sub-modelling**

Concrete masonry walls are a composite of different materials: masonry blocks and mortar. Modeling the global model (concrete masonry wall) with refined meshes can be time-consuming, and this can come with its own computational cost or errors. A solution to this is the use and analysis of a sub-model. Sub-modelling allows for a more detailed analysis of specific regions/sections of the complete model using finer refinements. This approach is useful when the aim is obtaining an accurate, detailed solution. This detailed solution has negligible effects on the overall solution [103].

Some sample models: full wall (12 courses), half wall (6 courses) and quarter wall (3 courses) were analyzed with the same mesh density. The results of the half wall and quarter wall was compared to determine their deviation from the full wall Figure 3-8. The unexposed side of the walls/blocks were the area of interest. The results as highlighted in Table 3-2 shows that for both the solid and hollow sections of the walls, the deviation from the full wall were all within acceptable ranges, and so both the half and quarter walls were deemed suitable.

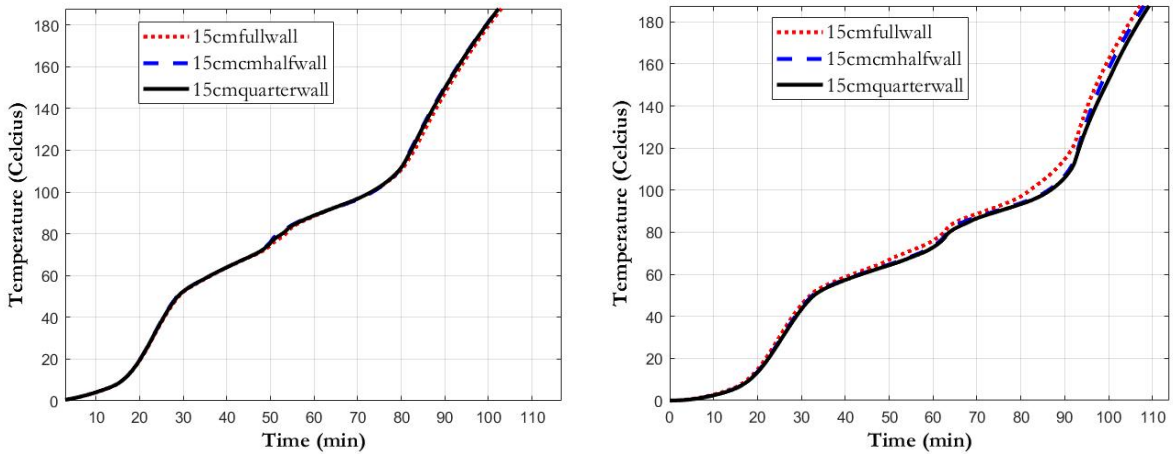

Figure 3-8 Comparing the sub-models a) Hollow section b) Solid web.

Table 3-2 Sub-model error check.

	Hollow section	Solid section
15cmfull (12-course)	-	-
15cmhalf (6-course)	0.6%	1.3%
15cmquarter (3-course)	0.6%	2.3%

3.2.6. **Meshing**

The mesh module involves specifying a mesh density, assigning element type, and defining a mesh control. Several techniques can be used to create meshes. The selection of a mesh density largely on the computational time and its closeness to the experimental results. For the 3D parts created, a hexahedra quadrilateral 8-node linear heat transfer type (DC3D8) was assigned to the assembly since the FEM simulation was focused on a heat transfer analysis Figure 3-9. Depending on the element type, two types of meshing control can be

used – top-down and bottom-up meshing controls [103]. The top-down control is a more automated technique, while the bottom-up technique gives the user the most control over the meshing. For simplification, a structured or sweep mesh control was selected for the parts because they generated suitable meshes. The meshing was done on individual parts and not as an assembly because some parts were earlier assigned master and slave surfaces, and thus, needed to be given individual mesh densities.

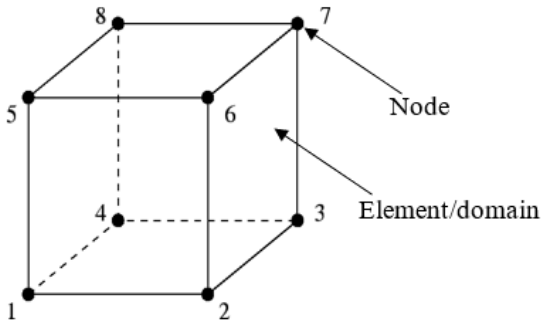

Figure 3-9: DC3D8 8 node linear heat transfer solid brick.

3.2.7. **Processing (FEA)**

The Abaqus analysis commences with the default initial step, followed by an analysis step. The initial step cannot be modified in any way [103]. This step considers set boundary conditions, contact interactions set to the initial step, and predefined fields. A predefined ambient temperature was assigned to the entire model in the initial step. A value of 27.5 ºC was used for Test 1 and a value of 28.1 ºC was used for Test 2. Boundary conditions were

not set in the finite element modeling process, as the experimental walls were not under any form of restrain. The analysis step is where the transient heat transfer analysis occurs, computing the temperature rise within the concrete masonry wall.

3.3. Model calibration

The necessary steps taken to ensure that the results from the finite element analysis closely matches the experimental results are discussed in this section. To correctly verify the finite element model, key thermal parameters such as the surface emissivity, convective heat transfer, and mesh sensitivity were taken into consideration.

3.3.1. Convective heat transfer

The combined effects of convection and radiation is of major importance in the heat transfer step. Heat transfer occurs via convection and radiation from the fire to the exposed face of the wall, through the cells and from the unexposed face of the wall to the atmosphere. In the experimental test, the thermocouples on the unexposed face of the wall had pads over them that reduced the effect of heat transfer to the surrounding. As such, the effects of convection and radiation to the atmosphere were ignored on the finite element model. They were only accounted for on the fire side of the wall and in the hollow cells. The heat transfer on the fire side of the wall was incorporated into the DFLUX subroutine file, while those for the hollow cells and frog cells were manually modelled in Abaqus.

Two approaches were used in determining the most effective value for the convective heat transfer coefficient that produces a temperature profile similar to the experimental results. The first approach assumed a single heat transfer coefficient value throughout the test. The values used for the trial analyses were 15 W/m^2K, 20 W/m^2K, 21 W/m^2K, and 25 W/m^2K. For the second approach, temperature dependant heat transfer coefficient values were estimated according to Equation 3-5. To estimate these values, the thermophysical properties of air at different temperatures (See Appendix C) according to SFPE [85] were used.

$$h = \frac{NuK}{L} \qquad \text{Equation 3-5}$$

The Nusselt number Nu was estimated according to Equation 3-6; where R_e represents the Reynolds number and P_r represents the Prandtl number.

$$Nu = 0.664\, R_e^{1/2}\, P_r^{1/3} \qquad \text{Equation 3-6}$$

Reynolds number was estimated according to Equation 3-7; where ρ is density, u is flow speed, L is the characteristic linear dimension, and μ is the fluid viscosity.

$$R_e = \frac{\rho u L}{\mu}$$ Equation 3-7

The temperature dependant heat transfer coefficient values used in the finite element model are summarized in below Table 3-3.

Table 3-3 Temperature-dependent convective heat transfer coefficients for FEM model.

Temperature (ºC)	h (W/m^2K)
0	11.5
27	12.1
77	13.75
127	15.42
177	16.99
227	18.52
277	19.96
327	21.35
377	22.68
427	23.97
477	25.19

The temperature profile for the hollow cell Figure 3-10a and solid web Figure 3-10b of the single and temperature dependent heat transfer coefficients were compared with the experimental results. It is evident that the single convective heat coefficient value (21 W/m^2K) and the temperature dependent value (TempDep) both had almost similar hollow cell results with only a slightly different in the solid webs plot. They also both had the

closest results to the experimental result, however, TempDep had better results and was thus used for the rest of the analysis.

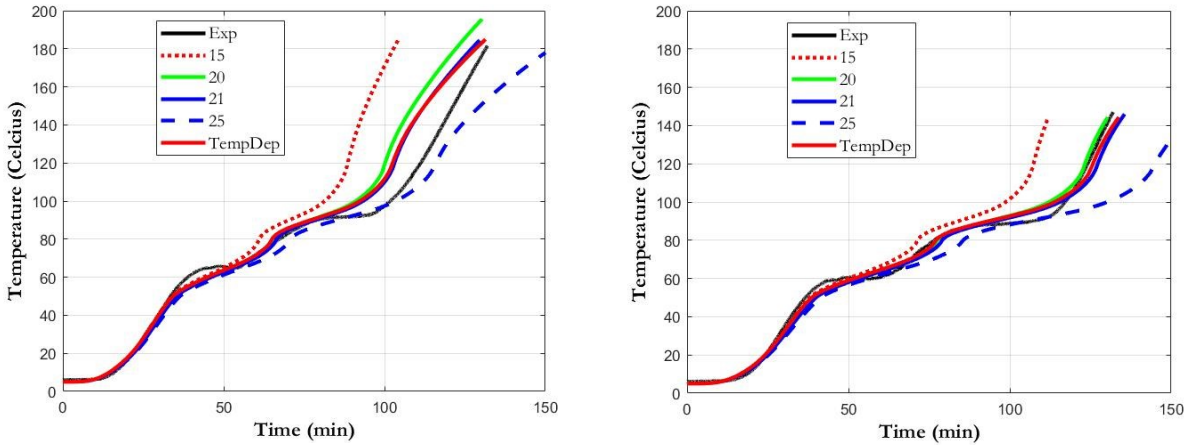

a. b.

Figure 3-10: Comparing convective heat transfer coefficient values: a) Hollow cell; b) Solid webs.

3.3.2. **Surface emissivity**

Heat transfer via radiation in the hollow cells of the concrete masonry blocks is dependent on the absorptivity to emissivity ratio. Based on the emissivity ranges suggested by different authors (see Section 2.3.2.4), four (4) values were chosen 0.8, 0.85, 0.9, and 0.94, and assigned to the developed models to check for the most optimal. The temperature profile for the hollow cell and solid web was compared with the experimental results Figure 3-11. The discrepancy in the plots start around 90 ◦C when moisture loss from the concrete wall occurs. This discrepancy is as a result of the model simplification done by increasing

the specific heat values of concrete. The emissivity values of 0.90 and 0.94 gave the closest results. In both, the model did not radiate out some heat and so they were left hotter than the experiment was until towards the end of the test where they coincided again. Emissivity value of 0.94 gave the closest result and so was used for the rest of the analysis.

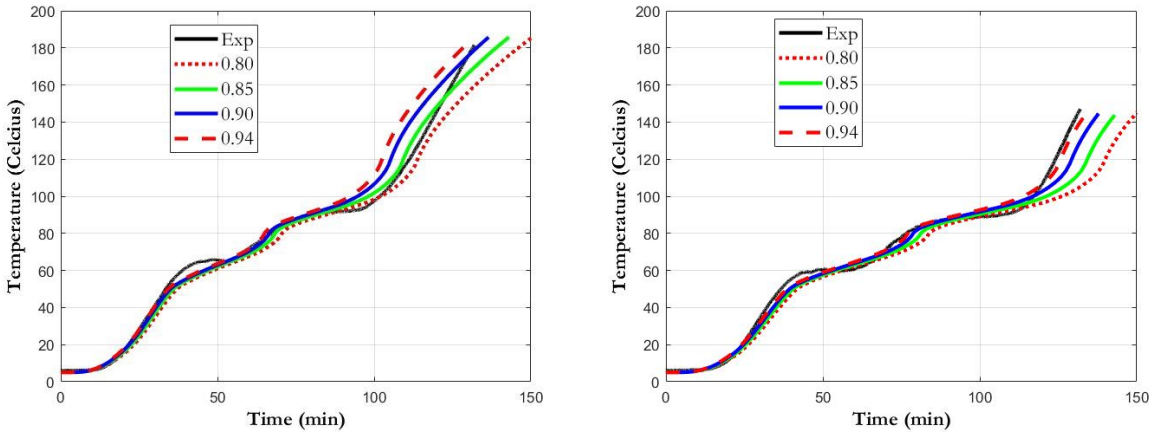

a. b.

Figure 3-11 Comparing emissivity values: a) Hollow cell; b) Solid webs.

3.3.3. **Mesh refinement**

The individual components of a concrete masonry wall exhibit an isotropic behavior, but this changes when these components form an assembly. The anisotropic nature of concrete masonry walls is present through the bed joint, head joint, and hollow cells, all in different directions [105]. For this reason, finite element mesh refinement is necessary. It is an important step in any finite element analysis as the accuracy of the results depends largely

on it. It can be achieved by increasing the element order or dividing the model into smaller elements/domains. As the elements get smaller, the meshes get refined, and the solution begins to converge towards the true solution. Increasing the domains increase the complexity of the analysis and computational time. Thus, the choice of an optimal solution depends not only on the accuracy of the solution but also on the computational time.

For this research, five (5) different mesh grades were used. These mesh grades ranged from coarse to fine meshes Figure 3-12. For each of the mesh grade, different mesh sizes were used depending on the masonry unit. Across all five (5) grades, the mortar was meshed more finely than the blocks because in the interaction module, they were assigned slave surfaces. Based on the mesh sizes for each grade, the total number of sub-elements created is also specified in Table 3-4.

Table 3-4 Mesh grades for concrete masonry wall.

	Extra coarse		Coarse		Normal		Fine		Extra fine	
Masonry Unit	Mesh Size	No. of Elements	Mesh Size	No. of Elements	Mesh Size	No. of Elements	Mesh Size	No. of Elements	Mesh Size	No. of Elements
Middle Block	30	954	25	1456	20	2180	15	3770	10	9994
Corner Block	30	726	25	1280	20	2090	15	3796	10	9766
Half Block	30	378	25	632	20	900	15	1742	10	4712
Bed Joint	25	64	20	80	15	106	10	158	5	632
Head Joint	25	16	20	20	15	26	10	38	5	152
Total		2138		3468		5302		9504		25256

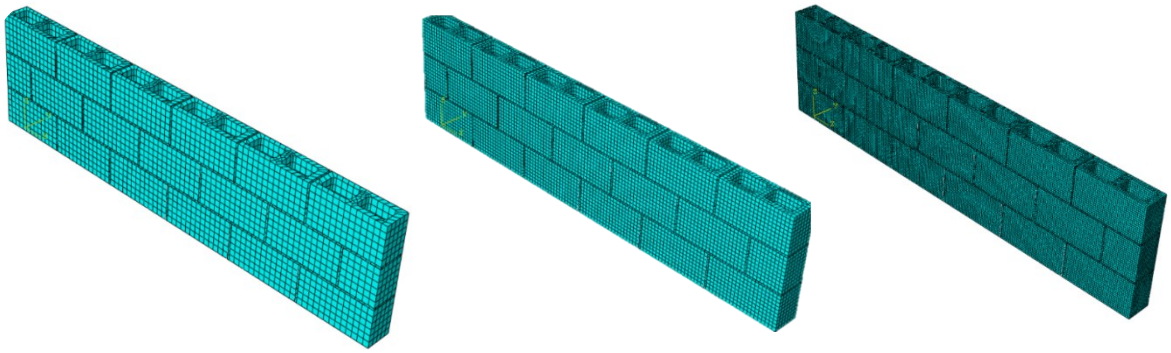

Figure 3-12 Mesh grades: Coarse (L), Normal (M), and Fine (R).

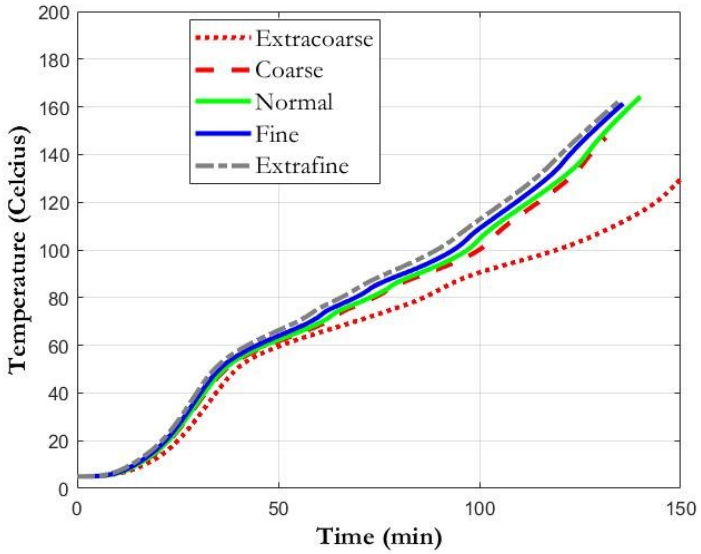

Figure 3-13: Mesh sensitivity.

The different mesh grades were plotted Figure 3-13 and the area under each graph was calculated to check their deviation from the extra fine mesh grade. Only the Fine mesh had a percentage error below 5% while the coarser meshes had errors ranging from 7% - 11% Table 3-5. This high percentage errors were due to the inaccessibility of nodal temperatures in selected areas like the mid point of the solid webs and hollow cells. The meshes were

too large and so the results obtained from those meshes were inaccurate. Narrowing down to the computational times, it was decided to use the fine mesh for the rest of the analysis as the analysis ran for 4.6 h lesser than the extra fine mesh took.

Table 3-5 Percentage error and computation time of mesh grades.

Meshes	Error (%)	CPU time (h)
Extra fine	-	7.10
Fine	2.89%	2.50
Normal	7.52%	1.00
Coarse	10.70%	0.73
Extra coarse	10.63%	0.57

Chapter 4: Results and discussions

In this section, the results from the experimental and numerical analysis of both the 20 cm wall and the 15 cm vermiculite wall will be analysed.

4.1. Wall without insulation – Test 1

This section contains the results for the 20 cm wall without insulation in the cells. The experimental and numerical test results were compared in order to verify the finite element model. Further discussions were done in this section, and conclusions were drawn from these results.

During the experimental test, a propane burner was used to subject to walls to fire according to the standard fire curve. The furnace temperature was mostly similar but for the drop in temperature after about 25 min Figure 4-1.

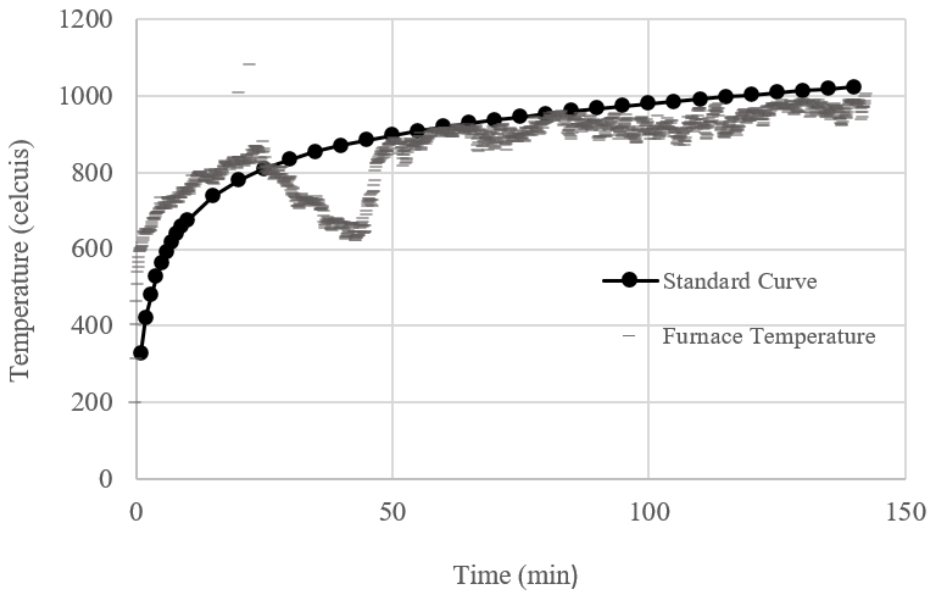

Figure 4-1 Comparison of the furnace temperature and the standard fire curve

The test was terminated after 2 h 22 min, and the corrected fire resistance period according to Equation 3-2 was calculated to be 2 h 15 min. There was just a time difference of 7 minutes.

4.1.1. **Failure time**

The insulation failure criterion was based on an average temperature increase of 140 ºC on the unexposed face of the wall or an increase of 180 ºC at a single thermocouple point. The 20 cm NWC control wall reached the average temperature increase after 2 h 5 min and reached the single point increase within 1 h 56 min. By correcting the furnace temperature using the correction factor in Equation 3-2, the average failure time was corrected to 2 h

and the single failure time was corrected to 1 h 51 min. Since the single point thermocouple increase was reached first, conclusion can then be made that the 20 cm control wall failed due to the 180 ºC insulation failure criteria after 1 h 51 min.

4.1.2. **Heavily instrumented block results**

The temperature profile of the control wall at the three distinct locations (H5, S3 and M3) show that the sections remain at ambient temperature for the first 10 mins of the test Figure 4-2. On the unexposed surface of the wall, it was observed that the hollow cell H5 heated up quicker than the other locations and it remained the hottest through out the duration of the test. This was due to the effect of radiation and convection that were the predominant mode of heat transfer in the cells.

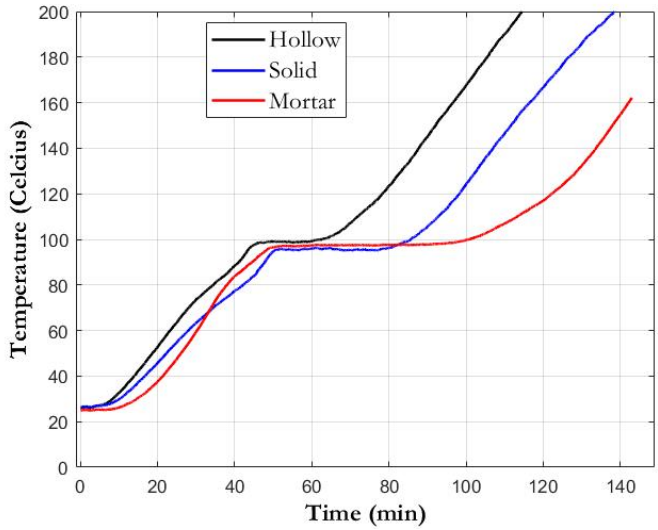

Figure 4-2 Temperature profile of control wall at H5, S3, and M3.

The plateau period of the wall occurred around 100 ºC. During this phase, the free moisture evaporated from the concrete. The length of the plateau stage is determined by the time required for the moisture contained in the concrete block or mortar to be completely evaporated. This plateau stage is associated with the energy absorption allowing this moisture to be converted into vapour. Plateau periods in concrete have been associated with their high permeability and gas pressure within their pores [106]. The mortar (M3) had the longest plateau spanning for about 50 min. This means that it contained the greatest amount of free moisture compared to the hollow cell or solid webs. This free moisture allowed the mortar section to remain at a constant temperature and only began to increase in temperature after 1 h 40 min. The solid webs plateaued for a duration of 30 mins, while the hollow cell plateaued for a duration of about 20 mins.

The main factors that influenced the thermal response of the hollow cell, solid webs and mortar joints were the heating rate, the moisture contents, and the thermal properties of the concrete blocks and mortar.

4.1.3. **Thermal image contour**

To continually monitor the temperature profile along the unexposed surface of the control wall, a thermal imagining camera collected data that were used to draw contours of the non-uniform temperature profile of the wall Figure 4-3. The first frame was the temperature

of the wall at ambient conditions i.e., 25.8 ºC. After about 15 mins, the unexposed surface began to heat up (frame 2). With the obvious hot spots in the cells, it is evident that the hollow sections are the hottest regions of wall, closely followed by the solid webs and then the mortar joint. A similar pattern is also noticed in frames 3 and 4. The presence of the buoyant air moving freely in the cells causes heat transfer to be more potent in this hollow cells. By the 3rd frame, cracks had begun forming at the top section of the wall. This might have been as a result of the heat accumulated in the upper layers of the wall. This accumulation resulted in the top section being considerably hotter than the bottom section. It can then be concluded that when a wall is subjected to fire, the hot gases in the hollow cells travel vertically upwards. However, this phenomenon did not cause a drastic damage to the blocks located at the upper layer.

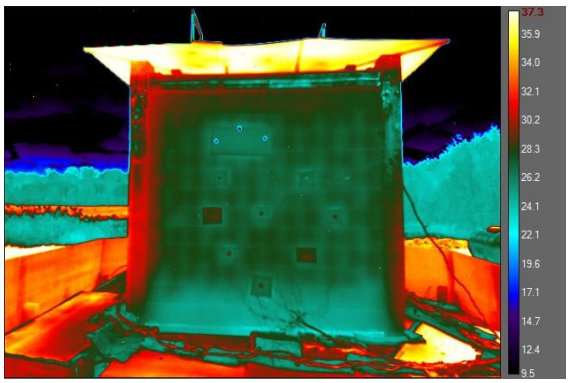

Frame 1 - At ambient

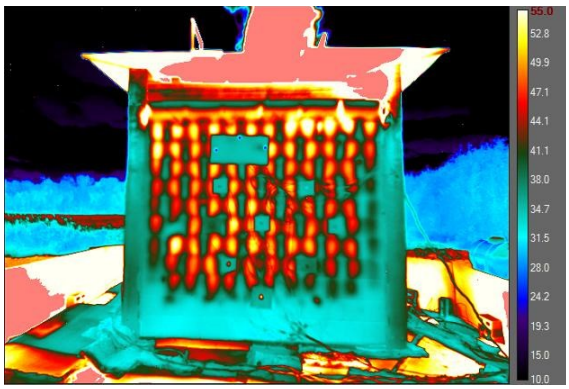

Frame 2 - At 15 mins

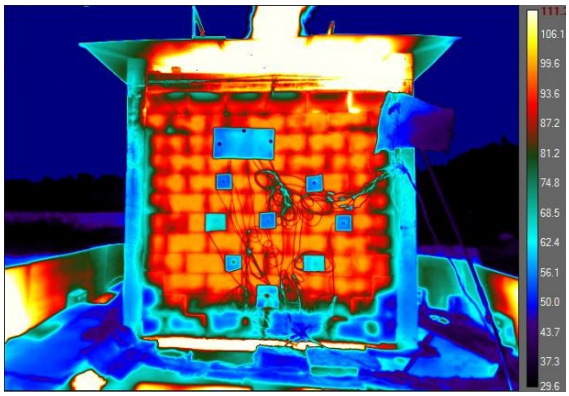

Frame 3 - At 1 h

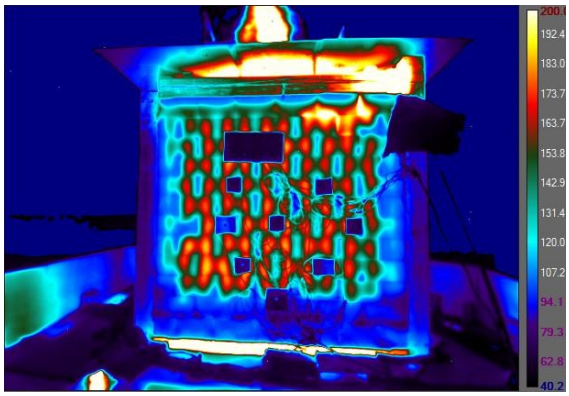

Frame 4 - At 2 h 20 min

Figure 4-3 thermal imaging contour frames for 20cm NWC wall.

With the thermal images, the thermocouples were able to be validated. There were no regions outside the thermocouple locations where the temperature readings became critical throughout the test duration.

4.1.4. **Verified finite element model**

This section looks at the verification of the finite element model. With the experimental work results, it is possible to check that the finite element works accurately.

4.1.4.1. **Average temperature profile**

The finite element model was verified by comparing the average temperature profile on the unexposed face of the wall with the Test 1 experimental results Figure 4-4. The finite element method was adopted to simulate the fire performance of the masonry wall. This numerical approach was adopted because of the difficulties with solving complex equations.

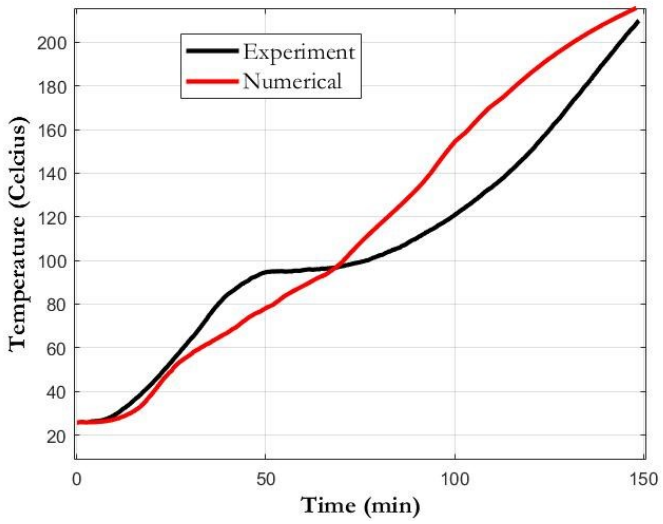

Figure 4-4: Average temperature profile on the unexposed face of the wall (Experimental and numerical).

The finite element analysis showed a reasonable agreement with the test data. Failure occurred after 1 h 47 min. The failure times for both the physical test and the FE model were almost identical, with both being slightly away from a 2-hour rating. The inability for ABAQUS to directly show the evaporation of the free water resulted in the absence of the horizontal plateau. This caused the model to remain hotter than the physical test after the 100 ºC mark, but it eventually converged to the physical test result towards the end of the test.

4.1.4.2. Control wall and validated model (H5, S3 and M3)

Nodal temperatures for the different sections on the unexposed face of the wall were taken and compared with the physical test Figure 4-5. Like with the physical results, the finite element analysis results were also similar, with H5 being the hottest section from the onset of the analysis to the end of the analysis. It was followed closely by S3 and then M3 was the coolest Figure 4-5. The finite element model was able to depict a similar pattern because of the thermophysical properties of the concrete and mortar incorporated into the model, interaction between the individual masonry units and the user defined DFLUX subroutine file attached in the analysis.

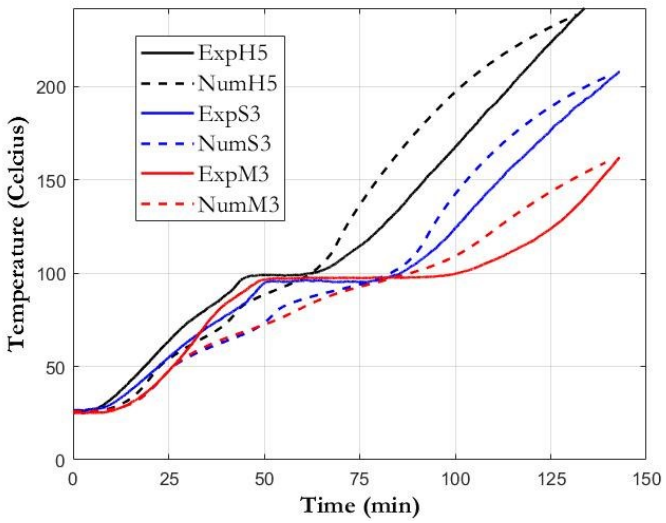

Figure 4-5 Comparison between the temperature profiles on the unexposed face (Experimental and numerical).

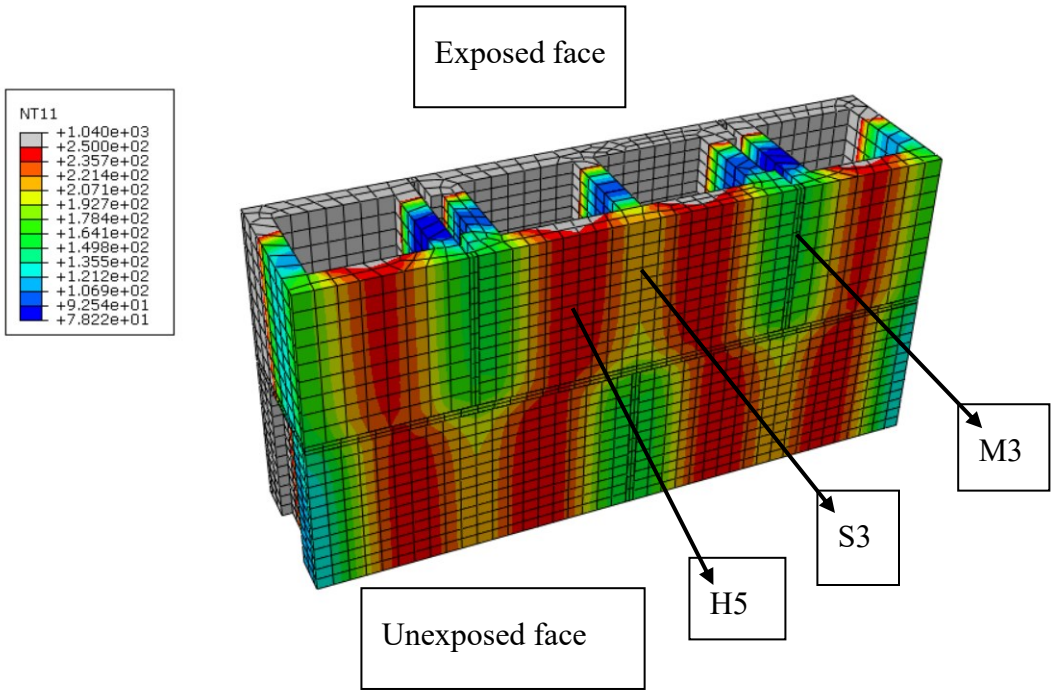

Figure 4-6 ABAQUS contour for 20cm NWC wall at failure.

4.1.4.3. Model accuracy

To check the accuracy of the verified model, the failure times between the finite element analysis and the control experimental wall were compared. The FE analysis deviated from the experimental failure time by 3.7%. This value fell within an acceptable range and the model was certified verified. With this, further analysis was conducted.

4.2. Wall with vermiculite insulation – Test 2

This section contains the results for the 15 cm wall with expanded vermiculite in the cells. The experimental and numerical test results were compared in order to validate the finite element model. Further discussions were done in this section, and conclusions were drawn from these results.

4.2.1. Furnace temperature

The furnace temperature was a close match to the standard curve temperature Figure 4-7.

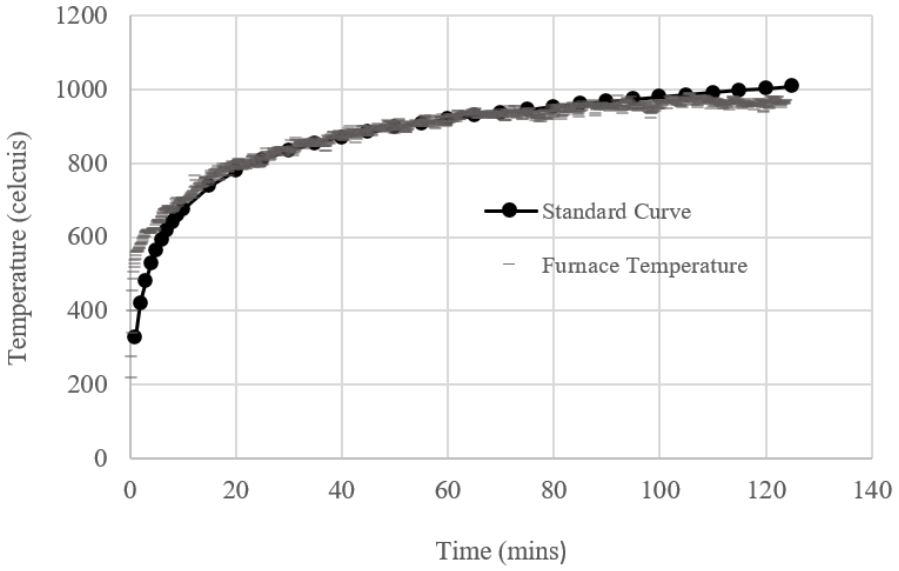

Figure 4-7 Comparison of the furnace temperature and the standard fire curve.

The experimental test was terminated after 2 h 4 min due to a sudden downpour of rain. The corrected fire resistance period according to Equation 3-2 was calculated to be 2 h 3 min.

4.2.2. **Failure time**

As a result of the premature termination of the physical test, the 15 cm expanded vermiculite insulated NWC wall did not reach its failure time. With its early termination after 2 h 4 min, it implies that the fire rating definitely surpasses the 2-hour mark. This is because both the average temperature increase, and maximum single point increase were never reached. Conclusions can then be made that this is a huge increase in the fire resistance rating when compared to a 15 cm uninsulated NWC wall that has a minimum

rating of 1 h. Hence, the fire rating can be improved using expanded vermiculite in the block cells.

4.2.3. **Effect of the vermiculite**

Regardless of the fact that the test 2 was terminated early, the average temperature profile plot can be compared with that of a 20 cm NWC uninsulated wall with a fire rating of 2 h Figure 4-8. By comparing these plots, an idea of the thermal performance of the fully insulated vermiculite wall can be determined. From the onset of the test, the 15 cm NWC wall was shown to heat up faster than the 20 cm NWC wall. This was due to the thinner face shells of the 15 cm NWC blocks. The 15 cm NWC wall had a horizontal plateau at about 120 ^{o}C. This period lasted for about 40 mins. During this period, as the free water began to evaporate out of the block, the 20 cm wall continued to increase in temperature and eventually surpassed the 15 cm NWC wall after 1 h 30 min into the test. The plot after the 1 h 30 min mark shows that the 15 cm NWC – vermiculite wall outperforms the 20 cm NWC – uninsulated wall. This could be due to the moisture retained by the vermiculite. At elevated temperatures, this moisture consumes heat energy which has a cooling effect that delays the temperature rise.

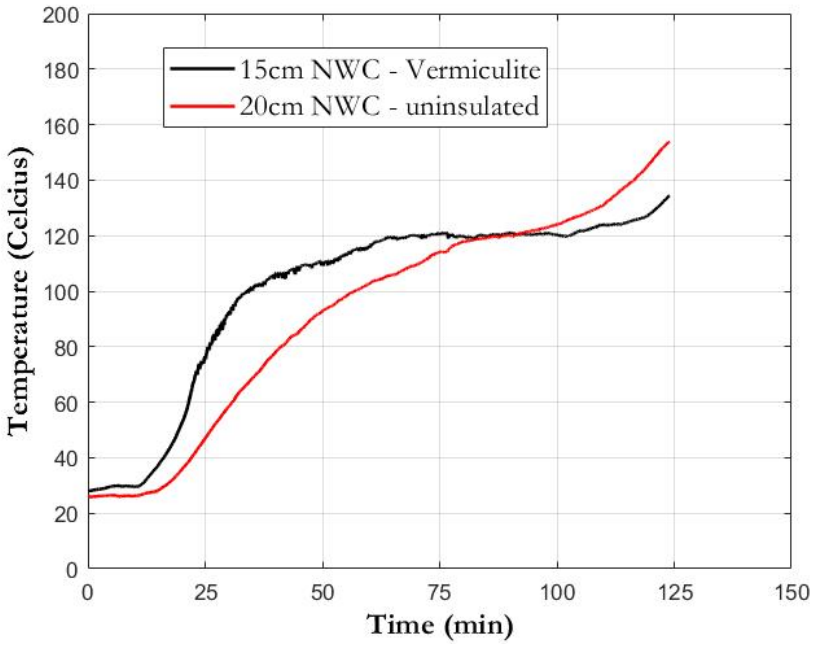

Figure 4-8 Average temperature profile on unexposed face of the wall (Experimental).

Unlike Test 1, the results to this test had a different pattern. At the start of the experiment, the solid web and hollow cell had a steady but gradual increase in temperature while the mortar had a rather steep and sudden increase in temperature.

The mortar surface was able to reach the plateau phase first, before the solid webs and hollow cell. This behaviour is as a result of the higher thermal conductivity of mortar when compared to that of concrete. As discussed before, Section 4.1, the plateau period for an uninsulated masonry wall occurred at about 100 ºC. However, by having vermiculite in the cells, the plateau periods occurred at a slightly higher temperature, somewhere between 120 - 140 ºC. The mortar surface showed a much longer plateau length due to the moisture

contained in its mix. The plateau period for the three special locations ended after 1 h 40 min of the physical test after which the mortar temperature began to increase linearly. By having the cells completely filled with vermiculite, the hollow cells and solid webs were no longer an area of concern as the rate of heat transfer to these regions were drastically reduced. Hence, for an insulated wall, failure occurs at the mortar section.

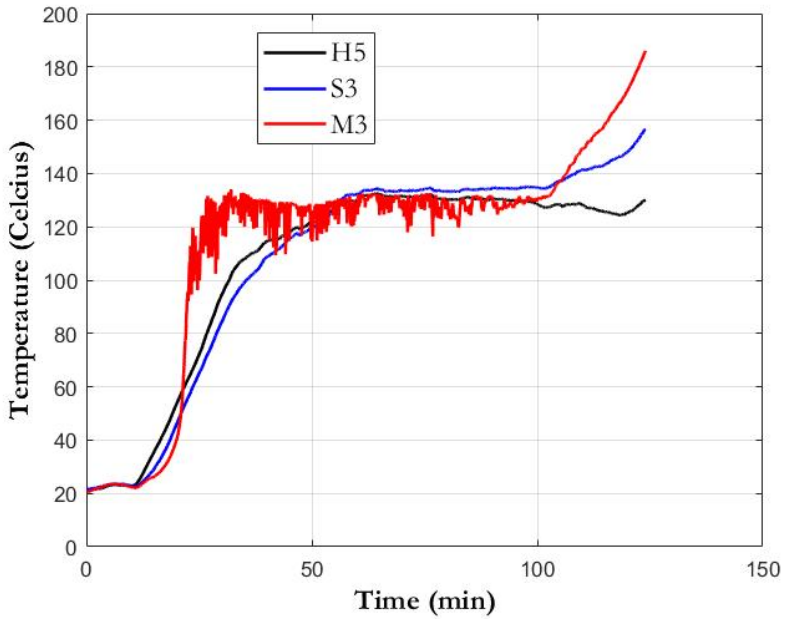

Figure 4-9 Temperature profile of fully insulated wall at H5, S3, and M3 (EXP).

It can be seen from the temperature difference between H2, H3 and H4 that regardless of the vermiculite fillings, heat is still transferred horizontally from the exposed surface of the wall, through the wall to the unexposed face of the wall Figure 4-10. H2 took a shorter time heating up while H3 and H4 spend slightly longer times heating up. This is because the expanded vermiculite has a much more improved thermal property at elevated temperatures

that allows it to heat up slowly. This makes the temperature difference between H2 and H3 much larger than the temperature difference between H3 and H4. The three thermocouple locations heated up at fairly similar rates until about 100 ºC. The plateau for H2 was almost nonexistent due to the direct heat received from the exposed surface. While that for H3 and H4 where much longer. This was as a result of the moisture loss from the expanded vermiculite also occurs at 100 ºC.

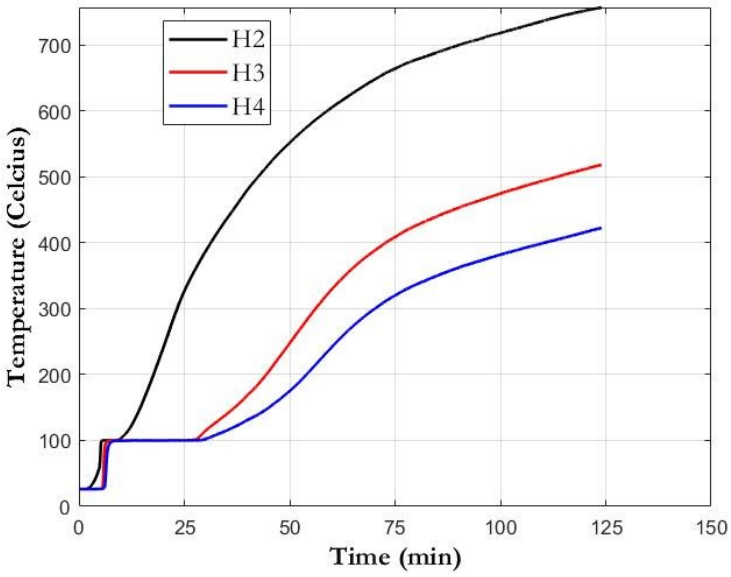

Figure 4-10 Hollow cell comparison.

4.2.4. **Thermal image contour**

After 15 min into the test, it is evident from frame 1 that the wall had started to heat up from the bottom Figure 4-11. After 45 mins into the test (frame 2), the bottom section of the wall still remained the hottest. Unlike an uninsulated wall where the hot air in the cells

are able to move vertically upwards, this was not the case for this wall. The vermiculite in the cells were able to impede this vertical heat flow. There were also noticeable cracks formed along the head joints at the top section of the wall. These cracks caused the mortar to be the hottest section of the wall. After 1 h into the test (frame 3), three hot cells were noticed at the middle of the wall. After 1 h 50 min, the three hot spots still remained the hottest part of the wall.

A couple of days after this test was carried out, the exposed and unexposed face of the wall were inspected. This inspection was done to investigate possible reasons behind why there where three (3) hot spots on the wall during the test. The exposed surface of the wall had spalled and there were also small noticeable holes at the middle of the wall and around the top section of the wall. with these openings, those spots were able to heat up well beyond the other areas of the wall.

Four (4) days after the physical test was carried out, a picture was taken to show the cracks formed on the unexposed face of the wall Figure 4-12. Majority of the cracks formed were along the bed and head mortar joints at both the top and bottom sections of the wall. but there were barely any cracks formed at the middle of the test wall

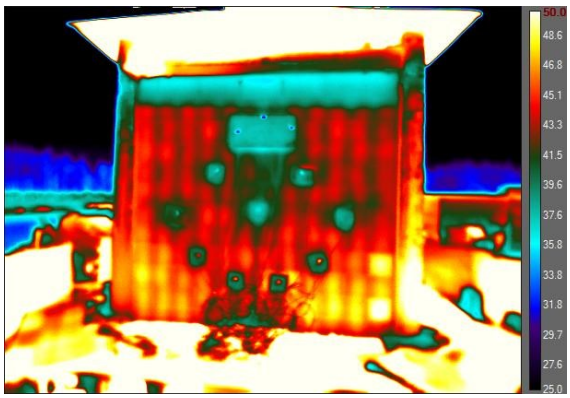

Frame 1 – At 15 mins

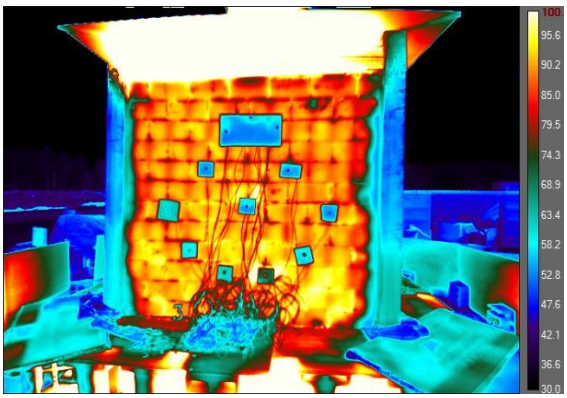

Frame 2 - At 45 mins

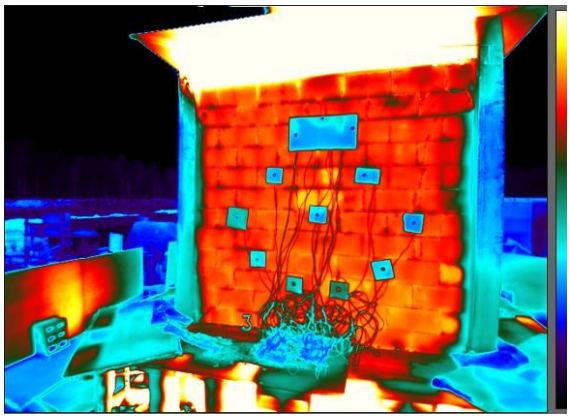

Frame 3 - At 1 h

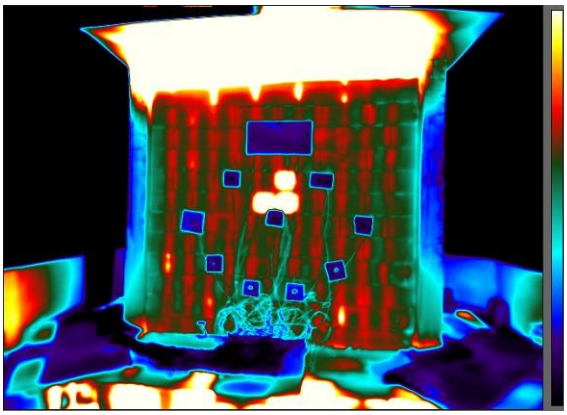

Frame 4 - At 1 h 50 min

Figure 4-11 Thermal imaging contour frames for fully insulated wall with vermiculite.

Figure 4-12 Crack on the unexposed face of fully insulated wall with vermiculite.

4.2.5. **Validation of finite element model**

As a result of vermiculites loose-fill nature, the wall was modelled similar to the physical test in such a way that the cells were completely filled as illustrated in Figure 4-13. The thermophysical properties incorporated into the FE model were gotten from past literature Table 4-1.

Table 4-1 Thermophysical properties of vermiculite [104].

	Thermal conductivity W/m.k	Density kg/m^3	Specific heat J/kg.k
Vermiculite	0.063	140	920

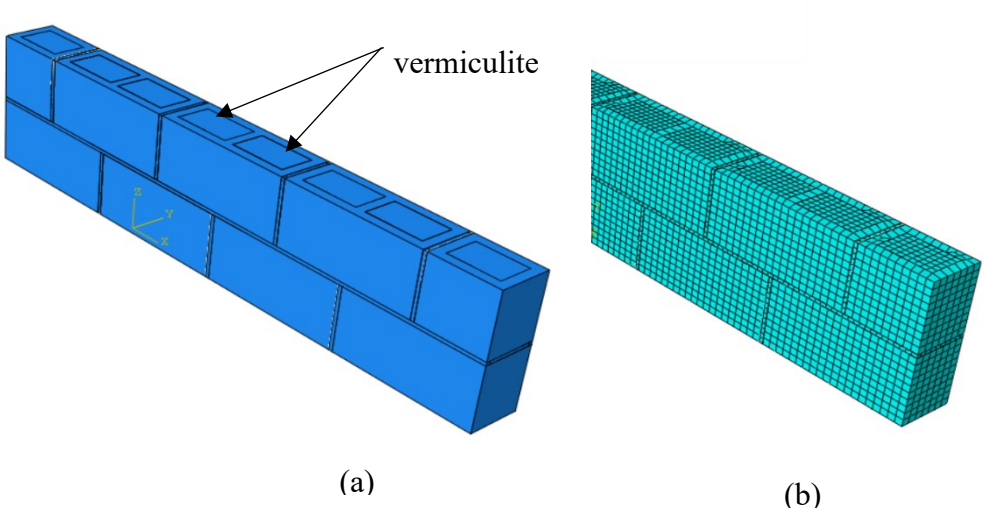

Figure 4-13 15 cm wall assembly fully insulated.

With the addition of the inserts in the cells, the interaction module was redone to consider the surface-to-surface contact between the masonry block, mortar and the vermiculite Figure 4-14. Since the insulation materials completely filled up the hollow and frog cells, the effects of radiation and convection were not considered.

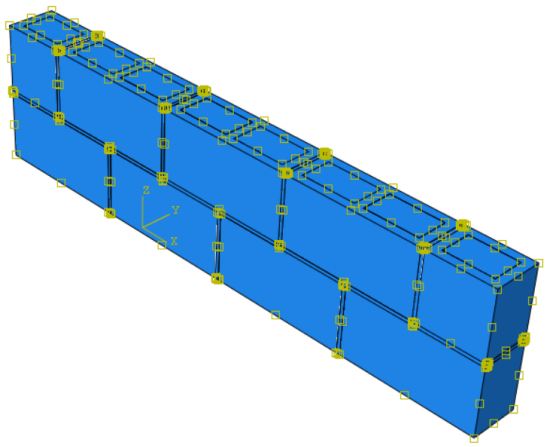

Figure 4-14: surface-to-surface contact interaction (conduction).

4.2.5.1. Heavily instrumented block results

By inputting the thermal properties highlighted in Table 4-1 into the model, the temperature profile along H5, S3 and M3 were compared with the experimental results. The FE analysis did not exactly depict the thermal response of the wall. The model was cooler than the experimental result across the hollow, solid and mortar sections Figure 4-15. Although a similar trend was observed between both results. The mortar joint was the hottest, followed by the solid webs and the hollow cells were the least critical, showing that the expanded vermiculite had an effect in reducing the impact of radiative or convective heat transfer in the cells.

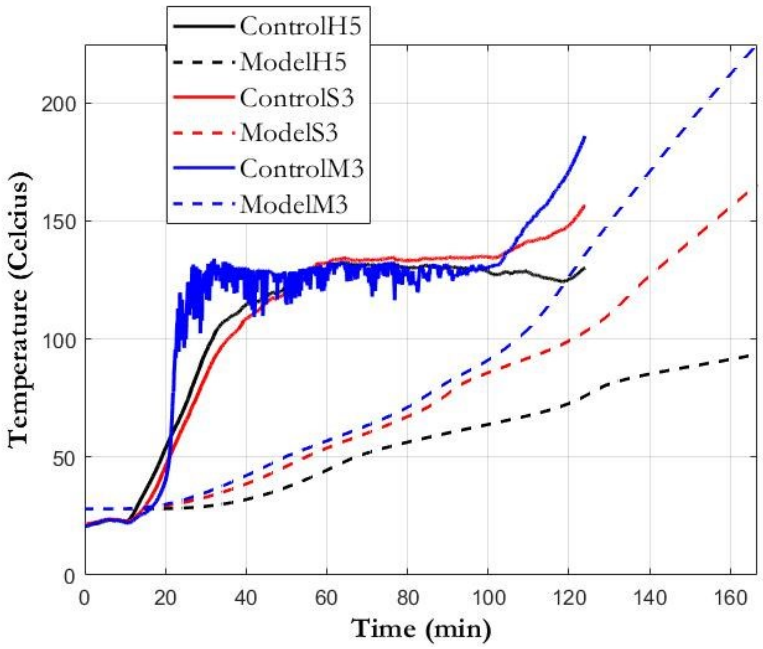

Figure 4-15 Temperature profile comparison at H5, S3, and M3 (control and FE model).

The experimental plots show that the plateau period ended after 100 minutes into the experiment. After this time, there was a sudden increase in heat transfer in the mortar, and a more gradual increase in the solid webs and hollow cells. During the experimental test, when the free water in the concrete and mortar begins to evaporate out of their pores, the vermiculite absorbs some of this moisture. Later in the test, this water in the expanded vermiculite also evaporates out.

Also, because ABAQUS was not able to directly incorporate the moisture loss behaviour during the finite element analysis, the sudden rise in the temperature after about 20 minutes and long plateau between 120 ºC - 140 ºC could not be reflected in the numerical plots. The results were left cooler. For the moisture loss effect to be indirectly incorporated into the model, the properties of vermiculite needed to be temperature dependant.

The average temperature profile on the unexposed face of the physical test (Test 2 results) and FE model were compared together Figure 4-16.

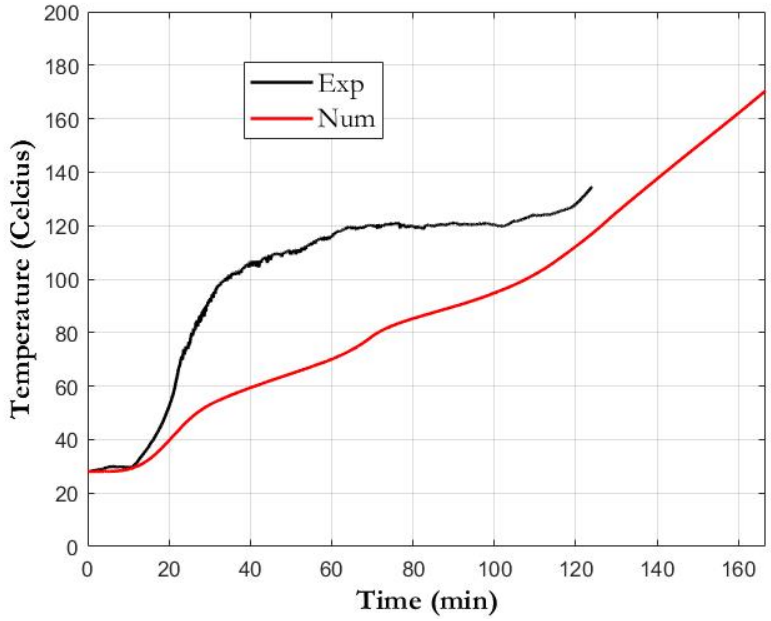

Figure 4-16 Average temperature profile of unexposed wall with vermiculite - Experimental and numerical.

The finite element model did not directly show the long horizontal plateau, but instead had a more gradual temperature increase. The model was able to predict a failure time of 2 h 36 min, which is over 2 h as predicted by the experimental results even though the test was terminated early.

4.3. Gypsum

Another 15cm fully insulated wall was modelled using gypsum as the cell filer. The thermophysical properties used were form existing literature. Density of 810 kg/m^3, thermal conductivity value of 0.28 W/mk and a specific heat of 1000 J/kg.k [93]. An ambient temperature of 28 ºC was used. The wall failed due to the 180 ºC insulation criteria after 153 minutes. The finite element analysis results were similar to a wall fully insulated with vermiculite. The hollow cells moved from being the most critical zone to being the least critical zone. The mortar became the most critical zone Figure 4-17.

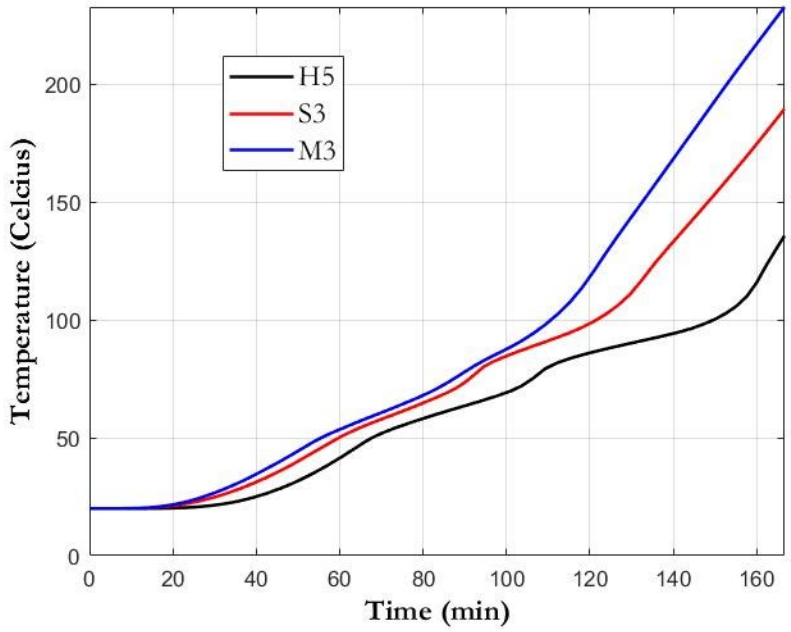

Figure 4-17 Temperature profile on the unexposed face - Numerical analysis.

The unexposed face of the wall did not begin to heat up until the first 20 minutes of the analysis. The mortar and solid webs had an almost equivalent temperature increase with time until about 100 ºC, after which there was a wider temperature difference.

4.4. Comparison between vermiculite wall and gypsum wall (Numerical)

It was decided to compare the temperature plots between the vermiculite wall (Numerical data) and the gypsum wall (Numerical data) Figure 4-18. The numerical results from both walls show that the vermiculite insulated wall heated up quicker than the gypsum insulated wall from the unset of the analysis. After 100 ºC, the vermiculite insulated wall had an increased heat transfer, causing it to heat up at a quicker rate, and eventually beyond the gypsum insulated wall. This reduced rate of heat transfer in the gypsum insulated wall is as a result of the calcination of gypsum that occurs after temperatures higher than 90 ºC, where the moisture contained is evaporated out at two different stages. Conclusions can

then be made that the vermiculite insulated wall has a slightly improved fire resistance than the gypsum insulated wall, with critical points being the mortar section.

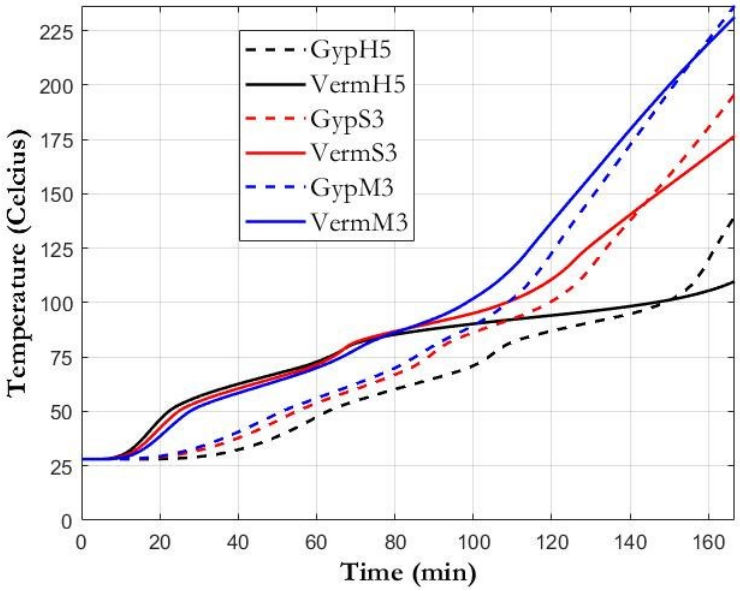

Figure 4-18 Comparison between the average temperature plots of the vermiculite wall and gypsum wall – Experimental.

4.5. Failure time summary

A summary of the failure times is summarized below in Figure 4-19. The fire resistance rating for a 15 cm wall is 1 hr, while that for a 20 cm wall is 2 hr. By having insulation materials such as vermiculite, and gypsum inside of the cells, a fire resistance rating of about 2 h – 2 hr 36 min was achieved. This was about a 43 – 45% increase in the fire rating.

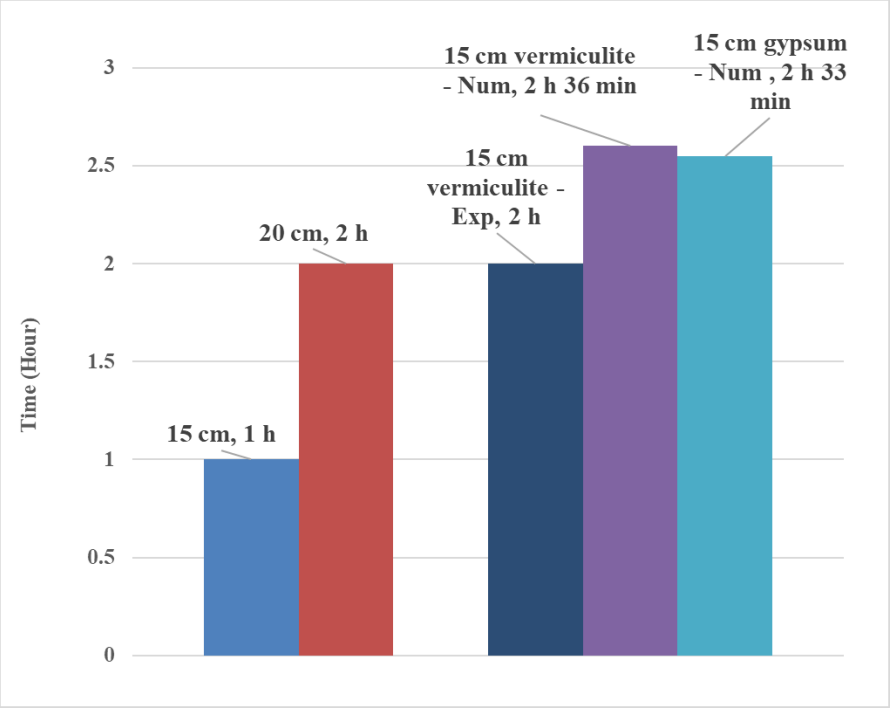

Figure 4-19 Failure time summary.

Chapter 5: Conclusions, limitations, and recommendations.

This study was undertaken to study the fire behaviour of masonry walls with lightweight insulation materials in the cells. Following the physical tests conducted, a three-dimensional thermal model was developed using ABAQUS to predict the behaviour of masonry walls when exposed to a standard fire. The masonry walls were made of 15 cm NWC blocks, as the focus was on non-loadbearing walls. The lightweight insulation materials used were vermiculite and gypsum (inorganic insulation material). The finite element model was first verified using a result from an uninsulated 20 cm NWC wall. It was later validated using results from a fully insulated 15 cm NWC wall with vermiculite. When the finite element model was validated, it was used for further studies, to predict the behavior of the walls with other insulation materials.

The thermal behaviour of the wall assemblies, alongside their time – temperature plots generally showed a good agreement with the results from the physical tests conducted. The model predictions of the fire resistance were within a reasonable variation from the experimental test results for walls uninsulated or walls insulated with an inorganic material. This variation could be as a result of the type of convection and radiation interaction

module used for the analysis, the meshing technique used or the thermophysical properties used.

5.1. Research conclusion

The conclusions from this study are summarized as follows:

1. Vermiculite and gypsum are suitable lightweight insulation materials that are able to restrict the effects of radiation and convection when used as a cell filler. The fire resistance rating of the 15 cm block was improved from 1 h to at least 2 h.
2. Finite element analysis is successful at predicting the heat transfer through concrete masonry that was insulated or uninsulated.
3. Finite element analysis can reduce the need for a full-scale fire resistance test on concrete masonry walls. With proper verification and validation of the model, further numerical simulations can be carried out to study the thermal response of concrete masonry with less need for expensive and time-consuming experimental testing.
4. For any heat transfer analysis to be accurately carried out, the density, thermal conductivity and specific heat values must be specified. During the numerical simulation, it was found that the density of a material had less effect on the thermal response of a masonry wall. However, Materials with a low thermal conductivity

and a high specific heat capacity showed good improvements to the fire resistance values.

5. Masonry walls that are fully insulated or partially insulated showed some level of improvement in the fire resistance rating of the wall. Especially because the hollow cells are usually the critical points. As fully or partially reducing the convective and radiative air circulation in the cells would always result in an improvement in the fire ratings of a block.
6. Masonry blocks with thicker face shells have a better thermal response to fire or elevated temperatures, than blocks with thinner face shells.
7. When the dead load is not of major concern, a 20cm NWC block can be substituted with a 15 cm block with cell fillers. With this substitute, a higher fire resistance rating can be achieved.

5.2. Limitations of study

Some limitations encountered in this study are listed as follows:

1. This research was conducted as a pure heat transfer analysis of non-load bearing walls. The mechanical properties were not considered

2. It was difficult in deciding on the thermo-physical properties to be used when modelling the insulation materials. This is because across literature, temperature

conditions or factors surrounding the choice of the values used were not consistent throughout as they are proprietary materials. Most of the properties stated did not also account for moisture absorption or evaporation. Much closer results could have been attained with temperature dependant thermo-physical properties.

5.3. Recommendations for future research

Recommendations for future studies are outlined as follows:

1. Small scall experimental tests were conducted on GPS insulation material that showed a potential for a good fire insulation. However, it was not reported in this thesis. There is a need to carry out a wall size tests to obtain a more conclusive result.
2. Laboratory works could also be conducted to determine the temperature dependent thermal properties of the insulation materials. With these, the behaviour of the material can be approximately replicated in any numerical analysis and the finite element model can be correctly validated or verified.
3. As a few thermocouples ended up malfunctioning during the tests, it is recommended that double the number needed should be used. With this, there would always be a backup test data that would be useful for further analysis.

Appendices

Appendix A1 - Thermo-physical properties of concrete

Concrete					
Thermal conductivity (W/m.k)		Specific heat capacity (J/kg.k)		Density (kg/m^3)	
20	1.60	20	600	20	2300
50	1.55	50	650	200	2200
100	1.50	70	700	400	2200
150	1.40	80	4000	600	2200
200	1.35	100	900	800	2200
250	1.30	200	105	900	2200
300	1.25	400	115	1000	2200
350	1.20	600	122		
400	1.15	700	126		
450	1.15	800	130		
500	1.10				
550	1.05				
600	1.00				
650	0.95				
700	0.90				
750	0.85				
800	0.85				

Appendix A2 - Thermo-physical properties of mortar

Mortar					
Thermal conductivity (W/m.k)		Specific heat capacity (J/kg.k)		Density (kg/m^3)	
20	1.20	20	750	20	1900
80	1.87	80	6000	50	1880
100	1.89	100	800	100	1860
200	2.90	200	850	150	1830
400	1.40	400	1050	200	1800
600	1.40	600	1150		
700	1.40	700	1050		
800	1.40	800	900		

Appendix B - DFLUX subroutine file

```
      subroutine dflux(flux,sol,kstep,kinc,time,noel,npt,coords,
     1 jltyp,temp,press,sname)
c
      include 'aba_param.inc'
c
      character*80 sname
      real :: Tf
      dimension flux(2),time(1),coords(3)
      parameter (sita=5.67d-11,emi=0.94,hc=0.021)
c
      flux(1)=0.0
      flux(2)=0.0
      Tf=20+750*(1-exp(-0.49*sqrt(time(1)/60)))+22*sqrt(time(1)/60)
      if (Tf.gt.sol) then
          flux(1)=hc*(Tf-sol)+sita*emi*((Tf+273)**4-(sol+273)**4)
          flux(2)=-hc-4*sita*emi*(sol+273)**3
      else
      end if
c
      return
      end
```

Appendix C - Thermophysical properties of air

T K	ρ kg/m^3	c_p kJ/kg·K	$\mu \cdot 10^7$ N·s/m^2	$\nu \cdot 10^6$ m^2/s	$k \cdot 10^3$ W/m·K	$\alpha \cdot 10^6$ m^2/s	Pr
100	3.5562	1.032	71.1	2.00	9.34	2.54	0.786
150	2.3364	1.012	103.4	4.426	13.8	5.84	0.758
200	1.7458	1.007	132.5	7.590	18.1	10.3	0.737
250	1.3947	1.006	159.6	11.44	22.3	15.9	0.720
300	1.1614	1.007	184.6	15.89	26.3	22.5	0.707
350	0.9950	1.009	208.2	20.92	30.0	29.9	0.700
400	0.8711	1.014	230.1	26.41	33.8	38.3	0.690
450	0.7740	1.021	250.7	32.39	37.3	47.2	0.686
500	0.6964	1.030	270.1	38.79	40.7	56.7	0.684
550	0.6329	1.040	288.4	45.57	43.9	66.7	0.683
600	0.5804	1.051	305.8	52.69	46.9	76.9	0.685
650	0.5356	1.063	322.5	60.21	49.7	87.3	0.690
700	0.4975	1.075	338.8	68.10	52.4	98.0	0.695
750	0.4643	1.087	354.6	76.37	54.9	109	0.702
800	0.4354	1.099	369.8	84.93	57.3	120	0.709
850	0.4097	1.110	384.3	93.80	59.6	131	0.716
900	0.3868	1.121	398.1	102.9	62.0	143	0.720
950	0.3666	1.131	411.3	112.2	64.3	155	0.723
1000	0.3482	1.141	424.4	121.9	66.7	168	0.726
1100	0.3166	1.159	449.0	141.8	71.5	195	0.728
1200	0.2902	1.175	473.0	162.9	76.3	224	0.728
1300	0.2679	1.189	496.0	185.1	82	238	0.719
1400	0.2488	1.207	530	213	91	303	0.703
1500	0.2322	1.230	557	240	100	350	0.685
1600	0.2177	1.248	584	268	106	390	0.688
1700	0.2049	1.267	611	298	113	435	0.685
1800	0.1935	1.286	637	329	120	482	0.683
1900	0.1833	1.307	663	362	128	534	0.677
2000	0.1741	1.337	689	396	137	589	0.672
2100	0.1658	1.372	715	431	147	646	0.667
2200	0.1582	1.417	740	468	160	714	0.655
2300	0.1513	1.478	766	506	175	783	0.647
2400	0.1448	1.558	792	547	196	869	0.630
2500	0.1389	1.665	818	589	222	960	0.613
3000	0.1135	2.726	955	841	486	1570	0.536

List of references

[1] S. W. Wafeek, "Ancient Masonry work in Egypt, china, and Rome: A comparative study," in 13th International Brick and Block Masonry Conference, Amsterdam, 2004.

[2] "How much did the September 11 terrosit attack cost America?," Institute for the analysis of global security., [Online]. Available: http://www.iags.org/costof911.html. [Accessed 22 Feburary 2021].

[3] Wikipedia contributors, "Wikipedia, The Free Encyclopedia.," 17 February 2021. [Online]. Available: https://en.wikipedia.org/w/index.php?title=Casualties_of_the_September_11_attacks&oldid=1007300254. [Accessed 22 February 2021].

[4] A. H. Buchanan, Structural design for fire safety, John Wiley & Sons., 2002.

[5] R. G. Drysdale and A. A. Hamid, "Masonry structures: Behaviour and Design," Canada Masonry Design Centre, 2005.

[6] J. E. Oti, J. M. Kinuthia and J. Bai, "Engineering properties of unfired clay masonry bricks," Engineering Geology, vol. 107, no. 3-4, pp. 130-139, 2009.

[7] K. J. J. G. H. D. Wild S., "Effect of partial substitution of lime with ground granulated blast furnace slag (GGBS) on the strength properties of lime-stabilized sulphate-bearing clay soils," Engineering Geology, vol. 51, no. 4, pp. 37-53, 1998.

[8] F. R. R. Ayala, "Mechanical properties and structural behaviour of masonry at elevated temperatures," United Kingdom, 2010.

[9] M. Building , "Building materials," Blogger, 16 March 2012. [Online]. Available: http://buildingmaterialassignment.blogspot.com/. [Accessed 4 April 2020].

[10] Z. Guo, Principles of Reinforced Concrete, Butterworth-Heinemann, 2014.

[11] C.-2. ACI, "Guide for structural lightweight aggregate concrete: Committee 213," American Concrete Institute, p. 27, 1999.

[12] U. B. Code, "Uniform building code," in International conference of building officials, Whittier, California, USA, 1997.

[13] M. S. J. Gan, Cement and Concrete, CRC Press, 1997.

[14] G.-F. Peng and Zhi-Shan Huang, "Change in microstructure of hardened cement paste subjected to elevated temperatures.," Construction and Building Materials, vol. 22, no. 4, pp. 593-599, 2008.

[15] I. Hager, "Behaviour of cement concrete at high temperature," Bulletin of the Polish Academy of Sciences. Technical Sciences, vol. 61, no. 1, pp. 145-154, 2013.

[16] A. Al-Sibahy and R. Edwards, "Thermal behaviour of novel lightweight concrete at ambient and elevated temperatures: Experimental, modelling and parametric studies," Construction and building materials, vol. 31, pp. 174-187, 2012.

[17] U. Schnider, "Concrete at high temperatures-A general review," Fire Safety Journal, vol. 13, pp. 55-68, 1988.

[18] G. GÖRHAN and G. KÜRKLÜ, "The Investigation of Heat Performance and Thermal Conductivity of Different Wall Materials at High Temperatures," Journal of Natural and Applied Sciences, vol. 22, no. 2, pp. 536-544, 2018.

[19] B. Jonaitis and P. Vytautas, "Effect of long-term loading and fire temperatures on mechanical properties of concrete," Journal of Civil Engineering and Management, vol. 11, no. 4, pp. 283-288, 2005.

[20] G. A. Khoury, "Effect of fire on concrete and concrete structures," Progress in Structural Engineering and Materials, vol. 2, no. 4, pp. 429-447, 2000.

[21] J. P. Ingham, "Application of petrographic examination techniques to the assessment of fire-damaged concrete and masonry structures," Materials characterization, vol. 60, no. 7, pp. 700-709, 2009.

[22] H. Pope, "Improving the fire resistance of concrete masonry walls," Ottawa, 2021.

[23] T. Muhammad, S. Khan, G. Bora and W. Jianqiang, "Effect of Elevated Temperature on Mechanical Properties of Limestone, Quartzite and Granite Concrete," International Journal of Concrete Structures and Materials, vol. 11, no. 1, pp. 17-28, 2017.

[24] S. Smeplass, "Effect of the aggregate type on the compressive strength and E-modulus of the aggregate," Trondheim, Norway, 1992.

[25] EN 1994-1-2, "Eurocode 4: Design of composite steel and concrete structures. Part 1-2: General rules - Structural fire design," Brussels, 2005.

[26] T. Zandbergen, Fire resistance of existing structures: Assessing the fire resistance of existing concrete buildings., 2016.

[27] ACI Committee 122, Guide to Thermal Properties of Concrete and Masonry systems, 2002.

[28] I. C. Mikron, "Table of emissivity of various surfaces".

[29] British Standards Institution, "Eurocode 2: Design of concrete structures. Part 1-2: General rules – Structural fire design," in British Standards Institution, Brussels, 2005.

[30] Y. Qin, H. Yuhui , W. Bo, M. Shaokun and Z. Xingui, "Regulating top albedo and bottom emissivity of concrete roof tiles for reducing building heat gains," Energy and Buildings, vol. 156, pp. 218-224, 2017.

[31] M. P. A. MPA, "MPA, The concrete Centre," [Online]. Available: https://www.concretecentre.com/Performance-Sustainability-(1)/Thermal-Mass/Surface-emissivity-why-this-matters.aspx#:~:text=Emissivity%20matters%20because%20matt%20surfaces,absorbing%20and%20emitting%20radiant%20heat.. [Accessed 15 December 2020].

[32] J. Lindgard and T. A. Hammer, "Fire resistance of structural lightweight aggregate concrete a literature survey with focus on spalling.," in NORDIC CONCRETE RESEARCH-PUBLICATIONS, 1998.

[33] R. Alghamri, A. Kanellopoulos and A. Al-Tabbaa, "Impregnation and encapsulation of lightweight aggregates for self-healing concrete.," Construction and Building Materials, vol. 124, pp. 910-921, 2016.

[34] P. Code, "Eurocode 4 Design of Composite Steel and Concrete Structures: Part 1.2: General Rules, Structural Fire Design, EN 1994-1-2," Brussels, 2005.

[35] O. A. Abdou and S. M. Kris, "The effect of air cells and mortar joints on the thermal resistance of concrete masonry walls," Energy and buildings, vol. 21, no. 2, pp. 111-119, 1994.

[36] V. Nežerka, J. Antoš, J. Litoš, P. Tesárek and J. Zeman, "An integrated experimental-numerical study of the performance of lime-based mortars in masonry piers under eccentric loading.," Construction and Building Materials, vol. 114, pp. 913-924, 2016.

[37] N. Arjun, "The constructor: Civil Engineering Home," [Online]. Available: https://theconstructor.org/building/brick-mortar-joint-types/24636/. [Accessed 08 May 2020].

[38] M. Zedan, S. Al-Sanea, A. Al-Mujahid and Z. Al-Suhaibani, "Effect of thermal bridges in insulated walls on air-conditioning loads using whole building energy analysis," Sustainability, vol. 8, no. 6, p. 560, 2016.

[39] H. Keelson and E. Zalok , "DO RAKED JOINTS AFFECT THE FIRE RESISTANCE OF CONCRETE MASONRY?," in 13th Canadian Masonry Symposium, Halifax, 2017.

[40] M. S. Cülfik and T. Özturan, "Effect of elevated temperatures on the residual mechanical properties of high-performance mortar," Cement and Concrete Research, vol. 32, no. 5, pp. 809-816, 2002.

[41] M. S. M, R. M. A and S. S. S, "EFFECT OF ELEVATED TEMPERATURE ON COMPRESSIVE STRENGTH OF BLENDED CEMENT MORTAR," Building research journal, vol. 56, pp. 173-185, 2008.

[42] M. S. M, A.-s. A. Y and A. S. Abbas, "Behavior of blended cement mortars containing nano-metakaolin at elevated temperatures," Construction and Building Materials, vol. 35, pp. 900-905, 2012.

[43] R. Černý, M. Totová, J. Poděbradská, J. Toman, J. Drchalová and P. Rovnaníková, "Thermal and hygric properties of Portland cement mortar after high-temperature exposure combined with compressive stress," Cement and Concrete Research, vol. 33, no. 9, pp. 1347-1355, 2003.

[44] J. Poděbradská, J. Pavlík, J. Toman and R. Černý, "Specific heat capacity of cementitious composites in high-temperature range," Working Group of the Slovak Physical Society,, pp. 18-23, 2003.

[45] J. Toman, J. NĚMEČKOVÁ and R. ČERNÝ, "Specific heat capacity of building materials at high temperatures," Roczniki Inżynierii Budowlanej, vol. 7, pp. 119-122, 2007.

[46] A. A, A.-t. T and Z. Z, "Numerical simulation of coupled heat transfers by conduction, natural convection and radiation in hollow structures heated from below or above," International Journal of Thermal Sciences , vol. 47, pp. 378-387, 2008.

[47] T. D. Nguyen and F. Meftah, "Behavior of clay hollow-brick masonry walls during fire. Part1: Experimental analysis," Fire Safety Journal, vol. 52, pp. 55-64, 2012.

[48] H. Pope and E. Zalok, "ISSUES WITH MASONRY AND FIRE: SPALLING AND THERMAL BOWING," in 13th Canadian Masonry Symposium, 2017.

[49] J. Sala, A. Urresti, K. Martin, I. Flores and A. Apaolaza , "Static and dynamic thermal characterisation of a hollow brick wall: Tests and numerical analysis.," Energy and Buildings, vol. 40, no. 8, pp. 1513-1520, 2008.

[50] B. Nagy, "Hygrothermal modelling of masonry blocks filled with thermal insulation.," in MATEC Web of Conferences., 2018.

[51] G. M. E. Cooke, "Thermal bowing and how it affects the design of fire," Interflam, 1988.

[52] S. M. Bryne, "Fire resistance of load-bearing masonry walls.," Fire technology, vol. 15, no. 3, pp. 180-188, 1979.

[53] R. J. Connolly, "The spalling of concrete in fires," 1995.

[54] P. Sullivan and A. Zaman, "Explosive spalling of concrete exposed to high temperatures," 1971.

[55] A. Faris, N. Ali, S. Gordon and A.-T. Abid, "Outcomes of a major research on fire resistance of concrete columns," Fire Safety Journal, vol. 39, pp. 433-445, 2004.

[56] A. Paul, "Spalling of Concrete – Causes, Prevention & Repair," 2014.

[57] H. Ke-cheng , G. Rong-xin , M. Qian-min, Y. Feng, L. Zhi-wei and S. Yan-Lin, "Experimental Research on High Temperature Resistance of Modified Lightweight Concrete after Exposure to Elevated Temperatures," Advances in Materials Science and Engineering, 2016.

[58] S. Yannas, "CONSERVATION PRACTICES AND POTENTIAL IN VARIOUS CLIMATES," in Passive and Low Energy Ecotechniques, 1985.

[59] Wikipedia contributors, "Building insulation materials," Wikipedia, The Free Encyclopedia, 11 March 2021. [Online]. Available: https://en.wikipedia.org/w/index.php?title=Building_insulation_materials&oldid=1011532359. [Accessed 23 March 2021].

[60] H. Zhang, Building Materials in Civil Engineering, Elsevier science, 2011.

[61] L. Aditya, T. M. I. Mahlia, B. Rismanchi, H. M. Ng, M. H. Hasan, H. S. C. Metselaar, M. Oki and H. B. Aditiyah, "A review on insulation materials for energy conservation in buildings.," Renewable and sustainable energy reviews, vol. 73, pp. 1352-1365, 2017.

[62] H. Yang, Y. Jiang, H. Liu, D. Xie, C. Wan, H. Pan and S. Jiang, "Mechanical, thermal and fire performance of an inorganic-organic insulation material composed of hollow glass microspheres and phenolic resin," Journal of colloid and interface science, vol. 580, pp. 163-170, 2018.

[63] S. Victoria, "Insulation," in Energy Smart Housing Manual, 2010.

[64] L. M. Al-Hadhrami and A. A. , "Assessment of thermal performance of different types of masonry bricks used in Saudi Arabia.," Applied thermal engineering, vol. 29, no. 5-6, pp. 1123-1130, 2009.

[65] Al-Hazmy and M. Majed, "Analysis of coupled natural convection–conduction effects on the heat transport through hollow building blocks," Energy and Buildings, vol. 38, no. 5, pp. 515-521, 2006.

[66] Z. Pavlík, M. Jerman, A. Trník, V. Kočí and R. Černý, "Effective thermal conductivity of hollow bricks with cells filled by air and expanded polystyrene.," Journal of building physics , vol. 37, no. 4, pp. 436-448, 2014.

[67] Z. Pavlík, M. Jerman, J. Fořt and R. Černý, "Monitoring thermal performance of hollow bricks with different cell fillers in difference climate conditions," International Journal of Thermophysics, vol. 36, no. 2-3, pp. 557-568, 2015.

[68] Y. Li and S. Ren, Building decorative materials, Elsevier, 2011.

[69] J. V. Ryan, "Study of Gypsum Plasters Exposed to Fire," Journal of Research of the National Bureau of Standards – C. Engineering and Instrumentation, vol. 66, no. 4, pp. 373-387, 1962.

[70] M. A. Sultan, "A model for predicting heat transfer through noninsulated unloaded steel-stud gypsum board wall assemblies exposed to fire.," Fire Technology, vol. 32, pp. 239-259, 1996.

[71] T. Z. Harmathy, "Properties of Building Materials," The SFPE Handbook of Fire Protection Engineering, pp. 378-391, 1988.

[72] J. R. Mehaffey, P. Cuerrier and G. Carisse, "A model for predicting heat transfer through gypsum-board/wood-stud walls exposed to fire," Fire and Materials, vol. 18, no. 5, pp. 297-305, 1994.

[73] A. O. Mydin, "Gypsum Board Thermal Properties Exposed to High Temperature and Fire Condition," rties Exposed to High Temperature and Fire Condition. Buletinul Institutului Politehnic din lasi. Sectia Constructii, Arhitectura, vol. 58, no. 4, p. 31, 2012.

[74] A. Oliver, "Thermal characterization of gypsum boards with PCM included: Thermal energy storage in buildings through latent heat," Energy and Buildings, vol. 48, pp. 1-7, 2012.

[75] D. Kontogeorgos and F. M., "Numerical investigation of simultaneous heat and mass transfer mechanisms occurring in a gypsum board exposed to fire conditions," Applied Thermal Engineering, vol. 30, no. 11-12, pp. 1461-1469, 2010.

[76] F. koksal, G. Osman and K. Mehmet , "Combined effect of silica fume and expanded vermiculite on properties of lightweight mortars at ambient and elevated temperatures.," Construction and Building Materials, vol. 88, pp. 175-187, 2015.

[77] M. Hall, "Inorganic mineral materials for insulation in buildings," in Materials for energy efficiency and thermal comfort in buildings, Elsevier, 2010, pp. 193-228.

[78] European Manufacturers of Expanded Polystyrene , "Behavious of EPS in case of fire," August 2002. [Online]. [Accessed 12 March 2021].

[79] A. V. Sowriraajan and C. B. Dixit, "IMPROVEMENT OF FIRE SAFETY IN ROOMS WITH EXISTING EXPANDED POLYSTYRENE ROOF INSULATION.," in PROCEEDINGS OF FIRE SCIENCE AND TECHNOLOGY - RESEARCH & ITS IMPLEMENTATIONS, 2011.

[80] M. Khoukhi, "The combined effect of heat and moisture transfer dependent thermal conductivity of polystyrene insulation material: Impact on building energy performance," Energy and buildings, vol. 169, pp. 228-235, 2018.

[81] S. A. Al-Ajlan, "Measurements of thermal properties of insulation materials by using transient plane source technique.," Applied thermal engineering, vol. 26, no. 17-18, pp. 2184-2191, 2006.

[82] B. Nagy and T. Elek , "Hygrothermal behaviour of hollow and filled ceramic masonry blocks," RILEM Proc, vol. 112, pp. 279-288, 2016.

[83] T. Z. Harmathy, "The Fire Resistance Test and its Relation to Real-world Fires," Fire and Materials, vol. 5, no. 3, pp. 112-122, 1981.

[84] D. Yang, W. Sun, Z. Liu and K. Zheng, "Research on improving the heat insulation and preservation properties of small-size concrete hollow blocks.," Cement and concrete research, vol. 33, no. 9, pp. 1357-1361, 2003.

[85] M. Al-Nasra and Z. Torbica, "Concrete Made for Energy Conservation Using Recycled Rubber Aggregates," International Journal of Engineering Science Invention, vol. 2, pp. 10-16, 2013.

[86] B. Yesilata, H. Bulut and P. Turgut, "Experimental study on thermal behavior of a building structure using rubberized exterior-walls.," Energy and Buildings, vol. 43, no. 2-3, pp. 393-399, 2011.

[87] B. Yesilata, Y. Isıker and P. Turgut, "Thermal insulation enhancement in concretes by adding waste PET and rubber pieces," Construction and Building Materials, vol. 23, no. 5, pp. 1878-1882, 2009.

[88] J. Gong, Z. Duan, K. Sun and M. Xiao, "Waterproof properties of thermal insulation mortar containing vitrified microsphere.," Construction and Building Materials, pp. 274-280, 2016.

[89] Z. Zhang, J. L. Provis, A. Reid and H. Wang, "Geopolymer foam concrete: An emerging material for sustainable construction.," Construction and Building Materials, vol. 56, pp. 113-127, 2014.

[90] P. Duan, L. Song, C. Yan, D. Ren and Z. Li, "Novel thermal insulating and lightweight composites from metakaolin geopolymer and polystyrene particles.," Ceramics International, vol. 43, no. 6, pp. 5115-5120, 2017.

[91] M. Antar and H. Baig, "Conjugate conduction-natural convection heat transfer in a hollow building block.," Applied Thermal Engineering, vol. 29, pp. 3716-3720, 2009.

[92] I. :. 3952, Specification for Burnt Clay Hollow Bricks for Walls and Partitions. Bureau of Indian Standards, New Delhi, 1988.

[93] L. P. Li, Z. G. Wu, Y. L. He, G. Lauriat and W. Q. Tao, "Optimization of the configuration of 290× 140× 90 hollow clay bricks with 3-D numerical simulation by finite volume method.," Energy and Buildings, vol. 40, no. 10, pp. 1790-1798, 2008.

[94] D. P. Aviram, A. N. Fried and J. J. Roberts, "Thermal properties of a variable cell wall.," Building and Environment, vol. 36, no. 9, pp. 1057-1072, 2001.

[95] P. J. B. B. Lourenço, Computational strategies for masonry structures, Netherlands: Delft University Press, 1997.

[96] A. Nadjai, M. O'Garra, F. Ali and D. Laverty, "A numerical model for the behaviour of masonry under elevated temperatures," Fire and materials, vol. 27, no. 4, pp. 163-182, 2003.

[97] W. contributors, "Abaqus," 1 November 2020. [Online]. Available: https://en.wikipedia.org/wiki/Abaqus. [Accessed 26 November 2020].

[98] CAN/ULC-S101, Standard Methods of Fire Endurance Tests of Building Construction and Materials, Scaborough, Canada, 2007.

[99] Wikipedia contributors, "Thermocouple," Wikipedia, The Free Encyclopedia, 7 December 2020. [Online]. Available: https://en.wikipedia.org/w/index.php?title=Thermocouple&oldid=992898540. [Accessed 8 December 2020].

[100] D. Logan, Finite element method, CA, US: Brooks/Cole,, 2002.

[101] H. A. Keelson, "Fire Resistance Quantification of Non-Loadbearing Masonry Walls–Numerical Study," Ottawa, 2018.

[102] L. F. Smith and R. W. Bletzacher, "Fire Endurance of Wall Assemblies Constructed with Concrete Masonry Units.," in Canadian Masonry Symposium., Canada, 1986.

[103] Dassaut Systemes Simulia Corps, ABAQUS/CAE Version 6.13 Standard Manual, Rhode Island, USA, 2013.

[104] T.-D. Nguyen, F. Meftah, R. Chammas and A. Mebarki, "The behaviour of masonry walls subjected to fire: Modelling and parametrical studies in the case of hollow burnt-clay bricks," Fire Safety Journal, vol. 44, no. 4, pp. 629-641, 2009.

[105] M. Smilovic, J. Radnic, N. Grgic and G. Baloevic, "Effect of anisotropy of masonry on the behaviour of unreinforced and confined masonry walls under ground motion," In Engineering Design Applications , pp. 173-186, 2019.

[106] F. Al Nahhas, R. Ami Saada, G. Bonnet and P. Dekmotte , "Resistance to fire of walls constituted by hollow blocks: Experiments and thermal modelling," Applied Thermal Engineering, vol. 27, pp. 258-267, 2007.

[107] A. Papadopoulos, "State of the art in thermal insulation materials and aims for future developments," Energy and Buildings, vol. 37, pp. 77-86, 2004.